University of Alberta

New Diversity Combiners and the Impact of Fading Correlation on Diversity Systems

by

Yunxia Chen 

A thesis submitted to the Faculty of Graduate Studies and Research in partial fulfillment of the requirements for the degree of **Master of Science**.

Department of Electrical and Computer Engineering

Edmonton, Alberta
Fall 2004

Your file Votre référence
ISBN: 0-612-95721-7
Our file Notre référence
ISBN: 0-612-95721-7

I dedicate this thesis to my parents for their endless encouragement, love and support.

Acknowledgements

It is with great pleasure that I take this opportunity to thank numerous individuals who have supported me throughout the course of my study.

First, I would like to thank my supervisor Dr. Tellambura for his valuable advice and constant encouragement. His insight, kindness and genuine concern for his students made working with him a memorable experience. I am grateful to him for leading me into this exciting area of wireless communications.

I wish to thank Dr. Xiaodai Dong and Dr. Peter Hooper for serving on my thesis committee.

My special thanks go to Luqing Wang who provided me with invaluable help and advice for my school life here. My gratitude also goes to my current labmates for providing such a creative, intellectually stimulating and fun environment.

My deepest gratitude goes to my parents and my boyfriend, Shuzhen, for their affection, understanding, patience and support. Every time in my life, they are always the source of my power and courage. I also extend my sincere thanks to my former classmates, my bridge teacher, Weiguo Zheng, and my bridge teammates for their encouragement.

Last, I would like to thank the Natural Sciences and Engineering Research Council (NSERC) and the Alberta Informatics Circle of Research Excellence (iCORE) for their financial support.

Contents

List of Tables

List of Figures

List of Symbols

Symbol	Definition
${}_1F_1(a, c; z)$	confluent hypergeometric function [3, Eq. (9.210.1)]
${}_2F_1(a, b; c; z)$	Gauss hypergeometric function [3, Eq. (9.100)]
$C(\mu, \sigma^2)$	complex Gaussian distribution with mean μ and variance σ^2
$D_{-2}(z)$	parabolic cylinder function [3, Eq. (9.240)]
$D(z)$	Dawson's integral [4]
$E(X)$	average of a RV X
$F_A(\cdot; \cdot; \cdot; \cdot)$	the n-th order Appell hypergeometric function [3, (9.180.2)]
$F_X(x)$	cdf of the RV X
$N(\mu, \sigma^2)$	real Gaussian distribution with mean μ and variance σ^2
i	$\sqrt{-1}$
$I_m(z)$	the m-th order modified Bessel function of the first kind [3, Eq. (8.406.3)]
$J_m(z)$	the m-th order Bessel function of the first kind [3, Eq. (8.402)]
$p_X(x)$	pdf of the RV X
$P(a, x)$	normalized incomplete gamma function
$Q_m(a, b)$	the m-th order Marcum Q-function [5, Eq. (1)]
$Q(x)$	Q-function [6, Eq. (2-1-97)]
$\mathcal{R}(K, \Omega)$	Ricean distribution with Rice factor K and average power Ω
$\Re(z)$	real part of z
$u(x)$	unit step function
$X_{(n)}$	the n-th largest element in $\{X_k\}$
x^*	complex conjugate of x
$\|x\|$	absolute value of x
$\chi_n(s, \sigma^2)$	non-central chi-square distribution with n degrees of freedom and non-centrality parameter s^2
$\chi_n(0, \sigma^2)$	central chi-square distribution with n degrees of freedom
δ_{jk}	Kronecker delta function

Symbol	Definition
$\gamma(a, x)$	incomplete Gamma function [3, Eq. (8.350.1)]
$\Gamma(a)$	Gamma function [3, Eq. (8.310.1)]
$\Gamma(a, x)$	complementary incomplete Gamma function [3, Eq. (8.350.2)]

List of Abbreviations

Abbreviation	Definition
AOA	angle-of-arrival
AWGN	additive white Gaussian noise
BER	bit error rate
cdf	cumulative distribution function
CEP	conditional error probability
CGRV	complex Gaussian random variable
chf	characteristic function
CSI	channel state information
DPSK	differential phase-shift-keying
EGC	equal gain combining
FSK	frequency-shift-keying
GSC	generalized selection combining
i.i.d.	independently and identically distributed
i.n.d.	independently and non-identically distributed
LOS	line-of-sight
mgf	moment generating function
MRC	maximal ratio combining
MSK	minimum-shift-keying
OFDM	orthogonal frequency division multiplexing
PAM	pulse amplitude modulation
pdf	probability density function
PDP	power delay profile
PSK	phase-shift-keying
QAM	quadrature amplitude modulation
RV	random variable
SER	symbol error rate

Abbreviation	Definition
SC	selection combining
SNR	signal-to-noise ratio
SWC	switched combining
PSD	power spectral density
UWB	ultra wide-band

Chapter 1

Introduction

Wireless communication has been one of the fastest growing fields over the past several years. The tremendous demand for wireless services has led to a renewal of the research activities related to wireless techniques. The fundamental limit to reliable wireless communications is the severe random fading phenomenon inherent in wireless channels; unlike the wired environment, the wireless channels are non-stationary and less predictable due to the radio propagation effects. To overcome this problem, many techniques are employed including: diversity techniques, smart antennas, adaptive filters and equalizers and orthogonal frequency division multiplexing (OFDM) [7].

1.1 Multi-path Fading

In wireless communications, the radio signals may not reach the receiver antennas directly. In fact, due to reflection, diffraction and scattering by the surrounded buildings, trees and other obstacles, the received signal is a superposition of radio signals coming from different directions with random amplitudes and phases. These multiple signals can interfere constructively or destructively. Consequently, the amplitudes of the received signal can fluctuate widely and this effect is known as multi-path fading or simply fading [8].

1.1.1 Statistical Models

Fading is modelled or described using several statistical models. To characterize the statistical channel models, the cumulative distribution function (cdf), the probability density function (pdf) and the moment generating function (mgf) of the fading amplitudes are of-

ten required. The cdf of a RV X, $F_X(x)$, is defined as the probability that the RV X is no greater than a fixed value of x [9, Eq. (4-1)]:

$$F_X(x) = \Pr[X \leq x]. \tag{1.1}$$

The corresponding pdf, which indicates the relative frequency of the occurrence of the event $\{X = x\}$, is obtained by differentiating the cdf with respect to x [9, Eq. (4-13)]:

$$p_X(x) = \frac{d}{dx} F_X(x). \tag{1.2}$$

The mgf of a RV X is defined as the Laplace transform of the corresponding pdf:

$$M_X(s) = \int_0^\infty p_X(x) e^{-sx}\, dx. \tag{1.3}$$

The mgf is related to another statistical function, the characteristic function (chf), as

$$\phi_X(i\omega) = M_X(-i\omega). \tag{1.4}$$

Next, we will introduce several widely-used, statistical fading channel models.

Rayleigh distribution

Rayleigh distribution is frequently used to model the amplitudes of the received signals in urban and suburban areas [10–12]. Let $R = \sqrt{X_1^2 + X_2^2}$, where X_1 and X_2 are zero-mean independent Gaussian random variables (RVs) with common variance $E(X_1^2) = E(X_2^2) = \sigma^2$, where $E(X)$ is the mean of the RV X, i.e., $X_1, X_2 \sim N(0, \sigma^2)$. It can be shown that R is Rayleigh distributed and its pdf is given by [6]

$$p_R(r) = \frac{r}{\sigma^2} e^{-\frac{r^2}{2\sigma^2}}, \quad r \geq 0. \tag{1.5}$$

The corresponding squared-envelope is central chi-square distributed with two degrees of freedom, i.e., $R^2 \sim \chi_2(0, \sigma^2)$ or exponential distributed, whose cdf, pdf and mgf are given respectively by [6]

$$F_{R^2}(y) = 1 - \exp\left(-\frac{y}{2\sigma^2}\right), \quad y \geq 0, \tag{1.6a}$$

$$p_{R^2}(y) = \frac{1}{2\sigma^2} \exp\left(-\frac{y}{2\sigma^2}\right), \quad y \geq 0, \tag{1.6b}$$

$$M_{R^2}(s) = \frac{1}{1 + 2\sigma^2 s}, \quad s > -\frac{1}{2\sigma^2}. \tag{1.6c}$$

Ricean distribution

In rural regions, which often lack tall structures, the received signal contains a direct line-of-sight (LOS) component; so the Ricean distribution is more suitable in such channels. Let $R = \sqrt{X_1^2 + X_2^2}$, where X_1 and X_2 are independent Gaussian RVs with non-zero means m_1, m_2 and common variance $E[(X_1 - m_1)^2] = E[(X_2 - m_2)^2] = \sigma^2$, i.e., $X_1 \sim N(m_1, \sigma^2)$ and $X_2 \sim N(m_2, \sigma^2)$. Then R is Ricean distributed with the Rice factor $K = \frac{m_1^2+m_2^2}{2\sigma^2}$ and the average power $\Omega = E(R^2) = m_1^2 + m_2^2 + 2\sigma^2$, i.e., $R \sim \mathcal{R}\left(\frac{m_1^2+m_2^2}{2\sigma^2}, m_1^2 + m_2^2 + 2\sigma^2\right)$, and its pdf is given by [6]

$$p_R(r) = \frac{2r(K+1)}{\Omega} \exp\left[-K - \frac{(K+1)r^2}{\Omega}\right] I_0\left(2r\sqrt{\frac{K(K+1)}{\Omega}}\right), \quad r \geq 0, \tag{1.7}$$

where $I_0(x)$ is the zero-th order modified Bessel function of the first kind which can be found [3, Eq. (8.406.3)]:

$$I_0(x) = \frac{1}{\pi} \int_0^{\pi} e^{x\cos\theta}\, d\theta. \tag{1.8}$$

The squared-envelope of a Ricean RV is non-central chi-square distributed with two degrees of freedom and non-centrality parameter $\frac{K\Omega}{K+1}$, i.e., $R^2 \sim \chi_2\left(\sqrt{\frac{K\Omega}{K+1}}, \sigma^2\right)$, whose cdf, pdf and mgf are given respectively by [6]

$$F_{R^2}(y) = 1 - Q\left(\sqrt{2K}, \sqrt{\frac{2(K+1)y}{\Omega}}\right), \quad y \geq 0, \tag{1.9a}$$

$$p_{R^2}(y) = \frac{K+1}{\Omega} \exp\left[-K - \frac{(K+1)y}{\Omega}\right] I_0\left(2\sqrt{\frac{K(K+1)y}{\Omega}}\right), \quad y \geq 0, \tag{1.9b}$$

$$M_{R^2}(s) = \frac{1+K}{1+K+s\Omega} \exp\left(-\frac{sK\Omega}{1+K+s\Omega}\right), \quad s > -\frac{1+K}{\Omega}, \tag{1.9c}$$

where $Q(a, b)$ is the first order Marcum Q-function. The m-th order Marcum Q-function $Q_m(a, b)$ is given by [5, Eq. (1)]

$$Q_m(a, b) = \int_b^{\infty} x \left(\frac{x}{a}\right)^{m-1} \exp\left[-\frac{x^2 + a^2}{2}\right] I_{m-1}(ax)\, dx \tag{1.10}$$

where $I_m(x)$ is the m-th order modified Bessel function of the first kind [3, Eq. (8.406.3)]. As expected, when $K = 0$, (1.9) reduces to (1.6). That is, the Rayleigh distribution is a special case of the Ricean distribution.

Lognormal distribution

The above two channel models are only valid in relatively small areas where the local mean of the envelope is approximately constant [13]. In larger areas, where the local mean fluctuates due to shadowing effects, the lognormal distribution is used [12, 14]. The lognormal pdf is given by [15]

$$p_R(r) = \frac{2}{\sqrt{2\pi}\xi\sigma r} \exp\left[-\frac{(10\log_{10} r^2 - \mu_{(\mathrm{dB})})^2}{2\sigma^2}\right], \quad r \geq 0, \tag{1.11}$$

where $\xi = \ln 10/10$, μ and σ^2 are the mean and variance of $10\log_{10}(r^2)$, respectively.

Nakagami-m distribution

The Nakagami-m distribution is a versatile statistical distribution which can accurately model a variety of fading environments. It has greater flexibility in matching some empirical data than the Rayleigh, Ricean or Lognormal distribution. It also includes the Rayleigh and the one-sided Gaussian distributions as special cases. Moreover, the Nakagami-m distribution can closely approximate the Ricean and the Hoyt distributions [16]. The pdf for this distribution is given by [6]

$$p_R(r) = \frac{2}{\Gamma(m)}\left(\frac{m}{\Omega}\right)^m r^{2m-1} \exp\left(-\frac{mr^2}{\Omega}\right), \quad r \geq 0, \tag{1.12}$$

where $\Omega = E(R^2)$ is the average envelope power, $\Gamma(m)$ is the Gamma function [3, Eq. (8.310.1)] which is related to the factorial by $\Gamma(n) = (n-1)!$ when n is a positive integer and the fading figure m is defined as

$$m = \frac{\Omega^2}{E[(R^2 - \Omega)^2]}, \quad m \geq 0.5. \tag{1.13}$$

When $m = 1$ and $m = 0.5$, Nakagami-m distribution reduces to the Rayleigh and the one-sided Gaussian distributions, respectively. The squared-envelope of a Nakagami-m RV is Gamma distributed with cdf, pdf and mgf given by [15]

$$F_{R^2}(y) = 1 - \frac{1}{\Gamma(m)}\Gamma\left(m, \frac{my}{\Omega}\right), \quad y \geq 0, \tag{1.14a}$$

$$p_{R^2}(y) = \frac{1}{\Gamma(m)}\left(\frac{m}{\Omega}\right)^m y^{m-1} \exp\left(-\frac{my}{\Omega}\right), \quad y \geq 0, \tag{1.14b}$$

$$M_{R^2}(y) = \left(\frac{m}{m + s\Omega}\right)^m, \quad s > -\frac{m}{\Omega}, \tag{1.14c}$$

where $\Gamma(a, x)$ is the complementary incomplete gamma function which can be defined as a finite integral [3, Eq. (8.310.1)]

$$\Gamma(n, x) = \int_x^\infty t^{n-1} e^{-t}\, dt, \quad n \geq 0. \tag{1.15}$$

1.1.2 Performance Loss due to Multi-path Fading

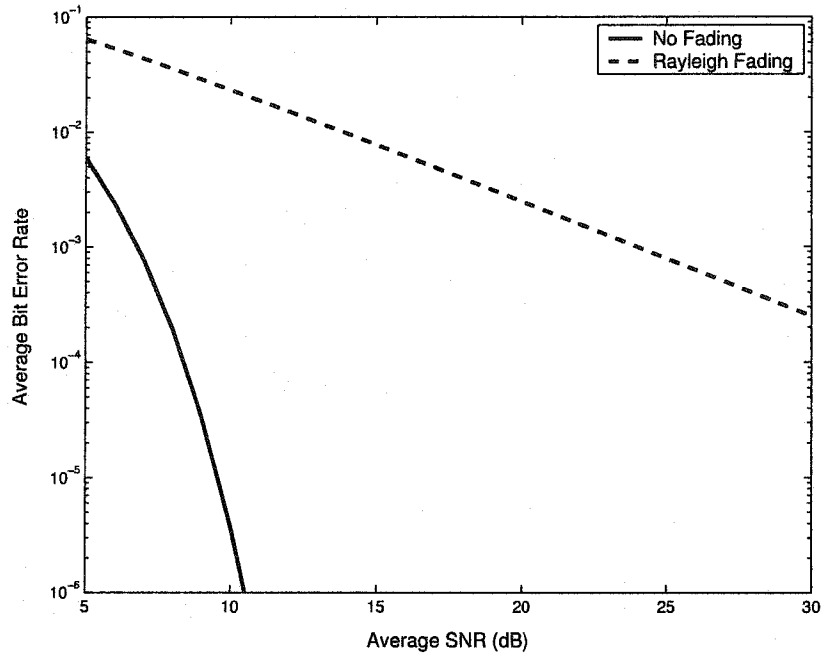

Figure 1.1: The effect of Rayleigh fading on the BER of BPSK.

Multi-path fading significantly impairs the quality of wireless communications [17]. For example, the bit error rate (BER) of uncoded binary phase-shift-keying (BPSK) in additive white Gaussian noise (AWGN) channel (i.e., no fading) is given by [6]

$$P_e = Q\left(\sqrt{2\gamma}\right) \approx e^{-\gamma}, \quad \text{as } \gamma \to \infty, \tag{1.16}$$

where γ is the signal-to-noise ratio (SNR) and $Q(x)$ is the area under the tail of the Gaussian pdf [6, Eq. (2-1-97)]. The BER decays exponentially with the increasing SNR. However, if the signal is transmitted through a Rayleigh fading channel, the average BER of BPSK is given by [15]:

$$\bar{P}_e = \frac{1}{2}\left[1 - \sqrt{\frac{\bar{\gamma}}{1+\bar{\gamma}}}\right] \approx \frac{1}{4\bar{\gamma}}, \quad \text{for } \bar{\gamma} \gg 1. \tag{1.17}$$

Hence, Rayleigh fading converts the exponential dependency of BER on SNR into an inverse linear one.

Fig. 1.1 shows the effect of Rayleigh fading on the BER of BPSK as compared to that in AWGN. Clearly, Rayleigh fading significantly degrades the performance of BPSK. For example, Rayleigh fading causes a 17dB SNR penalty at a BER of 10^{-3}, as compared to the AWGN case. In other words, to maintain the same average BER as that of an unfaded wireless link, the transmit power in a Rayleigh fading wireless link must increase by a factor of 50! Appropriate countermeasures should therefore be taken to mitigate the effect of multi-path fading.

1.2 Diversity Techniques

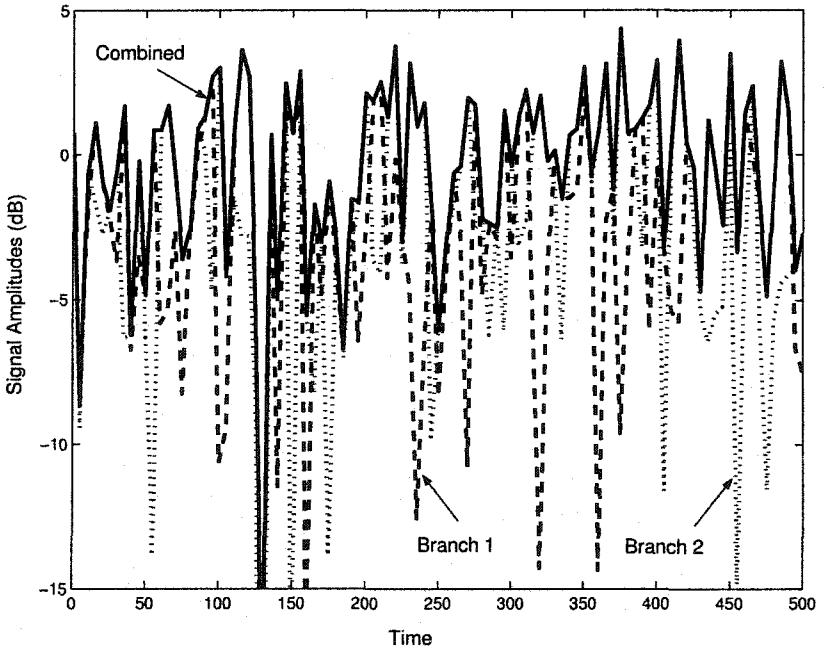

Figure 1.2: Diversity benefit.

Diversity is an effective means to reduce the effect of multi-path fading on the performance of wireless communication systems. The basic idea of diversity is simple. Multiple copies of the transmitted signal are collected using so-called diversity branches. Let $p \ll 1$ be the probability that the received signal at one diversity branch experiences severe fading.

For L identically and independently faded branches, the probability that all the received signals fade simultaneously is p^L, which is much smaller than p.

Fig. 1.2 shows the diversity benefit. Branch 1 and branch 2 are independently faded. Observe that the amplitudes of the received signals at each diversity branch fluctuate widely, which degrades the performance of wireless communication systems significantly (see Fig. 1.1). However, if we make use of both branches by selecting the better one as an output, the combined signal experiences less severe fading than either diversity branch. Hence, diversity techniques can be used to mitigate the effect of the deep fades experienced in wireless fading channels.

1.2.1 Types of Diversity

Diversity can be achieved by many methods. **Time diversity** is achieved by transmitting the same signal at different time slots. This, however, is rarely used in practice, because unacceptable delay can be introduced by delayed retransmission. **Frequency diversity** is obtained by transmitting the same signal at different carrier frequencies, which is undesirable when bandwidth is limited. Compared with the above two methods, **space diversity**, using multiple transmitter or receiver antennas, is preferred. No time delay or additional bandwidth is required in space diversity. **Multi-path diversity**, resolving the multi-path components at different delays, is also an attractive type of diversity in wide-band communications. A Rake receiver, which employs a single delay line through which the received signal is passed to collect the signal energy from the resolvable multi-paths, is often used to achieve multi-path diversity. Other types of diversity include angle diversity, polarization diversity and feedback diversity [15].

1.2.2 Diversity Combining Schemes

Consider a diversity combiner system with L branches which produce L replicas of the same transmitted signal using one of the above methods (see Fig. 1.3). Notice that the L diversity branches can be L receiver antennas in space diversity systems, L Rake fingers in multi-path diversity systems, L time slots in time diversity systems and so on. It is common to refer to L as the diversity order.

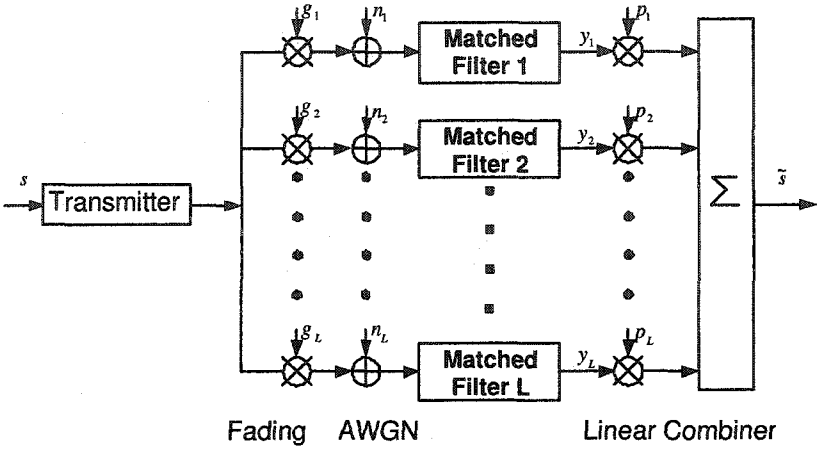

Figure 1.3: System Model.

The received signal after the matched filter at the k-th diversity branch can be written as

$$y_k = g_k s + n_k \tag{1.18}$$

where g_k is the random channel gain or fading gain associated with the k-th branch, s is the transmitted signal with energy E_s and n_k is AWGN at the k-th branch with identical power spectral density (PSD) $\frac{N_0}{2}$ per dimension. We assume that the noise components at different diversity branches are independent of the fading components, i.e., $E(n_j g_k^*) = 0$ for any j and k, where x^* is the complex conjugate of x, and uncorrelated with each other, i.e., $E(n_j n_k^*) = N_0 \delta_{jk}$ where δ_{jk} is the Kronecker delta function defined as

$$\delta_{jk} = \begin{cases} 1, & j = k, \\ 0, & j \neq k. \end{cases} \tag{1.19}$$

We consider only slow and flat fading channels, which means that the channel gains g_k's, where $k \in \{1, \ldots, L\}$, remain constant for the duration of the signaling interval and for all the frequencies of the transmitted signal (that is, g_k is not a function of time t or frequency f). Note that the channel gains g_k's have to be estimated in practice. In this context, g_k's are also known as channel state information (CSI). We assume that the diversity receiver has perfect CSI, i.e., it knows the values of g_k's exactly. This assumption is reasonable for slow fading communications. In Section 3.3.5, we briefly discuss the impact of imperfect CSI on the performance of diversity systems.

The instantaneous and the average SNRs at the k-th diversity branch are given by

$$\gamma_k = |g_k|^2 \frac{E_s}{N_0}, \tag{1.20}$$

$$\bar{\gamma}_k = E(\gamma_k) = E(|G_k|^2) \frac{E_s}{N_0}, \tag{1.21}$$

where $|x|$ is the absolute value of x and g_k denotes a realization of the RV G_k. Throughout this thesis, all RVs are denoted by capital letters and the corresponding realizations are denoted by small letters. The average branch SNRs in identically distributed fading channels are denoted by $\bar{\gamma}_k = \bar{\gamma}$ for $k \in \{1, \ldots, L\}$.

Once the L replicas of the same transmitted signal are obtained, the problem is how to make use of these signals. We use linear diversity combiner that linearly weights the L received signals by weighting factors $\{p_1, \ldots, p_L\}$ and then sums them up to form an output. The output signal of a linear combiner can be written as [18]

$$\tilde{s} = \sum_{k=1}^{L} p_k y_k = \left(\sum_{k=1}^{L} p_k g_k \right) s + \sum_{k=1}^{L} p_k n_k. \tag{1.22}$$

One can also develop non-linear diversity combiners, which will not be considered in this thesis as linear combiners are much more popular. Different weighting factors for the linear combiners have been proposed and studied in the literature [15, 17–19]. Several diversity combiners are briefly discussed next. The first three are well-known classical techniques and the rest are recent innovations.

Maximal Ratio Combining (MRC)

The optimal linear combiner in noise-limited channel is one in which the received signals are multiplied by the conjugates of the corresponding channel gains, i.e., $p_k = g_k^*$. The optimality can be readily proven using Cauchy-Schwarz inequality [19]. The instantaneous SNR of the linear combiner output (1.22) is given by

$$\gamma_{\text{out}} = \frac{\left(\sum_{k=1}^{L} p_k g_k \right)^2 E_s}{\left(\sum_{k=1}^{L} |p_k|^2 \right) N_0} \leq \frac{E_s}{N_0} \sum_{k=1}^{L} |g_k|^2 \tag{1.23}$$

with equality when $p_k = C g_k^*$ for any arbitrary constant C. MRC, employing the weighting factors $p_k = g_k^*$ for $k \in \{1, \ldots, L\}$, thus achieves the maximal output SNR, which is the

sum of all the L branch SNRs as

$$\gamma_{\text{mrc}} = \sum_{k=1}^{L} \gamma_k. \tag{1.24}$$

MRC is widely studied as a performance benchmark. Although MRC performs optimally, it is fairly complicated to implement in dense multi-path fading channels where the number of the diversity branches is very large. This has motivated the development of reduced-complexity suboptimal diversity combining schemes.

Equal Gain Combining (EGC)

EGC is simpler than MRC because it avoids measuring the amplitudes of the channel gains $|g_k|$. The received signals at different diversity branches are co-phased and equally weighted, i.e., $p_k = e^{-i\theta_k}$ where θ_k is the angle of the channel gain g_k, and then summed up to form an output as

$$\tilde{s}_{\text{egc}} = \sum_{k=1}^{L} |g_k| s + \sum_{k=1}^{L} e^{-i\theta} n_k. \tag{1.25}$$

EGC thus only compensates for the phase shift in the channels. The instantaneous output SNR of EGC is obtained as

$$\gamma_{\text{egc}} = \left(\sum_{k=1}^{L} |g_k| \right)^2 \frac{E_s}{LN_0}. \tag{1.26}$$

EGC offers performance close to the optimal MRC but with greater simplicity (see [20] for an extended discussion on the EGC and MRC performance difference). However, its complexity still increases as L increases.

Selection combining (SC)

In SC, the branch with the highest SNR is selected as an output whose SNR is given by

$$\gamma_{\text{sc}} = \max(\gamma_1, \gamma_2, \cdots, \gamma_L). \tag{1.27}$$

SC is a simple combining scheme as it picks the best among L branches. Since it discards many branches with SNRs perhaps close to the largest, it has the worst performance compared with other diversity combiners.

Switched Combining (SWC)

SC system has to monitor all the L diversity branches simultaneously, which requires L detectors. Switched combining scans the L branches until finding one with the SNR exceeding a preset threshold and uses it until its SNR drops below the threshold. An advantage of switched combining is that only one detector is needed. However, the performance of switched combining is even worse than that of SC, because the unused branches may have SNRs larger than the branch in use. We will not consider SWC in this thesis.

Generalized Selection Combining (GSC(M, L))

An L-branch MRC performs the best with the highest complexity and SC, on the other hand, performs the worst comparatively with the least complexity. This motivates the development of other diversity schemes whose complexity and performance lie between these two extreme cases. Therefore, several suboptimum hybrid diversity combining schemes that achieve a tradeoff between performance and implementation complexity have recently been proposed and studied in the literature. One such recent innovation is GSC(M, L), which is also known as hybrid SC/MRC. Here, M ($1 \leq M \leq L$) branches with the largest instantaneous SNRs out of L branches are coherently combined as in MRC, i.e., $p_k = g_k^*$ if $\gamma_k \geq \gamma_{(M)}$, where $\gamma_{(1)} \geq \gamma_{(2)} \cdots \geq \gamma_{(L)}$, and $p_k = 0$ otherwise. The instantaneous output SNR of GSC(M, L) can be written as

$$\gamma_{\text{gsc}} = \sum_{k=1}^{M} \gamma_{(k)}. \tag{1.28}$$

Note that GSC(M, L) reduces to the traditional MRC and SC by setting $M = L$ and $M = 1$, respectively.

Absolute Threshold GSC (AT-GSC) and Normalized Threshold GSC (NT-GSC)

Research efforts have also been made to improve GSC(M, L) by allowing the number of the combined branches M to vary dynamically with channel fading conditions. Two GSC schemes where M is a random variable, are proposed and analyzed in the literature [21–25]. AT-GSC [22, 23] combines all the branches with SNRs exceeding a fixed threshold γ_{th},

whose instantaneous output SNR is given by

$$\gamma_{\text{at}} = \begin{cases} 0, & \text{if all } \gamma_k < \gamma_{\text{th}}, \\ \sum_{\gamma_k \geq \gamma_{\text{th}}} \gamma_k, & \text{if any } \gamma_k \geq \gamma_{\text{th}}. \end{cases} \tag{1.29}$$

The error state of AT-GSC in which no branch contributes to the combiner output occurs when all the branch SNRs fall below the threshold γ_{th} simultaneously. When it is taken into consideration, the AT-GSC performance degrades monotonically with the increasing γ_{th}. In fact, AT-GSC performs even worse than SC when the threshold γ_{th} is high.

NT-GSC [21,22] combines the branches whose branch relative strength (the ratio of the each branch SNR to the maximum branch SNR) exceeds a fixed normalized threshold T ($0 < T \leq 1$), whose instantaneous output SNR is given by

$$\gamma_{\text{nt}} = \sum_{\frac{\gamma_k}{\gamma_{(1)}} \geq T} \gamma_k. \tag{1.30}$$

Since the number of the combined branches varies according to the channel fading conditions, AT-GSC and NT-GSC are more flexible than GSC(M, L) in fading channels.

Partial MRC (P-MRC(M, L))

More recently, P-MRC(M, L) [26], which coherently combines the first M ($0 < M \leq L$) branches out of the L available branches, i.e., $p_k = g_k^*$ for $k \in \{1, \ldots, M\}$ and $p_k = 0$ otherwise, has been proposed for the Rake receivers. P-MRC(M, L) is equivalent to the classical MRC with reduced diversity order M. The instantaneous output SNR of P-MRC(M, L) is given by

$$\gamma_{\text{pm}} = \sum_{k=1}^{M} \gamma_k. \tag{1.31}$$

1.2.3 Performance Measures and Analysis Techniques

To characterize the performance of diversity systems in slow and flat fading channels, performance measures, such as the average error rate, the outage probability and the moments of the combiner output SNR, are frequently used in the literature. Next, we briefly introduce some commonly used performance analysis techniques.

Average Error Rate

The average error rate is the most commonly used performance criteria, which evaluates the effectiveness of digital modulations in wireless fading channels. The average error rate is obtained by averaging the conditional error probability (CEP) over the statistics of the fading amplitudes. Many approaches have been proposed to evaluate the average error rates of various digital modulations with diversity combiners in different fading channels. The most popular one is the pdf-based approach, which averages the CEP over the pdf of the diversity combiner output SNR:

$$\bar{P}_e = \int_0^\infty P_e(\gamma) p_{\text{out}}(\gamma)\, d\gamma \tag{1.32}$$

where $P_e(\gamma)$ is the probability of error of a certain digital modulation in AWGN channel for a given SNR γ at the combiner output and $p_{\text{out}}(\gamma)$ is the pdf of the diversity combiner output SNR in a specified fading channel.

Recently, the mgf-based approach has been widely used to evaluate the error rate performance of various digital modulations with coherent diversity combiners. The basic idea of the mgf-based approach is to find an exponential-type representation for the CEPs so that the average error rates can be expressed strictly in terms of the mgf of the combiner output SNR. For example, Craig [27] shows that the symbol error rate (SER) of any two-dimensional linear coherent modulations can be expressed as

$$P_e(\gamma) = \frac{1}{2\pi} \sum_{k=1}^{S} W_k \int_0^{\eta_k} \exp\left[\frac{-\gamma a_k \sin^2(\varphi_k)}{\sin^2(\theta + \varphi_k)}\right] d\theta \tag{1.33}$$

where S is the total number of signal points or decision subregions, $W_k > 0$ is the a priori probability of the symbol to which subregion k corresponds, $a_k > 0$ is a normalization factor, η_k and φ_k are parameters relating to decision subregion k and they are independent of the instantaneous SNR γ. Various common digital modulations can be described by choosing these parameters appropriately: for special cases of (1.33), see Section 2.4.1.

Thus, using the mgf-based approach with (1.33) yields the average SER as

$$\bar{P}_s = \frac{1}{2\pi} \sum_{k=1}^{S} W_k \int_0^{\eta_k} M_{\text{out}}\left(\frac{a_k \sin^2(\varphi_k)}{\sin^2(\theta + \varphi_k)}\right) d\theta \tag{1.34}$$

where $M_{\text{out}}(s)$ is the mgf of the diversity combiner output SNR.

However, the mgf-based approach fails to work in the analysis of coherent EGC receivers. The chf-based approach is proposed to unify the average error rate analysis of different digital modulations with various diversity combiners, including coherent EGC, within a single common framework [28]. The key idea of this approach is to express the CEPs in terms of the combiner output envelop $X = \sqrt{\gamma}$ and transform (1.32) into frequency domain using Parseval's theorem. The chf-based approach enables the average error rates analysis for coherent EGC systems [1,29] (see Section 4.4.2).

Outage Probability

Another commonly used performance measure is the outage probability, which is defined as the probability that the instantaneous output SNR γ falls below a certain given threshold γ_T. Outage probability is a useful statistical measure of the radio link performance of cellular systems in the presence of interference. The outage threshold γ_T is determined by many factors, such as the receiver structure and the propagation environment [15]. For example, if an equalizer is used, the receiver will be more tolerant to the interference and the threshold γ_T can be reduced [15].

The outage probability of a diversity combiner relates to the cdf of the combiner output SNR as follows:

$$P_{\text{out}}(\gamma_T) = \Pr(0 \leq \gamma \leq \gamma_T) = F_{\text{out}}(\gamma_T) \tag{1.35}$$

where $F_{\text{out}}(x)$ is the cdf of the combiner output SNR.

Moments

As an alternative to average error rate analysis, we can use performance measures based on the moments of a combiner output SNR. For example, the average output SNR is sometimes used as a performance measure. However, a single moment, such as the average output SNR, alone does not reveal enough information and the higher order moments can furnish additional information for system design. For example, if the variance of the output is small, large fades from the average is not likely (which follows from the Chebyshev inequality).

The moments of the combiner output SNR can be obtained using the output pdf or the output mgf as

$$\begin{aligned} m_n = E(\gamma_{\text{out}}^n) &= \int_0^\infty \gamma^n p_{\text{out}}(\gamma)\, d\gamma \\ &= (-1)^n \left. \frac{dM_{\text{out}}(s)}{ds} \right|_{s=0}. \end{aligned} \tag{1.36}$$

Using the output moments, we can obtain other useful statistical measures. Skewness is a measure of the asymmetry of the combiner output SNR around the mean value m_1 [30]:

$$\nu = \frac{\mu_3}{\mu_2^{\frac{3}{2}}} \tag{1.37}$$

where μ_n is the central moments defined as

$$\mu_n = E[(\gamma_{\text{out}} - m_1)^n] = \sum_{k=0}^{n} \binom{n}{k} m_k (-m_1)^{k-i}. \tag{1.38}$$

For symmetric distributions, $\nu = 0$. If $\nu > 0$, the output SNRs are spread out more to the right. If $\nu < 0$, the output SNRs are spread out more to the left.

Kurtosis is a measure of the 'tail weight' of distribution, which is defined as [30]

$$\kappa = \frac{\mu_4}{\mu_2^2}. \tag{1.39}$$

For normal distribution, $\kappa = 3$. For a distribution, the greater the relative probability in one or both tails is, the larger κ will be.

Karl Pearson's coefficient of variation is defined as [30]

$$\text{cv} = \frac{\mu_2^{\frac{1}{2}}}{m_1}, \tag{1.40}$$

which is frequently used to describe the severity of the channel fading. For example, Win and Winters [31] used this output indicator to assess the effectiveness of GSC(M, L) scheme in Rayleigh fading channels. Charash [32] introduced the square value of the Karl Pearson's coefficient as a unified measure of the amount of fading (AF). More recently, Alouini and Simon [33] derived closed-form expressions for AFs of dual diversity combiners in correlated log-normal fading channels.

1.3 The Contribution of this Thesis

Traditional diversity combining techniques, such as MRC, EGC and SC, have long been employed to mitigate the effect of multi-path fading on wireless communication systems. Recent rapid growth in the use of wireless technology has revitalized this classic research area and two broad trends have emerged. First, research shows that the use of a large number of multiple antennas and ultra wide-band (UWB) systems can support high data rate communications, where diversity receivers have to process a large number of diversity branches. Second, the wireless receivers, for example, wireless handsets, are continually being miniaturized. This makes it difficult to provide complete independence among antenna elements. These two trends suggest that emphasis should be placed upon designing reduced-complexity suboptimal diversity algorithms and analyzing the impact of correlation among antenna elements. In contrast, in classical diversity theory, optimal algorithms and independent antennas are considered. Hence, in this thesis, we develop suboptimal diversity algorithms with reduced complexity and also develop analytic techniques for performance analysis of diversity systems in correlated fading.

With the former goal in mind, we propose two new diversity combining schemes, switching GSC (S-GSC) and adaptive MRC (A-MRC). S-GSC coherently combines all the branches whose SNRs exceed a preset threshold γ_{th}. If no branch SNR exceeds the threshold, S-GSC picks the best branch as the output. S-GSC outperforms the recently proposed AT-GSC with only slightly increased complexity. A-MRC adaptively combines the first N_c branches whose cumulative output SNR exceeds a preset threshold. A-MRC outperforms GSC(M, L) when the channel power decays rapidly. A-MRC does not require monitoring all the diversity branches and sorting them while GSC(M, L) does. Moreover, in both S-GSC and A-MRC, the number of the combined branches varies according to the channel fading conditions. These two schemes are more flexible than GSC(M, L) and P-MRC(M, L) in fading channels. We also provide a detailed theoretical analysis of the S-GSC and A-MRC performance in various fading channels. This allows for a comparative evaluation of our new schemes vis-a-vis other combining methods.

The maximum diversity gain occurs when the diversity branches experience identical

and independent fading. However, in some practical situations such as wireless communication handsets, fading is correlated because of the insufficient separation between the antennas. Correlated fading between diversity branches can significantly degrade the performance of diversity systems. A large number of experimental and theoretical studies have been devoted to evaluate the impact of correlation on the performance of diversity systems [34–38]. Thus, quantifying the resultant degradation of the performance of diversity systems is a long standing problem of importance [39–42].

Nevertheless, complete analytical results for all the diversity combiners are not known, except for MRC. Performance analysis of some diversity combiners requires distributional results for order statistics of correlated RVs, which are not available. This thesis, however, makes two specific contributions to the state-of-art. First, we develop a novel approach for analyzing the performance of multi-branch diversity combining systems in equally correlated Rayleigh, Ricean and Nakagami-*m* fading channels. The novel insight of our approach is that a set of independent complex Gaussian RVs (CGRVs) can be linearly combined to form a set of equally correlated CGRVs. Using this insight, we translate the problem of performance in equally correlated fading to the problem of performance in a *conditionally independent* fading environment. This reformulation allows us to extend known results for independent fading to analyze the multi-branch SC and EGC performance in correlated fading. Using our new representations for the channel gains, we derive the output cdfs, the output moments, the outage probabilities and the average error rates of a wide class of digital modulations for multi-branch SC and EGC systems.

Unlike the other existing methods for the SC performance analysis [43, 44], our results can handle any number of diversity branches as a single-fold integral (for the outage probability) or 2-dimensional integral (for the average error rates and the output moments). The complexity of our approach does not increase with the number of diversity branches. To the best of our knowledge, theoretical results for the multi-branch EGC performance in correlated fading channels do not exist in the literature. We therefore partially resolve the long-standing open problem of the multi-branch EGC performance in correlated fading channels. We also show that diversity gain still exists in correlated fading channels. Additional diversity gain diminishes as the diversity order increases. As the fading correlation

increases, the performance of a diversity system degrades and the rate of degradation increases. Higher-order diversity systems are much more sensitive to the fading correlation. We also find that the performance of diversity systems in correlated Ricean fading channels can be worse than that in correlated Rayleigh fading channels, which has never been observed for the independent fading case. These observations help the design of diversity systems.

Second, the channel gain representations developed in Chapter 4 holds only for equally correlated fading channels. For arbitrarily correlated fading channels, simple analytical performance results for multi-branch SC and EGC do not exist in the literature, as the joint distribution is not known for three or more arbitrarily correlated Rayleigh RVs. We thus redress this gap by deriving new infinite series representations for the joint pdf and the joint cdf of three and four correlated Rayleigh RVs. Bounds on the error resulting from truncating the infinite series are derived. A classical approach due to Miller is used to derive our results. Unfortunately, Miller's approach cannot be extended to more than 4 variates and, in fact, the quadri-variate case considered in this thesis appears to be the most general result possible. For brevity, we treat only a limited number of applications in this thesis. The new pdf and cdf expressions are used to evaluate the 3-branch SC performance, the moments of the 3-branch EGC output SNR and the mgf of the GSC(2,3) output SNR in arbitrarily correlated Rayleigh fading. A novel application of Bonferroni's inequalities allows new bounds for the complementary cdf (ccdf) of the multi-branch SC output SNR in arbitrarily correlated Rayleigh channels.

This thesis is organized as follows. Chapter 2 proposes a new hybrid diversity combining scheme, S-GSC, and analyzes its performance in independent fading channels. Numerical results which compare the S-GSC performance with AT-GSC and SC are also provided. Chapter 3 proposes another reduced-complexity diversity combining scheme, A-MRC, and analyzes its performance in various independent fading channels. The performance of A-MRC is also compared with that of GSC(M, L) and P-MRC(M, L). Chapter 4 develops new representations for the equally correlated Rayleigh, Ricean and Nakagami-m channel gains and uses the new results to evaluate the performance of multi-branch SC and EGC in such channels. Numerical and semi-analytical simulation results are provided to inves-

tigate the performance of multi-branch diversity combiner in various equally correlated fading channels. Chapter 5 derives new infinite series representations for the joint cdf and the joint pdf of the tri-variate and a certain class of quadri-variate Rayleigh distributions. The new results are further applied to solve certain long-standing diversity problems, such as the performance of 3-branch SC, EGC and GSC(2,3) systems in arbitrarily correlated Rayleigh fading channels. Chapter 6 concludes this thesis and outlines future work in this area.

Chapter 2

A New Switching Hybrid Combining Scheme

This chapter proposes a new hybrid combining scheme, switching GSC (S-GSC). Section 2.1 introduces a short background on the problem. Section 2.2 analyzes the effect of the threshold on the AT-GSC performance. Section 2.3 develops the new diversity combining scheme, S-GSC, and derives the mgf, pdf and cdf of its output SNR in independent fading channels. In Section 2.4, the average error rates of various modulation schemes, the outage probability and the output moments of S-GSC are evaluated. Section 2.5 presents some numerical results to compare S-GSC with other combining techniques. Section 2.6 concludes this chapter.

2.1 Introduction

As proven in (1.23), MRC is the optimal linear combiner in a noise-limited channel. All the other linear combiners are suboptimal and their performance cannot be better than that of MRC. In (1.29), we briefly described AT-GSC and found an error state in AT-GSC, which results in poor BER performance. We are therefore motivated to find diversity algorithms better than AT-GSC.

This chapter thus develops a new diversity combining scheme, referred to as switching GSC (S-GSC). This scheme combines all branches whose SNRs exceed a preset threshold γ_{th} as in AT-GSC and if all the branch SNRs drop below the threshold, the output is the single branch with the maximum SNR as in SC. The main difference between our proposed

S-GSC and AT-GSC is that S-GSC eliminates the error state that presents in AT-GSC. We prove that both the average error rate performance and the processing complexity of S-GSC lie between those of MRC and SC. Importantly, the complexity of S-GSC is only slightly above that of AT-GSC. We derive the mgf of the S-GSC output SNR in independent fading channels. For independently and identically distributed (i.i.d.) Rayleigh fading channels, we derive the pdf and cdf of the S-GSC output SNR and analyze the average error rate and the outage probability performance of S-GSC. Moments of the S-GSC output SNR are also derived. These theoretical results are sufficient to completely characterize the performance of S-GSC and enable one to compare S-GSC with conventional diversity schemes.

2.2 AT-GSC Performance as a Function of Threshold

Before developing S-GSC, we highlight why AT-GSC does not perform acceptably. We expect that as the threshold γ_{th} increases, fewer branches will be combined in AT-GSC, which results in higher error rate. We prove this intuitive notion rigorously by using the mgf of the AT-GSC output SNR. For i.i.d. Rayleigh fading channels, the output mgf of AT-GSC is given by [23]

$$M_{\text{at}}(s) = \left[1 - e^{-\frac{\gamma_{\text{th}}}{\bar{\gamma}}} + \frac{e^{-\frac{\gamma_{\text{th}}}{\bar{\gamma}}(1+s\bar{\gamma})}}{1+s\bar{\gamma}}\right]^L. \tag{2.1}$$

For any real value $s > 0$ and $\gamma_{\text{th}} > 0$, we have $M_{\text{at}}(s) > 0$ and

$$\frac{\partial M_{\text{at}}(s)}{\partial \gamma_{\text{th}}} = \frac{L}{\bar{\gamma}} e^{-\frac{\gamma_{\text{th}}}{\bar{\gamma}}} \left(1 - e^{-s\gamma_{\text{th}}}\right) \left[1 - e^{-\frac{\gamma_{\text{th}}}{\bar{\gamma}}} + \frac{e^{-\frac{\gamma_{\text{th}}}{\bar{\gamma}}(1+s\bar{\gamma})}}{1+s\bar{\gamma}}\right]^{L-1} > 0. \tag{2.2}$$

Hence the output mgf $M_{\text{at}}(s)$ monotonically increases with γ_{th}. Combining (2.2) and (1.34), we find that the average error rate of any two-dimensional coherent modulations with AT-GSC monotonically increases with γ_{th}, which means that the AT-GSC performance degrades monotonically as γ_{th} increases.

Fig. 2.1 shows that for a fixed average branch SNR $\bar{\gamma}$ and the diversity order L, the average BER $\bar{P}_e$ of BPSK with AT-GSC increases dramatically as the preset threshold γ_{th} increases. It approaches 1/2 in the worst case. This makes AT-GSC unsuitable for practical applications and motivates improvements for AT-GSC.

2.3 S-GSC

To mitigate the worsening system performance of AT-GSC as the threshold γ_{th} increases, we present S-GSC, in which all the branches with SNRs exceeding γ_{th} are combined as the output. If no branch SNR exceeds γ_{th}, the branch with the largest SNR is selected. S-GSC switches therefore between AT-GSC and SC depending on how many branch SNRs exceed γ_{th}. Consequently, the S-GSC output SNR can be written as

$$\gamma_{\text{sg}} = \begin{cases} \max(\gamma_l), & \text{if all } \gamma_l < \gamma_{\text{th}}, \\ \sum\limits_{\gamma_l \geq \gamma_{\text{th}}} \gamma_l, & \text{otherwise.} \end{cases} \tag{2.3}$$

The first case of (2.3) accounts for the event that all the branch SNRs drop below the threshold and S-GSC switches to SC (this eliminates the error state of AT-GSC). The second case corresponds to the event that some of the branch SNRs exceed the threshold and S-GSC combines them just like AT-GSC. Comparing the output SNR of S-GSC (2.3) with that of AT-GSC (1.29), we find that S-GSC eliminates the error state that presents in AT-GSC when all the branch SNRs drop below γ_{th} simultaneously.

To evaluate the performance of S-GSC, we derive the mgf of its output SNR. Using the previous analysis of SC [15] and AT-GSC [23], we derive a general expression for the mgf of the S-GSC output SNR in independent fading channels in terms of the cdfs $F_{\gamma_l}(x)$'s and the pdfs $p_{\gamma_l}(x)$'s of the branch SNRs as

$$\begin{aligned} M_{\text{sg}}(s) = & \sum_{l=1}^{L} \left[\int_0^{\gamma_{\text{th}}} \left(e^{-sx} p_{\gamma_l}(x) \prod_{j=1, j\neq l}^{L} F_{\gamma_j}(x) \right) dx \right] \\ & + \prod_{l=1}^{L} \left[F_{\gamma_l}(\gamma_{\text{th}}) + \int_{\gamma_{\text{th}}}^{\infty} p_{\gamma_l}(x) e^{-sx}\, dx \right] - \prod_{l=1}^{L} F_{\gamma_l}(\gamma_{\text{th}}). \end{aligned} \tag{2.4}$$

When $\gamma_{\text{th}} = 0$ and $\gamma_{\text{th}} = \infty$, S-GSC reduces to classical MRC and SC, respectively.

1. When $\gamma_{\text{th}} = 0$, all the branch SNRs exceed the threshold γ_{th}. S-GSC thus combines all the branches and its output mgf (2.4) simplifies to

$$M_{\text{sg}}(s) = \prod_{l=1}^{L} \left[\int_0^{\infty} p_{\gamma_l}(x) e^{-sx}\, dx \right], \tag{2.5}$$

which is equivalent to the case of MRC.

2. When $\gamma_{\text{th}} = \infty$, no branch SNR exceeds the threshold γ_{th}. S-GSC always selects the best branch and its output mgf (2.4) reduces to

$$M_{\text{sg}}(s) = \sum_{l=1}^{L} \left[\int_0^{\infty} \left(e^{-sx} p_{\gamma_l}(x) \prod_{j=1, j\neq l}^{L} F_{\gamma_j}(x) \right) dx \right], \tag{2.6}$$

which is equivalent to the case of SC.

Note that (2.4) is general enough to handle any independent fading channels. For independently and non-identically distributed (i.n.d.) and i.i.d. Rayleigh fading channels, (2.4) reduces to

$$\begin{aligned} M_{\text{sg}}(s) = & \sum_{\substack{b_j=0,1 \\ b_1+\cdots+b_L=1}}^{L} (-1)^{b_1+\cdots+b_L+1} \left(\sum_{l=1}^{L} \frac{b_l}{\bar{\gamma}_l} \right) \frac{1 - e^{-\left(s+\sum_{l=1}^{L} \frac{b_l}{\bar{\gamma}_l}\right)\gamma_{\text{th}}}}{s + \sum_{l=1}^{L} \frac{b_l}{\bar{\gamma}_l}} \\ & + \prod_{l=1}^{L} \left[1 - e^{-\frac{\gamma_{\text{th}}}{\bar{\gamma}_l}} + \frac{e^{-\left(s+\frac{1}{\bar{\gamma}_l}\right)\gamma_{\text{th}}}}{1 + s\bar{\gamma}_l} \right] - \prod_{l=1}^{L} \left[1 - e^{-\frac{\gamma_{\text{th}}}{\bar{\gamma}_l}} \right], \end{aligned} \tag{2.7}$$

and

$$\begin{aligned} M_{\text{sg}}(s) = & \sum_{n=1}^{L} \binom{L}{n} (-1)^{n+1} n \frac{1 - e^{-\frac{\gamma_{\text{th}}}{\bar{\gamma}}(n+\bar{\gamma}s)}}{n + \bar{\gamma}s} \\ & + \sum_{l=1}^{L} \binom{L}{l} [1 - e^{-\frac{\gamma_{\text{th}}}{\bar{\gamma}}}]^{L-l} \left[\frac{e^{-\frac{\gamma_{\text{th}}}{\bar{\gamma}}(1+\bar{\gamma}s)}}{1 + \bar{\gamma}s} \right]^{l}, \end{aligned} \tag{2.8}$$

respectively. Differentiating (2.8) with respect to γ_{th}, we can show that for a certain $\bar{\gamma}$ and real $s > 0$, $M_{\text{sg}}(s) > 0$ and $\frac{\partial M_{\text{sg}}}{\partial \gamma_{\text{th}}} > 0$. Hence, the output mgf increases monotonically with γ_{th}. Noticing that the average SER of any two-dimensional coherent modulations can be expressed in terms of the output mgf $M_{\text{sg}}(s)$ (1.34), we can prove that the error rate performance of S-GSC is upper bounded by MRC ($\gamma_{\text{th}} = 0$) and lower bounded by SC ($\gamma_{\text{th}} = \infty$).

The pdf of the S-GSC output SNR in i.i.d. Rayleigh fading channels can be derived using the properties of Laplace transform as,

$$\begin{aligned} p_{\text{sg}}(x) = & \frac{L}{\bar{\gamma}} (1 - e^{-\frac{x}{\bar{\gamma}}})^{L-1} e^{-\frac{x}{\bar{\gamma}}} [1 - u(x - \gamma_{\text{th}})] \\ & + \frac{1}{\bar{\gamma}} \sum_{l=1}^{L} \binom{L}{l} \frac{1}{(l-1)!} (1 - e^{-\frac{\gamma_{\text{th}}}{\bar{\gamma}}})^{L-l} e^{-\frac{x}{\bar{\gamma}}} \left(\frac{x - l\gamma_{\text{th}}}{\bar{\gamma}} \right)^{l-1} u(x - l\gamma_{\text{th}}) \end{aligned} \tag{2.9}$$

where $u(x)$ is the step function defined as

$$u(x) = \begin{cases} 0, & x < 0, \\ 1, & x \geq 0. \end{cases} \tag{2.10}$$

2.4 Performance Analysis

Using (2.8), we next derive the average error rates, the outage probability and several output quality measures of S-GSC in i.i.d. Rayleigh fading channels. For other independent fading channels, the S-GSC performance can be readily evaluated using (2.4). For brevity, we do not develop such results here.

2.4.1 Average Error Rate

The mgf-based approach [45, 46] can be readily applied with (2.8) to evaluate the average error rates of a multitude of digital modulations with S-GSC in i.i.d. Rayleigh fading channels. We show that the average error rates can be expressed as either a finite integral of the output mgf or the output mgf itself.

BPSK and Binary Frequency-Shift-Keying (BFSK)

BPSK has been adopted for reverse link in the CDMA2000 systems due to its high power efficiency.

The CEP for BPSK and BFSK in AWGN channel is in the form of Q-function [6], which can be expressed in a finite integral form as

$$P_e(\gamma) = Q\left(\sqrt{2\alpha\gamma}\right) = \frac{1}{\pi}\int_0^{\frac{\pi}{2}} \exp\left(-\frac{\alpha\gamma}{\sin^2\theta}\right) d\theta, \qquad \alpha = \begin{cases} 1, & \text{for BPSK,} \\ \frac{1}{2}, & \text{for BFSK.} \end{cases} \tag{2.11}$$

The advantage of the exponential representation for error rate analysis is that the final average error rates can be expressed strictly in terms of the mgf of the combiner output SNR. Using the definition of the mgf (1.3) and substituting (2.11) into (1.32), we obtain the average BER of BPSK and BFSK as a finite integral of the output mgf [47]

$$\bar{P}_e = \frac{1}{\pi}\int_0^{\frac{\pi}{2}} M_{\text{sg}}\left(\frac{\alpha}{\sin^2\theta}\right) d\theta. \tag{2.12}$$

For example, the average BER of BPSK with S-GSC is given by

$$\begin{aligned}\bar{P}_e = &\frac{1}{2} - Q\left(\sqrt{2\gamma_{\text{th}}}\right)[1-(1-e^{-\frac{\gamma_{\text{th}}}{\bar{\gamma}}})^L] \\ &+ \sum_{n=1}^{L}\binom{L}{n}(-1)^n\sqrt{\frac{\bar{\gamma}}{\bar{\gamma}+n}}\left[\frac{1}{2} - Q\left(\sqrt{\frac{2\gamma_{\text{th}}(n+\bar{\gamma})}{\bar{\gamma}}}\right)\right] \\ &+ \frac{1}{\pi}\sum_{l=1}^{L}\binom{L}{l}[1-e^{-\frac{\gamma_{\text{th}}}{\bar{\gamma}}}]^{L-l}\int_0^{\pi/2}\left\{\frac{e^{-\frac{\gamma_{\text{th}}}{\bar{\gamma}}\left(1+\frac{\bar{\gamma}}{\sin^2\theta}\right)}}{1+\frac{\bar{\gamma}}{\sin^2\theta}}\right\}^l d\theta\end{aligned} \tag{2.13}$$

Since (2.13) is a simple, finite range integral of exponential and trigonometric functions, it can easily be evaluated numerically using any common mathematical software such as Matlab and Maple. The same applies to all formulas derived for the average error rates in this section.

Non-Coherent BFSK and Binary Differential PSK (DPSK)

Since the coherent diversity combiners, such as MRC and GSC(M, L), require phase coherency, they are typically employed with coherent modulations. However the analysis of non-coherent and differentially coherent modulation schemes with coherent diversity combiners is also of interest because they provide a lower bound on the average error rates with non-coherent diversity combiners.

The CEP for non-coherent BFSK and binary DPSK is an exponential function [6]

$$P_e(\gamma) = \frac{1}{2}e^{-\alpha\gamma}, \qquad \alpha = \begin{cases}1, & \text{for binary DPSK,}\\ \frac{1}{2}, & \text{for non-coherent BFSK.}\end{cases} \tag{2.14}$$

The average BER of non-coherent BFSK and binary DPSK with coherent S-GSC can be directly obtained using the output mgf as,

$$\bar{P}_e = \frac{1}{2}M_{\text{sg}}(\alpha). \tag{2.15}$$

Using (2.8), we obtain closed-form expression for (2.15).

M-ary PSK and M-ary DPSK

Noise resistance and the ease of implementation have made M-ary PSK being adopted for various kinds of third generation (3G) standards. For example, 4PSK is used for the forward

link in ETSI/Europe (European Telecommunications Standards Institute) and ARIB/Japan (Association of Radio Industries and Business), and 8PSK is adopted in EDGE (Enhanced Data for Global Evolution).

Expressing the CEP of M-ary PSK as an exponential-type finite integral, we obtain the corresponding average SER as [47]

$$\bar{P}_e = \frac{1}{\pi}\int_0^{\pi-\frac{\pi}{M}} M_{\text{sg}}\left(\frac{\sin^2\left(\frac{\pi}{M}\right)}{\sin^2\theta}\right) d\theta. \tag{2.16}$$

Pawula [48] showed that the CEP of M-ary DPSK can also be written as a finite integral of an exponential function. Hence, the corresponding average SER is obtained as a finite integral of the output mgf as

$$\bar{P}_e = \frac{1}{\pi}\int_0^{\pi-\frac{\pi}{M}} M_{\text{sg}}\left(\frac{\sin^2\left(\frac{\pi}{M}\right)}{1+\cos\left(\frac{\pi}{M}\right)\theta}\right) d\theta. \tag{2.17}$$

M-ary quadrature amplitude modulation (QAM)

M-ary QAM, which applies amplitude modulation on quadrature carries, is another attractive modulation scheme due to its spectral efficiency. 16-QAM and 64-QAM are adopted in the IEEE 802.11a standard.

Utilizing the exponential integral representation for the Q-function, we obtain the average SER of M-ary QAM as [47]

$$\begin{aligned}\bar{P}_e = &\frac{4}{\pi}\left(1-\frac{1}{\sqrt{M}}\right)\int_0^{\frac{\pi}{2}} M_{\text{sg}}\left(\frac{\alpha}{\sin^2\theta}\right) d\theta \\ &-\frac{4}{\pi}\left(1-\frac{1}{\sqrt{M}}\right)^2\int_0^{\frac{\pi}{4}} M_{\text{sg}}\left(\frac{\alpha}{\sin^2\theta}\right) d\theta\end{aligned} \tag{2.18}$$

where $\alpha = \frac{3}{2(M-1)}$.

$\pi/4$-Quadrature DPSK ($\pi/4$-QDPSK)

The performance analysis of $\pi/4$-QDPSK has received considerable attention, owing to its adoption in the second generation of North American and Japanese digital cellular standards, such as the North American IS-54 and Japanese PDC (Personal Digital Cellular) (see [49–51] and their references).

Using the CEP expression for $\pi/4$-QDPSK with Gray coding [52], we obtain the corresponding average SER as

$$\bar{P}_e = \frac{1}{2\pi}\int_0^{\pi} M_{\text{sg}}\left(\frac{2}{2-\sqrt{2}\cos\theta}\right) d\theta. \tag{2.19}$$

2.4.2 Outage Probability

As discussed in Section 1.2.3, the outage probability is a common performance measure of digital communication systems. Since the outage probability is related to the output cdf as (1.35), the outage probability of S-GSC in i.i.d. Rayleigh fading channels can be obtained by integrating the output pdf of S-GSC (2.9) as

$$\begin{aligned} P_{\text{out}}(\gamma_T) &= (1-e^{-\frac{\gamma_T}{\bar{\gamma}}})^L[1-u(\gamma_T-\gamma_{\text{th}})] + (1-e^{-\frac{\gamma_{\text{th}}}{\bar{\gamma}}})^L \\ &\quad \times u(\gamma_T-\gamma_{\text{th}}) \sum_{m=1}^{\min\{L,\lfloor\gamma_T/\gamma_{\text{th}}\rfloor\}} \binom{L}{m}(1-e^{-\frac{\gamma_{\text{th}}}{\bar{\gamma}}})^{L-m} \\ &\quad \times \left[1-e^{-\frac{\gamma_T-m\gamma_{\text{th}}}{\bar{\gamma}}}\sum_{j=0}^{m-1}\frac{\left(\frac{\gamma_T-m\gamma_{\text{th}}}{\bar{\gamma}}\right)^{m-1-j}}{(m-1-j)!}\right] \end{aligned} \tag{2.20}$$

where $\lfloor x \rfloor$ denotes the largest integer which is smaller than x.

2.4.3 Moments of the Output SNR

The output moments of S-GSC in i.i.d. Rayleigh fading channels can be obtained using the output pdf (2.9) or the output mgf (2.8) with (1.36) (see Section 1.2.3 for details). For example, the average output SNR of S-GSC is obtained as

$$\begin{aligned} m_1 = \bar{\gamma}\sum_{n=1}^{L}\binom{L}{n}\Bigg\{&(-1)^{n-1}\left(\frac{1}{n}\right) + e^{-\frac{n\gamma_{\text{th}}}{\bar{\gamma}}} \\ &\times\left[(-1)^n\left(\frac{1}{n}+\frac{\gamma_{\text{th}}}{\bar{\gamma}}\right) + n(1-e^{-\frac{\gamma_{\text{th}}}{\bar{\gamma}}})^{L-l}\left(1+\frac{\gamma_{\text{th}}}{\bar{\gamma}}\right)\right]\Bigg\}. \end{aligned} \tag{2.21}$$

We also obtain the second order moment of the output SNR as

$$\begin{aligned} m_2 = \bar{\gamma}^2\sum_{n=1}^{L}\binom{L}{n}\Bigg\{&(-1)^{n-1}\frac{2}{n^2} + e^{-\frac{n\gamma_{\text{th}}}{\bar{\gamma}}}\left[(-1)^n\left(\frac{2}{n^2}+\frac{2\gamma_{\text{th}}}{n\bar{\gamma}}+\left(\frac{\gamma_{\text{th}}}{\bar{\gamma}}\right)^2\right)\right. \\ &\left.+n(1-e^{-\frac{\gamma_{\text{th}}}{\bar{\gamma}}})^{L-l}\left(1+l\left(1+\frac{\gamma_{\text{th}}}{\bar{\gamma}}\right)^2\right)\right]\Bigg\}. \end{aligned} \tag{2.22}$$

2.4.4 Number of the Combined Branches

The average number of the combined branches $\bar{N}_c$, which indicates how often channel estimation is required, may be considered as a measure of the processing complexity of a diversity combiner.

In S-GSC, the probability that $N_c = l$ out of L branches are combined as the output is given by

$$\Pr\{N_c = l\} = \begin{cases} [F_{\text{sg}}(\gamma_{\text{th}})]^L + L[1 - F_{\text{sg}}(\gamma_{\text{th}})][F_{\text{sg}}(\gamma_{\text{th}})]^{L-1}, & \text{for } l = 1, \\ \binom{L}{l}[F_{\text{sg}}(\gamma_{\text{th}})]^{L-l}[1 - F_{\text{sg}}(\gamma_{\text{th}})]^l, & \text{for } 2 \le l \le L. \end{cases} \tag{2.23}$$

Thus, the average number of the combined branches of S-GSC in i.i.d. Rayleigh fading channels is derived as

$$\bar{N}_c = \sum_{l=1}^{L} l \Pr\{N_c = l\} = (1 - e^{-\frac{\gamma_{\text{th}}}{\bar{\gamma}}})^L + Le^{-\frac{\gamma_{\text{th}}}{\bar{\gamma}}}. \tag{2.24}$$

We compare the processing complexity of different diversity combiners by listing the average number of the combined branches for each:

$$\bar{N}_c = \begin{cases} L, & \text{MRC}, \\ 1, & \text{SC}, \\ Le^{-\frac{\gamma_{\text{th}}}{\bar{\gamma}}} + (1 - e^{-\frac{\gamma_{\text{th}}}{\bar{\gamma}}})^L, & \text{S-GSC}, \\ Le^{-\frac{\gamma_{\text{th}}}{\bar{\gamma}}}, & \text{AT-GSC}. \end{cases} \tag{2.25}$$

Eq. (2.25) shows that MRC is the most complicated scheme, while SC is the simplest one provided $\gamma_{\text{th}} < \bar{\gamma} \ln L$. As the threshold γ_{th} increases, the average number of the combined branches $\bar{N}_c$ of S-GSC approaches 1 and S-GSC reduces to SC. As γ_{th} decreases, $\bar{N}_c$ of S-GSC approaches L and S-GSC approaches MRC. The complexity of S-GSC lies between that of SC and MRC. S-GSC combines only $(1 - e^{-\frac{\gamma_{\text{th}}}{\bar{\gamma}}})^L < 1$ more branches than AT-GSC on average. When the diversity order L is large, the complexity of S-GSC is comparable to that of AT-GSC.

2.5 Numerical Results

Numerical results are presented to illustrate the performance of S-GSC in i.i.d. Rayleigh fading channels. In all the figures, the normalized threshold is defined as the threshold

normalized by the average branch SNR $\hat{\gamma}_{\text{th}} = \gamma_{\text{th}}/\bar{\gamma}$.

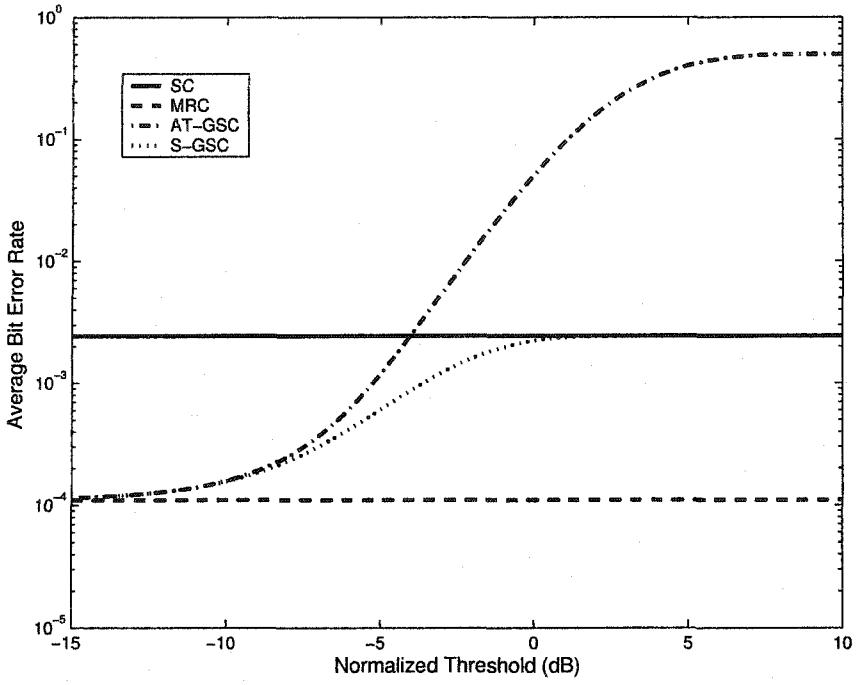

Figure 2.1: The average BER of BPSK with S-GSC, AT-GSC, MRC and SC as a function of the normalized threshold. $\bar{\gamma} = 5\text{dB}$, $L = 5$.

Fig. 2.1 shows the average BER of BPSK with several diversity schemes as a function of the normalized threshold $\hat{\gamma}_{\text{th}}$. Clearly, the MRC and SC performance does not change with the threshold. However, the AT-GSC and S-GSC performance is highly dependent on $\hat{\gamma}_{\text{th}}$. As $\hat{\gamma}_{\text{th}}$ increases, AT-GSC performs very poorly. When $\hat{\gamma}_{\text{th}} \gg 1$ (the threshold γ_{th} is much higher than the average SNR $\bar{\gamma}$), the average BER of AT-GSC approaches 1/2. Clearly, as the threshold increases, the probability that no branch is selected increases. However, the performance of our proposed S-GSC is less sensitive to the threshold compared to that of AT-GSC. When the threshold is low, S-GSC performs as well as AT-GSC. However, for high threshold values, the BER of S-GSC approaches that of SC, which is much lower than that of AT-GSC.

Fig. 2.2 compares the normalized average output SNR $\hat{\gamma}_{\text{out}} = \gamma_{\text{out}}/\bar{\gamma}$ achieved by different diversity schemes. As expected, the average output SNR of MRC increases linearly with the increasing diversity order L while for SC, it increases much more slowly. This

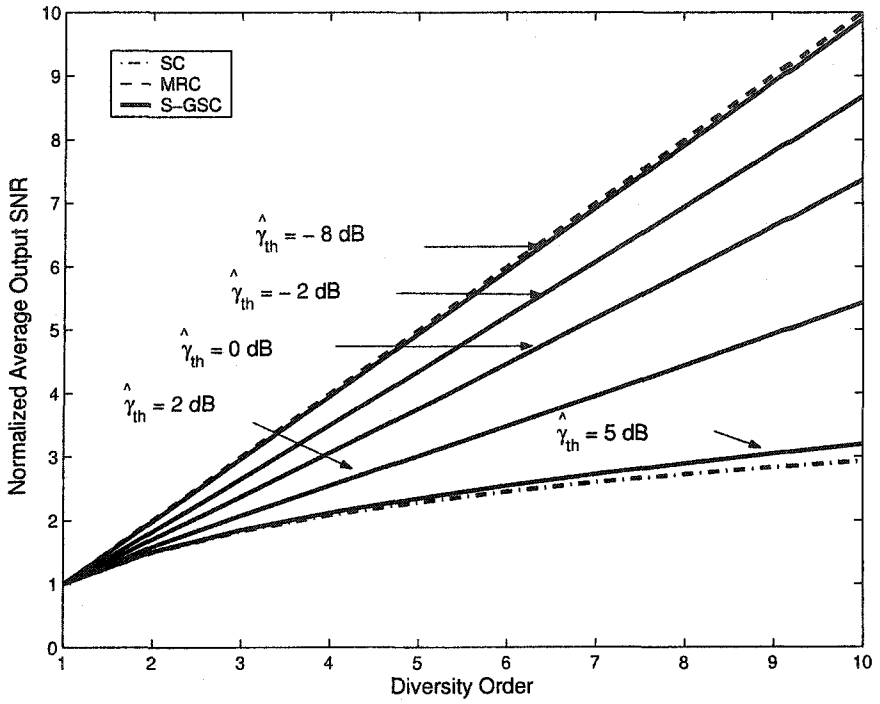

Figure 2.2: The normalized average output SNR $\hat{\gamma}_{\text{out}} = \gamma_{\text{out}}/\bar{\gamma}$ of S-GSC, MRC and SC.

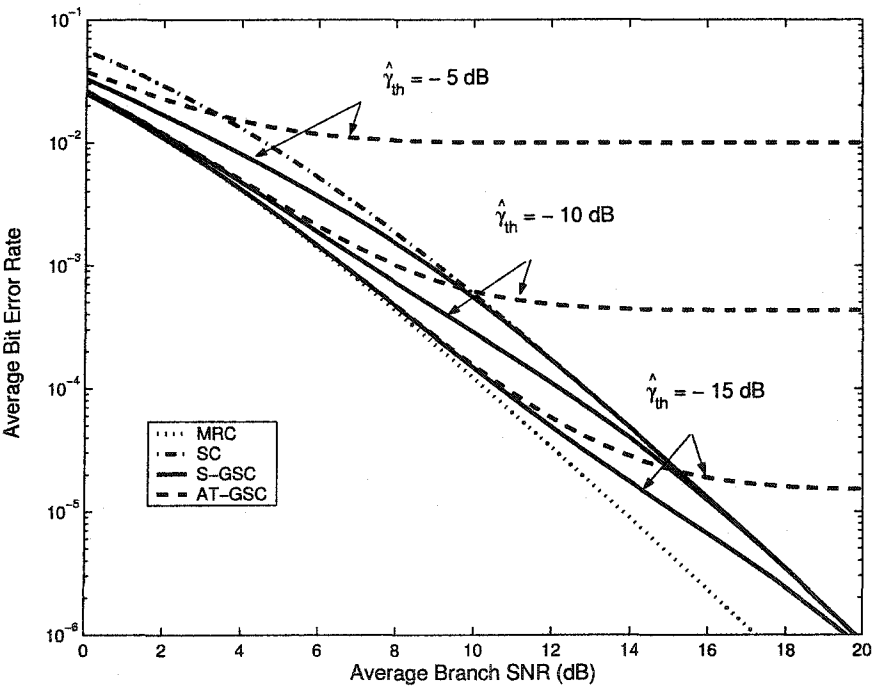

Figure 2.3: The average BER of binary DPSK with S-GSC, AT-GSC, MRC and SC. $L = 3$.

observation agrees with the result in [13]. The average output SNR of S-GSC is upper and lower bounded by that of MRC and SC, respectively. As the threshold $\hat{\gamma}_{\text{th}}$ decreases (S-GSC behaves more like MRC), the average output SNR of S-GSC increases. The average output SNR of S-GSC increases much faster when the normalized threshold $\hat{\gamma}_{\text{th}}$ is low. Therefore, lowering the threshold improves the average output SNR, especially for a higher diversity order.

The average BER of binary DPSK with different diversity combiners is shown in Fig. 2.3. As expected, MRC performs the best and AT-GSC performs even worse than SC when the normalized threshold $\hat{\gamma}_{\text{th}}$ is large. This is because high threshold sends AT-GSC to the error state (the event that all the branch SNRs drop below the threshold), which results in significantly high error rate. However, our proposed S-GSC outperforms both SC and AT-GSC.

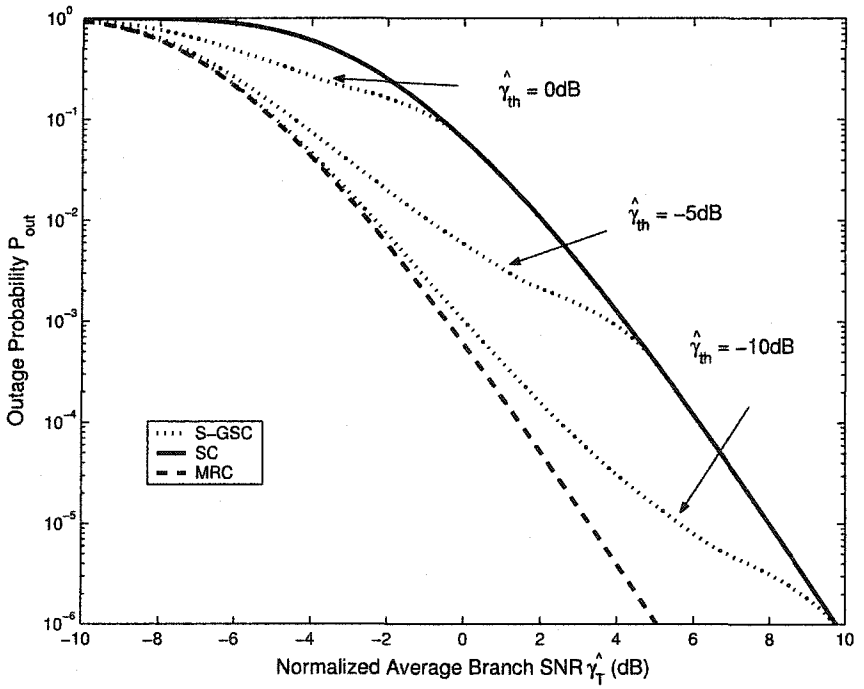

Figure 2.4: The outage probability of S-GSC, SC and MRC. $\hat{\gamma}_T = \bar{\gamma}/\gamma_T$, $L = 6$.

Fig. 2.4 compares the outage probability of S-GSC with those of SC and MRC. The outage probability of S-GSC approaches that of MRC when the normalized threshold $\hat{\gamma}_{\text{th}}$ is low. As $\hat{\gamma}_{\text{th}}$ increases, S-GSC performs close to SC.

2.6 Conclusion

This chapter has shown that AT-GSC performs poorly as the preset threshold γ_{th} increases. To improve system performance, we developed a new combining scheme, called S-GSC, which is a hybrid of SC and AT-GSC. We also developed theoretical performance results for S-GSC, which are general enough to handle any independent fading model. Results show that S-GSC outperforms both SC and AT-GSC. As the threshold decreases, the S-GSC performance improves but its processing complexity increases. We showed that both the performance and the complexity of S-GSC lie between those of MRC and SC. The number of the branches contributing to the output of S-GSC is not fixed, but varies corresponding to the channel fading conditions. Depending on the requirements of an application, S-GSC can be made to operate with different levels of complexity and performance.

Chapter 3

An Adaptive MRC Scheme

This chapter develops another suboptimal, reduced-complexity scheme called adaptive MRC (A-MRC). Section 3.1 compares the processing complexity of several coherent linear combining schemes. Section 3.2 introduces our A-MRC scheme and derives the mgf of its output SNR in independent Rayleigh and Nakagami-m fading channels. Section 3.3 analyzes the performance of a wide class of digital modulations with A-MRC in independent Rayleigh fading channels and also derives the mgf of the A-MRC output SNR with imperfect CSI in i.i.d. Rayleigh fading channels. Section 3.4 shows some numerical results that compare the performance of A-MRC with that of other combiners in different fading channels. Section 3.5 concludes this chapter.

3.1 Introduction

For emerging high data-rate wireless communication in dense multi-path channels, the number of the resolvable multi-path components (or diversity branches) can be very large. Rake receivers with a large number of fingers and MRC are optimal in this case. However, power consumption limits and implementation cost render MRC impractical in dense multi-path fading channels. For example, in UWB systems, the number of the resolvable multi-path components L can be up to several hundred paths [53]. To employ ideal MRC in this case requires channel estimation for all the L branches, clearly an extremely complicated task. GSC(M, L) has thus received much attention for Rake receiver design [47, 54–57]. However, in order to select the best M branches, GSC(M, L) measures the instantaneous SNRs of all the L branches and ranks them. This is just as complicated as MRC when L

Table 3.1: Processing Complexity of Diversity Combining Techniques

Diversity scheme	Measuring all the L paths	Ranking	Complexity
MRC	Yes	No	Fixed
GSC(M, L)	Yes	Yes	Fixed
P-MRC(M, L)	No	No	Fixed
AT-GSC	Yes	No	Variable
NT-GSC	Yes	Yes	Variable
S-GSC	Yes	Yes	Variable
A-MRC	No	No	Variable

is large. Therefore, P-MRC(M, L) [26] is proposed for Rake receptions. This approach reduces the number of branches which are needed to be measured and avoids the sorting operation as well. However, in time-varying channels, choosing an appropriate M for GSC(M, L) and P-MRC(M, L) may be difficult [22].

GSC may be improved by allowing the number of the combined branches M to vary dynamically with channel fading conditions. In AT-GSC, NT-GSC and our new proposed S-GSC, the number of the combined branches M is a random variable. These GSC derivatives are more flexible than GSC(M, L) in fading channels. However, they also require monitoring the instantaneous SNRs of all the L available branches.

This chapter proposes an adaptive MRC (A-MRC) scheme which coherently combines the first N_c ($0 < N_c \leq L$) branches whose cumulative output SNR is above a preset threshold γ_{th}. That is, A-MRC continues adding branches until the total output SNR exceeds γ_{th}. A-MRC only requires to monitor the first N_c branches where N_c varies depending on channel fading conditions. This is a desirable feature for a Rake receiver. When MRC or GSC(M, L) is used in Rake receiver, its output can only be formed after the combiner receives all the L multi-path components. This is both time and power consuming. A Rake receiver with A-MRC does not need to wait for the arrival of the last multi-path component. Once the cumulative sum of the branch SNRs exceeds the threshold, A-MRC will discard all the remaining branches and form an output immediately. Moreover, no sorting operation is needed in A-MRC, which reduces the computational complexity. Table 3.1 compares the processing complexity of several combining schemes.

We provide a detailed theoretical analysis of the A-MRC performance. This allows for a comparative evaluation of A-MRC vis-a-vis other GSC methods. We derive the mgf of the A-MRC output SNR in standard fading channels, such as Rayleigh and Nakagami-m fading. Asymptotic analysis of A-MRC in independent Rayleigh fading channels shows that the effective diversity order of A-MRC varies depending on the preset threshold γ_{th}. When γ_{th} is large, A-MRC has the same diversity order as MRC. Numerical results show that, A-MRC outperforms GSC(M, L) when the channel power decays rapidly. Note that our main analytical results are predicated on the availability of perfect CSI. However, the analysis can be made more realistic if channel estimation errors are taken into consideration. We thus develop theoretical performance results for A-MRC with Gaussian channel estimation errors in i.i.d. Rayleigh fading channels. These analytical results are sufficient to completely characterize the performance of A-MRC and enable one to compare A-MRC with other diversity schemes.

3.2 A-MRC

A-MRC coherently combines the first N_c ($0 < N_c \leq L$) branches whose cumulative output SNR is above a preset threshold γ_{th}. It behaves like MRC while the number of the combined branches N_c varies dynamically with the fading condition. The instantaneous output SNR of A-MRC is given by

$$\gamma_{\text{am}} = \sum_{k=1}^{N_c} \gamma_k. \tag{3.1}$$

Note that the number of the combined branches N_c is highly dependent on the preset threshold γ_{th} and the channel gains. Alternatively, the output SNR of A-MRC can be written as

$$\gamma_{\text{am}} = \begin{cases} \gamma_1, & \text{if } \gamma_1 \geq \gamma_{\text{th}}, \\ \displaystyle\sum_{k=1}^{N_c} \gamma_k, & \text{if } \displaystyle\sum_{k=1}^{N_c} \gamma_k \geq \gamma_{\text{th}} \text{ and } \sum_{k=1}^{N_c-1} \gamma_k < \gamma_{\text{th}}, \\ \displaystyle\sum_{k=1}^{L} \gamma_k, & \text{if } \displaystyle\sum_{k=1}^{L-1} \gamma_k < \gamma_{\text{th}}. \end{cases} \tag{3.2}$$

The first case in (3.2) accounts for the optimistic event that the first branch SNR exceeds the threshold, i.e., $\gamma_1 \geq \gamma_{\text{th}}$. Only the first branch is then applied to the A-MRC output

and all the remaining branches are not processed. The second case accounts for the event that N_c, $N_c \in \{2, \ldots, L-1\}$, branches are required to be coherently combined to form an output whose SNR exceeds the threshold γ_{th}. The third case corresponds to the worst case where the cumulative sum of the first $L-1$ branch SNRs does not exceed γ_{th} and all the L branches have to be combined as the output, just like MRC.

The following procedure describes the operation of A-MRC:

1. Initialize the number of the combined branches $N_c = 1$ and the cumulative sum of the branch SNRs $V = 0$. Select the threshold γ_{th} according to the system performance requirement.

2. Estimate the channel gain g_{N_c} and the instantaneous SNR γ_{N_c} at the N_c-th branch. Update $V = V + \gamma_{N_c}$.

3. Compare V with the preset threshold γ_{th}. If $V \geq \gamma_{\text{th}}$, discard the remaining branches and output the weighted sum of the first N_c branches; otherwise, let $N_c = N_c + 1$. If $N_c \geq L$, all the branches are combined to form the output and A-MRC is equivalent to MRC; otherwise, repeat step 2.

That is, A-MRC continues to add diversity branches until the cumulative sum of the branch SNRs exceeds the preset threshold. This method avoids the sorting operation required in GSC(M, L) and allows the number of the combined branches N_c to vary according to the channel fading conditions. Compared with MRC and GSC schemes, our proposed A-MRC only measures the first N_c branches instead of all the L branches.

3.2.1 General Independent Fading

Next we derive the mgf of the A-MRC output SNR in various fading channels:

$$M_{\text{am}}(s) = \int_{\gamma_{\text{th}}}^{\infty} p_{\gamma_1}(x) e^{-sx}\, dx + \sum_{j=2}^{L-1} \int_0^{\gamma_{\text{th}}} \int_{\gamma_{\text{th}}-v}^{\infty} p_{V_{j-1},\gamma_j}(v, x) e^{-s(v+x)}\, dx dv$$
$$+ \int_0^{\gamma_{\text{th}}} \int_0^{\infty} p_{V_{L-1},\gamma_L}(v, x) e^{-s(v+x)}\, dx dv \tag{3.3}$$

where $V_j = \sum_{l=1}^{j} \gamma_l$ is the sum of the first j branch SNRs and $p_{V_{j-1},\gamma_j}(v, x)$ is the joint pdf of V_{j-1} and γ_j, for $j \in \{2, \ldots, L\}$.

An immediate question is if there is a value of the threshold γ_{th} which is optimal in the average BER minimizing sense. We can answer this question in a fairly general setting (i.e., without assuming a particular fading distribution). Differentiating the output mgf (3.3) over γ_{th}, we obtain that for any real value $s > 0$,

$$\begin{aligned}\frac{\partial M_{\text{am}}(s)}{\partial \gamma_{\text{th}}} &= -e^{-s\gamma_{\text{th}}}\left[p_{\gamma_1}(\gamma_{\text{th}}) + \sum_{j=2}^{L-1}\int_0^{\gamma_{\text{th}}} p_{V_{j-1},x_j}(v, \gamma_{\text{th}} - v)\, dv \right. \\ &\qquad \left. + \sum_{j=2}^{L}\int_0^{\infty} p_{V_{j-1},x_j}(\gamma_{\text{th}}, x) e^{-sx}\, dx \right] \\ &= -e^{-s\gamma_{\text{th}}} \sum_{j=1}^{L-1}\left[p_{V_j}(\gamma_{\text{th}}) - \int_0^{\infty} p_{V_j,x_{j+1}}(\gamma_{\text{th}}, x) e^{-sx}\, dx \right] \\ &< -e^{-s\gamma_{\text{th}}} \sum_{j=1}^{L-1}\left[p_{V_j}(\gamma_{\text{th}}) - \int_0^{\infty} p_{V_j,x_{j+1}}(\gamma_{\text{th}}, x)\, dx \right] < 0.\end{aligned} \tag{3.4}$$

Hence, the output mgf monotonically decreases with γ_{th}. Noting the relation between the average error rates and the output mgf (1.34), we find that the average error rates of A-MRC decreases with γ_{th}. That is, as γ_{th} increases, the performance of A-MRC improves. Next, we consider two extreme cases of (3.3).

1. No diversity $\gamma_{\text{th}} = 0$. When $\gamma_{\text{th}} = 0$, A-MRC selects the first branch as the output. This is equivalent to no diversity case. As expected, the output mgf (3.3) reduces to

$$M_{\text{am}}(s) = \int_0^{\infty} e^{-sx} p_{\gamma_1}(x)\, dx. \tag{3.5}$$

2. MRC $\gamma_{\text{th}} = \infty$. When the threshold approaches infinity, all the available branches have to be combined a$M_{\text{am}}(s) = \int_0^{\infty} p_{V_L}(v) e^{-sv}\, dv,$ to

$$M_{\text{am}}(s) = \int_0^{\infty} p_{V_L}(v) e^{-sv}\, dv, \tag{3.6}$$

which is equivalent to the output mgf of MRC.

Note that (3.3) holds for arbitrary independent fading channels. Using (3.3), the output mgf of A-MRC for any standard fading distribution can be obtained. For brevity, we next analyze Rayleigh and Nakagami-m fading channels only.

3.2.2 Independent Rayleigh Fading

For independent Rayleigh fading channels, closed-form expressions for the mgf of the A-MRC output SNR can be readily derived. Noticing that the instantaneous branch SNR γ_k is exponentially distributed, whose pdf is given by (1.6b)

$$p_{\gamma_j}(x) = \frac{1}{\bar{\gamma}_j} e^{-\frac{x}{\bar{\gamma}_j}}, \quad x \geq 0, \tag{3.7}$$

we simplify (3.3) as

$$\begin{aligned} M_{\text{am}}(s) = &\frac{e^{-\frac{\gamma_{\text{th}}}{\bar{\gamma}_1}(1+s\bar{\gamma}_1)}}{1+s\bar{\gamma}_1} + \sum_{j=2}^{L-1} \frac{e^{-\frac{\gamma_{\text{th}}}{\bar{\gamma}_j}(1+s\bar{\gamma}_j)}}{1+s\bar{\gamma}_j} \int_0^{\gamma_{\text{th}}} p_{V_{j-1}}(v) e^{\frac{v}{\bar{\gamma}_j}} dv \\ &+ \frac{1}{1+s\bar{\gamma}_L} \int_0^{\gamma_{\text{th}}} p_{V_{L-1}}(v) e^{-sv} dv. \end{aligned} \tag{3.8}$$

Clearly, we need to find the pdf of the sum of exponential RVs $p_{V_j}(v)$. Next, we derive closed-from expressions for the output mgf (3.8) for different cases of independent Rayleigh fading. Asymptotic analysis results are also provided.

I.i.d. Rayleigh fading

In i.i.d. Rayleigh fading channels, all the average branch SNRs are identical to each other, i.e., $\bar{\gamma}_1 = \bar{\gamma}_2 = \ldots = \bar{\gamma}_L = \bar{\gamma}$. The pdf of a sum of j identical exponential RVs is given by [6]

$$p_{V_j}(v) = \frac{v^{j-1} e^{-\frac{v}{\bar{\gamma}}}}{(j-1)! \bar{\gamma}^j}, \quad v \geq 0. \tag{3.9}$$

Substituting (3.9) into (3.8), we obtain the output mgf of A-MRC in i.i.d. Rayleigh fading channels in closed-form as

$$M_{\text{am}}(s) = \frac{1}{(1+s\bar{\gamma})^L} + \frac{e^{-\frac{\gamma_{\text{th}}}{\bar{\gamma}}(1+s\bar{\gamma})}}{1+s\bar{\gamma}} \sum_{j=0}^{L-2} \frac{1}{j!} \left(\frac{\gamma_{\text{th}}}{\bar{\gamma}}\right)^j [1 - (1+s\bar{\gamma})^{j+1-L}]. \tag{3.10}$$

The corresponding output pdf can also be derived in closed-form as

$$\begin{aligned} p_{\text{am}}(x) = &\frac{x^{L-1} e^{-\frac{x}{\bar{\gamma}}}}{\bar{\gamma}^L (L-1)!} u(x) + \frac{e^{-\frac{x}{\bar{\gamma}}}}{\bar{\gamma}} \sum_{j=0}^{L-2} \frac{1}{j!} \left(\frac{\gamma_{\text{th}}}{\bar{\gamma}}\right)^j \\ &\times \left[1 - \frac{[(x-\gamma_{\text{th}})/\bar{\gamma}]^{L-j-1}}{(L-j-1)!}\right] u(x-\gamma_{\text{th}}) \end{aligned} \tag{3.11}$$

I.n.d. Rayleigh fading

We assume that the average SNRs at different branches are different from each other, i.e., $\bar{\gamma}_k \neq \bar{\gamma}_l$ for any $k \neq l$ and $k, l \in \{1, \ldots, L\}$. The pdf of the sum of the first j branch SNRs V_j can be obtained as [6]

$$p_{V_j}(v) = \sum_{k=1}^{j} \frac{\pi(k, j)}{\bar{\gamma}_k} e^{-\frac{v}{\bar{\gamma}_k}}, \quad v \geq 0, \tag{3.12}$$

where

$$\pi(k, j) = \prod_{\substack{l=1 \\ l \neq k}}^{j} \frac{\bar{\gamma}_k}{\bar{\gamma}_k - \bar{\gamma}_l}. \tag{3.13}$$

Substituting (3.12) into (3.8), we obtain the mgf of the A-MRC output SNR in i.n.d. Rayleigh fading channels as

$$\begin{aligned} M_{\text{am}}(s) =& \frac{e^{-\frac{\gamma_{\text{th}}}{\bar{\gamma}_1}(1+s\bar{\gamma}_1)}}{1+s\bar{\gamma}_1} + \sum_{j=1}^{L-2} \frac{e^{-\frac{\gamma_{\text{th}}}{\bar{\gamma}_{j+1}}(1+s\bar{\gamma}_{j+1})}}{1+s\bar{\gamma}_{j+1}} \sum_{k=1}^{j} \pi(k, j) \frac{1 - e^{-\frac{\gamma_{\text{th}}}{\bar{\gamma}_k}\left(1-\frac{\bar{\gamma}_k}{\bar{\gamma}_{j+1}}\right)}}{1 - \frac{\bar{\gamma}_k}{\bar{\gamma}_{j+1}}} \\ &+ \sum_{k=1}^{L-1} \pi(k, L-1) \frac{1 - e^{-\frac{\gamma_{\text{th}}}{\bar{\gamma}_k}(1+s\bar{\gamma}_k)}}{(1+s\bar{\gamma}_L)(1+s\bar{\gamma}_k)} \end{aligned} \tag{3.14}$$

where $\pi(k, j)$ is defined as (3.13).

General independent Rayleigh fading

More generally, we assume that the average SNRs of the first j branches $\{\bar{\gamma}_1, \ldots, \bar{\gamma}_j\}$ have $1 \leq n_j \leq j$ distinct values $\{\alpha_1, \ldots \alpha_{n_j}\}$. Without loss of generality, we assume that

$$\begin{aligned} \bar{\gamma}_1 = \ldots = \bar{\gamma}_{r_{j,1}} &= \alpha_1 \\ \bar{\gamma}_{r_{j,1}+1} = \ldots = \bar{\gamma}_{r_{j,1}+r_{j,2}} &= \alpha_2 \\ &\ldots \\ \bar{\gamma}_{r_{j,1}+\ldots+r_{j,n_j-1}+1} = \ldots = \bar{\gamma}_{r_{j,1}+\ldots+r_{j,n_j}} &= \alpha_{n_j} \end{aligned} \tag{3.15}$$

where $r_{j,k}$, $(k = 1, \ldots, n_j)$ is the number of the average branch SNRs which are equal to α_k among the first j branches. It is clearly that $r_{j,1} + \ldots + r_{j,n_j} = j$. Since the

channel is assumed to be independently faded, the mgf of the sum of the first j branch SNRs $V_j = \sum_{l=1}^{j} \gamma_l$ can be obtained as the product of the mgfs of the individual branch SNRs γ_l $(l = 1, \ldots, j)$:

$$M_{V_j}(s) = \prod_{l=1}^{j} \frac{1}{1 + s\bar{\gamma}_l} = \prod_{k=1}^{n_j} \left(\frac{1}{1 + s\alpha_k} \right)^{r_{j,k}}. \tag{3.16}$$

Using partial fraction-based techniques, we may derive a closed-form expression for the pdf of V_j, which is the inverse Laplace transform of (3.16) [58]

$$p_{V_j}(x) = A(j) \sum_{k=1}^{n_j} \sum_{l=1}^{r_{j,k}} \frac{\psi_{k,l}(j, \alpha_k)}{(l-1)!} \frac{x^{r_{j,k}-l} e^{-\frac{x}{\alpha_k}}}{(r_{j,k}-l)!} \tag{3.17}$$

where $A(j) = \prod_{l=1}^{n_j} \alpha_l^{1-r_{j,l}}$ and

$$\psi_{k,l}(j, t) = (-1)^{l-1}(l-1)! \sum_{\Omega} \prod_{\substack{q=1 \\ q \neq k}}^{n_j} \binom{s_q + r_{j,q} - 1}{s_q} \left(\frac{1}{\alpha_q} - \frac{1}{t} \right)^{-(r_{j,q}+s_q)} \tag{3.18}$$

where $\Omega : \sum_{q \neq k} s_j = l - 1$ and s_j is non-negative integer.

Substituting (3.17) into (3.8), we obtain the mgf of the A-MRC output SNR in general independent Rayleigh fading channels

$$\begin{aligned} M_{\text{am}}(s) = {} & \frac{e^{-\frac{\gamma_{\text{th}}}{\bar{\gamma}_1}(1+s\bar{\gamma}_1)}}{1 + s\bar{\gamma}_1} + \sum_{j=1}^{L-2} \frac{e^{-\frac{\gamma_{\text{th}}}{\bar{\gamma}_{j+1}}(1+s\bar{\gamma}_{j+1})}}{1 + s\bar{\gamma}_{j+1}} A(j) \sum_{k=1}^{n_j} \sum_{l=1}^{r_{j,k}} \frac{\psi_{k,l}(j, \alpha_k) g_{k,l}(j)}{(l-1)!(r_{j,k}-l)!} \\ & + A(L-1) \sum_{k=1}^{n_{L-1}} \sum_{l=1}^{r_{L-1,k}} \frac{\psi_{k,l}(L-1, \alpha_k) \gamma\left(r_{L-1,k} - l + 1, \frac{\gamma_{\text{th}}}{\alpha_k}(1 + s\alpha_k) \right)}{(r_{L-1,k}-l)!(l-1)!(1 + s\bar{\gamma}_L)(s + \frac{1}{\alpha_k})^{r_{L-1,k}-l+1}} \end{aligned} \tag{3.19}$$

where

$$g_{k,l}(j) = \begin{cases} \left(\frac{1}{\alpha_k} - \frac{1}{\bar{\gamma}_{j+1}} \right)^{-(r_{j,k}-l+1)} \gamma\left[r_{j,k} - l + 1, \frac{\gamma_{\text{th}}}{\alpha_k} \left(1 - \frac{\alpha_k}{\bar{\gamma}_{j+1}} \right) \right], & \alpha_k \neq \bar{\gamma}_{j+1}, \\ \frac{1}{r_{j,k} - l + 1} \gamma_{\text{th}}^{r_{j,k}-l+1}, & \text{otherwise,} \end{cases} \tag{3.20}$$

and $\gamma(n, x)$ is the incomplete gamma function which can be defined as a finite integral [3, Eq. (8.350.1)]

$$\gamma(n, x) = \int_0^x t^{n-1} e^{-t}\, dt, \quad n \geq 0. \tag{3.21}$$

When $n \geq 1$ is an integer, (3.21) can be expressed as a finite series:

$$\gamma(n, x) = (n-1)!\left(1 - e^{-x}\sum_{k=0}^{n-1}\frac{x^k}{k!}\right). \tag{3.22}$$

It can be shown that (3.10) and (3.14) are two special cases of (3.19).

Asymptotic Analysis

Asymptotic performance analysis provides an insight on the effective diversity order of a diversity system. Using (3.3) with the polynomial approximation for the pdf of the instantaneous branch SNR (3.7) in Rayleigh fading channels [59]

$$p_{\gamma_j}(x) \simeq \frac{1}{\bar{\gamma}_j}, \quad \text{for high average branch SNR } \bar{\gamma}_j, \tag{3.23}$$

we obtain the asymptotic mgf of the A-MRC output SNR as

$$M_{\text{am}}(s) \simeq \frac{1}{s^L \gamma_p} + e^{-s\gamma_{\text{th}}}\sum_{j=0}^{L-2}\frac{(s\gamma_{\text{th}})^j}{j!}\left[\frac{1}{s^{j+1}\prod_{l=1}^{j+1}\bar{\gamma}_l} - \frac{1}{s^L\gamma_p}\right] \tag{3.24}$$

where $\gamma_p = \prod_{l=1}^{L}\bar{\gamma}_l$ is the production of all the L average branch SNRs. Note that (3.24) holds for any kind of independent Rayleigh fading channels. For i.i.d. Rayleigh fading channels, (3.24) reduces to

$$M_{\text{am}}(s) \simeq \frac{1}{(s\bar{\gamma})^L} + e^{-s\gamma_{\text{th}}}\sum_{j=0}^{L-2}\frac{(s\gamma_{\text{th}})^j}{j!(s\bar{\gamma})^{j+1}}[1 - (s\bar{\gamma})^{j+1-L}]. \tag{3.25}$$

The diversity order L of A-MRC is highly dependent on the threshold γ_{th}. When γ_{th} approach infinity, $M_{\text{am}}(s) \simeq \frac{1}{(s\bar{\gamma})^L}$, i.e., A-MRC has the same diversity order L as that of MRC. However, when γ_{th} approach zero, $M_{\text{am}}(s) \simeq \frac{1}{s\bar{\gamma}}$, i.e., no diversity benefit can be achieved. As γ_{th} increases, the effective diversity order of A-MRC increases, which results in better performance.

3.2.3 Independent Nakagami-m Fading

In independent Nakagami-m fading channels, the instantaneous SNR of the j-th branch is gamma distributed whose pdf is given by (1.14b)

$$p_{\gamma_j}(x) = \frac{x^{m_j-1}e^{-\frac{x}{\eta_j}}}{\Gamma(m_j)\eta_j^{m_j}}, \quad x \geq 0, \tag{3.26}$$

where m_j is the fading severity parameters associated with the j-th branch and $\eta_j = \bar{\gamma}_j/m_j$.

Due to Moschopoulos [60], the pdf of the sum of the first j branch SNRs, i.e., the sum of independent gamma random variables, is given by

$$p_{V_j}(v) = \left[\prod_{n=1}^{j}\left(\frac{\eta_{1,j}}{\eta_n}\right)^{m_n}\right]\sum_{k=0}^{\infty}\frac{\epsilon_{j,k}v^{\beta_j+k-1}e^{-\frac{v}{\eta_{1,j}}}}{\eta_{1,j}^{\beta_j+k}\Gamma(\beta_j+k)}, \quad v \geq 0, \tag{3.27}$$

where $\beta_j = \sum_{n=1}^{j} m_n$, $\eta_{1,j} = \min\{\eta_1, \ldots, \eta_j\}$ and $\epsilon_{j,k}$ can be computed recursively as

$$\epsilon_{j,k} = \begin{cases} 1, & k = 0, \\ \frac{1}{k}\sum_{r=1}^{k}\epsilon_{j,k-r}\sum_{t=1}^{j}m_t\left(1-\frac{\eta_{1,j}}{\eta_t}\right)^r, & k = 1, 2, \ldots. \end{cases} \tag{3.28}$$

Using (3.26) and (3.27), we obtain the mgf of the A-MRC output SNR in independent Nakagami-m fading channels as

$$\begin{aligned} M_{\text{am}}(s) = {} & \frac{\Gamma\left[m_1, \left(s+\frac{1}{\eta_1}\right)\gamma_{\text{th}}\right]}{\Gamma(m_1)(1+s\eta_1)^{m_1}} + \sum_{j=2}^{L-1}\frac{1}{(1+s\eta_j)^{m_j}}\left[\prod_{n=1}^{j-1}\left(\frac{\eta_{1,j-1}}{\eta_n}\right)^{m_n}\right]\sum_{k=0}^{\infty}\frac{\epsilon_{j-1,k}}{\eta_{1,j-1}^{\beta_{j-1}+k}} \\ & \times \frac{1}{\Gamma(\beta_{j-1}+k)\Gamma(m_j)}\int_0^{\gamma_{\text{th}}}\Gamma\left[m_j, \left(s+\frac{1}{\eta_j}\right)(\gamma_{\text{th}}-y)\right]y^{\beta_{j-1}+k-1}e^{-\left(s+\frac{1}{\eta_{1,j-1}}\right)y}dy \\ & + \frac{1}{(1+s\eta_L)^{m_L}}\left[\prod_{n=1}^{L-1}\left(\frac{\eta_{1,L-1}}{\eta_n}\right)^{m_n}\right]\sum_{k=0}^{\infty}\frac{\epsilon_{L-1,k}\,\gamma\left[\beta_{L-1}+k, \left(s+\frac{1}{\eta_{1,L-1}}\right)\gamma_{\text{th}}\right]}{\Gamma(\beta_{L-1}+k)(1+s\eta_{1,L-1})^{\beta_{L-1}+k}}. \end{aligned} \tag{3.29}$$

Note that (3.29) is general enough to handle any kind of independent Nakagami-m fading channels, including the case where some of the fading severity parameters m_j's and/or some of the average branch SNRs $\bar{\gamma}_j$'s are identical and the others are different.

When all the fading severity parameters m_j's are integers, (3.29) can be simplified as

$$\begin{aligned} M_{\text{am}}(s) = {} & \frac{\Gamma\left[m_1, \left(s+\frac{1}{\eta_1}\right)\gamma_{\text{th}}\right]}{\Gamma(m_1)(1+s\eta_1)^{m_1}} + \sum_{j=2}^{L-1}\frac{1}{(1+s\eta_j)^{m_j}}\left[\prod_{n=1}^{j-1}\left(\frac{\eta_{1,j-1}}{\eta_n}\right)^{m_n}\right]\sum_{k=0}^{\infty}\frac{\epsilon_{j-1,k}}{\eta_{1,j-1}^{\beta_{j-1}+k}} \\ & \times \frac{e^{-\left(s+\frac{1}{\eta_j}\right)\gamma_{\text{th}}}}{(\beta_{j-1}+k-1)!}\sum_{t=0}^{m_j-1}\left(s+\frac{1}{\eta_j}\right)^t\sum_{r=0}^{t}(-1)^r\frac{1}{(t-r)!r!}\gamma_{\text{th}}^{t-r}f(\eta_{1,j-1}, \eta_j) \\ & + \frac{1}{(1+s\eta_L)^{m_L}}\left[\prod_{n=1}^{L-1}\left(\frac{\eta_{1,L-1}}{\eta_n}\right)^{m_n}\right]\sum_{k=0}^{\infty}\frac{\epsilon_{L-1,k}\gamma\left[\beta_{L-1}+k, \left(s+\frac{1}{\eta_{1,L-1}}\right)\gamma_{\text{th}}\right]}{(\beta_{L-1}+k-1)!(1+s\eta_{1,L-1})^{\beta_{L-1}+k}} \end{aligned} \tag{3.30}$$

where the incomplete gamma function $\gamma(n, x)$ can be evaluated using the finite series (3.22) and the complementary incomplete gamma function $\Gamma(n, x)$ is related to $\gamma(n, x)$ by

$$\Gamma(n, x) = \Gamma(n) - \gamma(n, x) = 1 - e^{-x} \sum_{k=0}^{n-1} \frac{x^k}{k!}, \quad \text{when } n \text{ is an integer,} \tag{3.31}$$

and

$$f(\eta_{1,j-1}, \eta_j) = \begin{cases} \dfrac{\gamma\left[\beta_{j-1} + k + r, \gamma_{\text{th}}\left(\frac{1}{\eta_{1,j-1}} - \frac{1}{\eta_j}\right)\right]}{\left(\frac{1}{\eta_{1,j-1}} - \frac{1}{\eta_j}\right)^{(\beta_{j-1}+k+r)}}, & \eta_{1,j-1} \neq \eta_j, \\ \dfrac{1}{\beta_{j-1} + k + r} \gamma_{\text{th}}^{\beta_{j-1}+k+r}, & \text{otherwise.} \end{cases} \tag{3.32}$$

3.3 Performance Analysis

We next use the output mgfs (3.10), (3.14) to evaluate the average error rates, the outage probability, the average output SNR and the average number of the combined branches of A-MRC in i.i.d. and i.n.d. Rayleigh fading channels. The same analysis can be performed for general independent Rayleigh fading and Nakagami-m fading with the aid of (3.19) and (3.29), respectively. For brevity, we do not develop such results here. We also derive the output mgf of A-MRC with imperfect CSI in i.i.d. Rayleigh fading channels.

3.3.1 Average Error Rate

As is shown in Chapter 2, the mgf-based technique [45, 46] can be readily applied with the output mgfs to evaluate the average error rates of a wide class of digital modulations with a certain diversity combiner. In the following, we provide just three examples of such analysis for brevity.

BPSK and Coherent BFSK

Replacing $M_{\text{sg}}(s)$ with $M_{\text{am}}(s)$ in (2.12), we obtain the average BER of BPSK and coherent BFSK with A-MRC as

$$\bar{P}_b = \frac{1}{\pi} \int_0^{\frac{\pi}{2}} M_{\text{am}}\left(\frac{g}{\sin^2\theta}\right) d\theta. \tag{3.33}$$

The infinite integral can be readily evaluated using simple numerical methods.

Alternatively, using the output pdf (3.11) and integrating by parts, we obtain the average BER of BPSK and coherent BFSK with A-MRC in i.i.d. Rayleigh fading channels as

$$\bar{P}_b = J(g) = \frac{1}{2} - \frac{1}{2}\sqrt{\frac{g\bar{\gamma}}{1+g\bar{\gamma}}}\left\{\sum_{k=0}^{L-1}\binom{2k}{k}\frac{1}{[4(1+g\bar{\gamma})]^k} + \sum_{j=0}^{L-2}\frac{1}{j!}\left(\frac{\gamma_{\text{th}}}{\bar{\gamma}}\right)^j \times \left[-2Q\left(\sqrt{2\omega}\right) + \frac{1}{\sqrt{\pi}}\sum_{l=0}^{L-j-1}\frac{1}{l!(1+g\bar{\gamma})^l}\sum_{t=0}^{l}\binom{l}{t}(-\omega)^t\Gamma\left(\frac{1}{2}+l-t,\omega\right)\right]\right\} \tag{3.34}$$

where $\omega = \frac{\gamma_{\text{th}}(1+g\bar{\gamma})}{\bar{\gamma}}$. We define $J(g)$ for subsequent use.

Binary DPSK and Non-Coherent BFSK

Similarly, replacing $M_{\text{sg}}(s)$ with $M_{\text{am}}(s)$ in (2.12) and using the output mgf (3.10), we obtain the closed-form expression for the average BER of binary DPSK and non-coherent BFSK in i.i.d. Rayleigh fading channels as

$$\bar{P}_b = \frac{1}{2(1+g\bar{\gamma})^L} + \frac{e^{-\frac{\gamma_{\text{th}}}{\bar{\gamma}}(1+g\bar{\gamma})}}{2(1+g\bar{\gamma})}\sum_{j=0}^{L-2}\frac{1}{j!}\left(\frac{\gamma_{\text{th}}}{\bar{\gamma}}\right)^j[1-(1+g\bar{\gamma})^{j+1-L}]. \tag{3.35}$$

16-QAM

16-QAM has a wide application in satellite and mobile communications. The BER of square 16-QAM is given by [61]

$$P_b(\gamma) = \frac{3}{2}Q\left(\sqrt{\frac{2\gamma}{5}}\right) + Q\left(3\sqrt{\frac{\gamma}{5}}\right) - \frac{1}{2}Q\left(5\sqrt{\frac{2\gamma}{5}}\right). \tag{3.36}$$

Hence, we obtain the average BER in terms of the output mgf as

$$\bar{P}_b = \frac{1}{\pi}\int_0^{\frac{\pi}{2}}\left[\frac{3}{2}M_{\text{am}}\left(\frac{1}{5\sin^2\theta}\right) + M_{\text{am}}\left(\frac{9}{10\sin^2\theta}\right) - \frac{1}{2}M_{\text{am}}\left(\frac{5}{\sin^2\theta}\right)\right]d\theta. \tag{3.37}$$

For i.i.d. Rayleigh fading channels, we can simplify the average BER as

$$\bar{P}_b = \frac{3}{2}J\left(\frac{1}{5}\right) + J\left(\frac{9}{10}\right) - \frac{1}{2}J(5) \tag{3.38}$$

where $J(g)$ is defined as (3.34).

3.3.2 Outage Probability

Noticing the relation between the outage probability and the output cdf (1.35), we obtain the outage probability of A-MRC in i.i.d. Rayleigh fading channels by integrating the output pdf (3.11) as

$$P_{\text{out}}(\gamma_T) = \frac{1}{(L-1)!}\gamma\left(L, \frac{\gamma_T}{\bar{\gamma}}\right) + u(\gamma_T - \gamma_{\text{th}}) \times \sum_{j=0}^{L-2} \frac{1}{j!}\left(\frac{\gamma_{\text{th}}}{\bar{\gamma}}\right)^j \left[e^{-\frac{\gamma_{\text{th}}}{\bar{\gamma}}} \frac{\Gamma\left(L-j, \frac{\gamma_T-\gamma_{\text{th}}}{\bar{\gamma}}\right)}{(L-j-1)!} - e^{-\frac{\gamma_T}{\bar{\gamma}}}\right]. \tag{3.39}$$

3.3.3 Average Output SNR

The average output SNR of A-MRC can be derived using the output mgf (3.10) for i.i.d. Rayleigh fading channels,

$$\bar{\gamma}_{\text{out}} = \bar{\gamma}\left[L - e^{-\frac{\gamma_{\text{th}}}{\bar{\gamma}}} \sum_{j=0}^{L-2} \frac{1}{j!}\left(\frac{\gamma_{\text{th}}}{\bar{\gamma}}\right)^j (L-j-1)\right]. \tag{3.40}$$

Note that as $\gamma_{\text{th}} \to \infty$, the average output SNR of A-MRC approaches $L\bar{\gamma}$, which is equivalent to that of MRC. Similarly, using (3.14), we obtain the average output SNR for i.n.d. Rayleigh fading channels as

$$\begin{aligned}\bar{\gamma}_{\text{out}} =& (\bar{\gamma}_1 + \gamma_{\text{th}})e^{-\frac{\gamma_{\text{th}}}{\bar{\gamma}_1}} + \sum_{j=1}^{L-2}(\bar{\gamma}_{j+1} + \gamma_{\text{th}})e^{-\frac{\gamma_{\text{th}}}{\bar{\gamma}_{j+1}}} \sum_{k=1}^{j} \pi(k,j) \frac{1 - e^{-\frac{\gamma_{\text{th}}}{\bar{\gamma}_k}\left(1-\frac{\bar{\gamma}_k}{\bar{\gamma}_{j+1}}\right)}}{1 - \frac{\bar{\gamma}_k}{\bar{\gamma}_{j+1}}} \\ &+ \sum_{k=1}^{L-1} \pi(k, L-1)[\bar{\gamma}_L + \bar{\gamma}_k - e^{-\frac{\gamma_{\text{th}}}{\bar{\gamma}_k}}(\bar{\gamma}_L + \bar{\gamma}_k + \gamma_{\text{th}})].\end{aligned} \tag{3.41}$$

Higher-order moments of the A-MRC output SNR can be obtained using the output mgfs. For brevity, we do not develop such results here.

3.3.4 Number of the Combined Branches

The number of the combined branches N_c of A-MRC varies dynamically with the channel fading conditions. We use the average number of the combined branches to evaluate the processing complexity of A-MRC.

For i.i.d Rayleigh fading channels, the probability that l branches are combined in A-MRC is given by

$$\Pr(N_c = l) = \begin{cases} \dfrac{1}{(l-1)!} e^{-\frac{\gamma_{th}}{\bar{\gamma}}} \left(\dfrac{\gamma_{th}}{\bar{\gamma}}\right)^{l-1}, & l = 1, \ldots, L-1, \\ 1 - e^{-\frac{\gamma_{th}}{\bar{\gamma}}} \displaystyle\sum_{j=0}^{L-2} \frac{1}{j!} \left(\frac{\gamma_{th}}{\bar{\gamma}}\right)^{j}, & l = L, \end{cases} \tag{3.42}$$

Thus, we can readily obtain the average number of the combined branches as

$$\bar{N}_c = L - e^{-\frac{\gamma_{th}}{\bar{\gamma}}} \left[\sum_{l=1}^{L-1} \left(\frac{\gamma_{th}}{\bar{\gamma}}\right)^{l-1} \frac{L-l}{(l-1)!} \right]. \tag{3.43}$$

From (3.43), we readily find that as γ_{th} increases, the average number of the combined branches $\bar{N}_c$ increases and so does the computational complexity of the system. As $\gamma_{th} \to \infty$, (3.43) approaches L, which is expected. Recall that as γ_{th} increases, the A-MRC performance improves. Hence, there is a tradeoff between performance and complexity. A-MRC can be made to operate with difference levels of complexity and performance according to the application requirements.

The variance of the number of the combined branches can also be obtained with (3.42) and (3.43) as

$$\mathrm{VAR}(N_c) = e^{-\frac{\gamma_{th}}{\bar{\gamma}}} \sum_{l=1}^{L-1} \left(\frac{\gamma_{th}}{\bar{\gamma}}\right)^{l-1} \frac{(L-l)^2}{(l-1)!} - e^{-\frac{2\gamma_{th}}{\bar{\gamma}}} \left[\sum_{l=1}^{L-1} \left(\frac{\gamma_{th}}{\bar{\gamma}}\right)^{l-1} \frac{L-l}{(l-1)!} \right]^2. \tag{3.44}$$

As $\gamma_{th} \to \infty$, (3.44) tends to zero, as expected.

For i.n.d. Rayleigh fading channels, the average and the variance of N_c are given by

$$\begin{aligned} \bar{N}_c =& e^{-\frac{\gamma_{th}}{\bar{\gamma}_1}} + \sum_{l=2}^{L-1} l e^{-\frac{\gamma_{th}}{\bar{\gamma}_l}} \sum_{k=1}^{l-1} \pi(k, l-1) \frac{1 - e^{-\frac{\gamma_{th}}{\bar{\gamma}_k}\left(1 - \frac{\bar{\gamma}_k}{\bar{\gamma}_l}\right)}}{1 - \frac{\bar{\gamma}_k}{\bar{\gamma}_l}} \\ &+ L \sum_{k=1}^{L-1} \pi(k, L-1)(1 - e^{-\frac{\gamma_{th}}{\bar{\gamma}_k}}) \end{aligned} \tag{3.45}$$

and

$$\begin{aligned} \mathrm{VAR}(N_c) =& e^{-\frac{\gamma_{th}}{\bar{\gamma}_1}} + \sum_{l=2}^{L-1} l^2 e^{-\frac{\gamma_{th}}{\bar{\gamma}_l}} \sum_{k=1}^{l-1} \pi(k, l-1) \frac{1 - e^{-\frac{\gamma_{th}}{\bar{\gamma}_k}\left(1 - \frac{\bar{\gamma}_k}{\bar{\gamma}_l}\right)}}{1 - \frac{\bar{\gamma}_k}{\bar{\gamma}_l}} \\ &+ L^2 \sum_{k=1}^{L-1} \pi(k, L-1)(1 - e^{-\frac{\gamma_{th}}{\bar{\gamma}_k}}) - \bar{N}_c^2. \end{aligned} \tag{3.46}$$

3.3.5 Imperfect Channel Estimation

Note that all the previous analysis is based on the assumption that CSI is perfectly known at the receiver. However, perfect CSI is not available in practice. For example, with pilot symbol assisted estimation, a Gaussian estimation error may arise in the estimate due to the large time or frequency separation between pilot and signal [62]. We next show that our results for the perfect A-MRC in i.i.d. Rayleigh fading channels can be readily used to analyze the A-MRC performance with Gaussian estimation errors in i.i.d. Rayleigh fading channels.

With pilot symbol assisted estimation, the channel estimate $\hat{g}_k$ can be written as

$$\hat{g}_k = g_k + e_k, \quad k \in \{1, \ldots, L\}, \tag{3.47}$$

where e_k is the difference between the estimate $\hat{g}_k$ and the actual channel gain g_k, which is assumed to be a zero-mean CGRV with identical variance $\sigma_e^2 = E(|e_k|^2)$. We assume that the Gaussian error e_k is independent of the actual channel gain g_k and the noise components, i.e., $E(e_j g_k^*) = E(e_j n_k^*) = 0$ for any j and k. Thus, g_k and $\hat{g}_k$ are joint complex Gaussian distributed with zero means and variances $E(|g_k|^2) = \sigma_g^2$ and $E(|\hat{g}_k|^2) = \hat{\sigma}_g^2 = \sigma_g^2 + \sigma_e^2$, respectively. The correlation between g_k and $\hat{g}_k$ is given by

$$\rho(g_k, \hat{g}_k) = \frac{\sigma_g}{\hat{\sigma}_g} = \frac{\sigma_g}{\sqrt{\sigma_g^2 + \sigma_e^2}}. \tag{3.48}$$

We express the actual channel gain g_k in terms of the estimate $\hat{g}_k$ as

$$g_k = \lambda \hat{g}_k + \tilde{e}_k \tag{3.49}$$

where $\lambda = \frac{\sigma_g^2}{\sigma_g^2 + \sigma_e^2}$ and $\tilde{e}_k$ is a zero-mean CGRV with variance $E(|\tilde{e}_k|^2) = \tilde{\sigma}_e^2 = \frac{\sigma_g^2 \sigma_e^2}{\sigma_g^2 + \sigma_e^2}$. Note that $E(\tilde{e}_j \hat{g}_k^*) = E(\tilde{e}_j n_k^*) = 0$ for all j and k.

Given the transmitted signal s and the channel estimates $\hat{g}_k$'s, we obtain the output signal of A-MRC as

$$\tilde{s} = \sum_{k=1}^{N_c} \hat{g}_k^* r_k = \underbrace{\lambda s \sum_{k=1}^{N_C} |\hat{g}_k|^2}_{\text{Desired signal}} + \underbrace{\sum_{k=1}^{N_c} \hat{g}_k^* s \tilde{e}_k}_{\text{Gaussian estimation error}} + \underbrace{\sum_{k=1}^{N_c} \hat{g}_k^* n_k}_{\text{AWGN}}. \tag{3.50}$$

Note that the second term in (3.50) is a zero-mean CGRV which can be regarded as the Gaussian noise from the estimator. Hence, the Gaussian estimation errors enlarge the noise components in the received signal. The output SNR conditioned on the channel estimates $\hat{g}_k$'s is given by

$$\gamma_{\text{am}} = \frac{|\lambda s \sum_{k=1}^{N_c} |\hat{g}_k|^2|^2}{E[|\sum_{k=1}^{N_c} \hat{g}_k^*(\tilde{e}_k s + n)|^2]} = \sum_{k=1}^{N_c} \mu_k \tag{3.51}$$

where μ_k is the instantaneous SNR of the k-th branch given by

$$\mu_k = |\hat{g}_k|^2 \frac{\lambda^2 E_s}{N_0 + \tilde{\sigma}_g^2 E_s} = \frac{|\hat{g}_k|^2}{(1+\kappa)^2 \left(\frac{E_s}{N_0}\right)^{-1} + \sigma_g^2 \kappa (1+\kappa)} \tag{3.52}$$

where $\kappa = \sigma_e^2/\sigma_g^2$. Hence, the average SNR of the k-th branch is given by

$$\bar{\mu} = E(\mu_k) = \frac{1}{(1+\kappa)\bar{\gamma}^{-1} + \kappa} \tag{3.53}$$

where $\bar{\gamma} = \sigma_g^2 \frac{E_s}{N_0}$ is the average SNR at the k-th branch when perfect CSI is available. Since $\kappa \geq 0$, we have $\bar{\mu} \leq \bar{\gamma}$ which means that the imperfect CSI decreases the average branch SNR, resulting in worse performance. When $\kappa = 0$, i.e., no estimation noise, (3.51) reduces to (3.1) for the perfect CSI case.

Assume that σ_g^2 and σ_e^2 are known at the receiver. The instantaneous output SNR of A-MRC with Gaussian estimation errors is given by

$$\gamma_{out} = \begin{cases} \mu_1, & \text{if } \mu_1 \geq \gamma_{\text{th}}, \\ \sum_{k=1}^{N_c} \mu_k, & \text{if } \sum_{k=1}^{N_c} \mu_k \geq \gamma_{\text{th}} \text{ and } 0 \leq \sum_{k=1}^{N_c-1} \mu_k < \gamma_{\text{th}}, \\ \sum_{k=1}^{L} \mu_k, & \text{if } 0 \leq \sum_{k=1}^{L-1} \mu_k < \gamma_{\text{th}}. \end{cases} \tag{3.54}$$

Comparing (3.51) and (3.1), we find that the instantaneous output SNR of A-MRC with imperfect CSI has the same distribution as that with perfect CSI but different mean values. Therefore, replacing the average branch SNR $\bar{\gamma}$ (for perfect CSI) in (3.10) with $\bar{\mu}$ (3.53) (for imperfect CSI), we can obtain the mgf of the A-MRC output SNR with imperfect CSI in i.i.d. Rayleigh fading channels. Other performance measures can then be readily derived using the output mgf.

For example, the BER of BPSK with imperfect A-MRC in i.i.d. Rayleigh fading channels is given by

$$\bar{P}_b = \frac{1}{2} - \frac{1}{2}\sqrt{\frac{g\bar{\mu}}{1+g\bar{\mu}}}\left\{\sum_{k=0}^{L-1}\binom{2k}{k}[4(1+g\bar{\mu})]^{(}-k) + \sum_{j=0}^{L-2}\frac{1}{j!}\left(\frac{\gamma_{\text{th}}}{\bar{\mu}}\right)^{j} \times \left[-2Q(\sqrt{2\omega_e}) + \frac{1}{\sqrt{\pi}}\sum_{l=0}^{L-j-1}\frac{1}{l!(1+g\bar{\mu})^{l}}\sum_{t=0}^{l}\binom{l}{t}(-\omega_e)^{t}\Gamma\left(\frac{1}{2}+l-t,\omega_e\right)\right]\right\} \tag{3.55}$$

where $\omega_e = \frac{\gamma_{\text{th}}(1+g\bar{\mu})}{\bar{\mu}}$.

3.4 Numerical Results

We now provide some numerical results to show the performance of A-MRC in independent Rayleigh and Nakagami-m fading channels. In all the figures, we assume that the total number of the resolvable multi-path components is $L = 10$. The normalized threshold $\hat{\gamma}_{\text{th}}$ is defined as the threshold normalized by the average SNR of the first branch, i.e., $\hat{\gamma}_{\text{th}} = \gamma_{\text{th}}/\bar{\gamma}_1$. The average receive SNR is defined as the sum of the average branch SNRs i.e.,$\gamma_b = \sum_{j=1}^{L}\bar{\gamma}_j$. In Figs. 3.1-3.7, we assume that perfect CSI is available at the receiver. In Figs. 3.1-3.5 and 3.7, the channel is assumed to have an exponential power delay profile (EPDP), i.e., the average received SNR at the j-th branch is given by $\bar{\gamma}_j = e^{-\delta(j-1)}\bar{\gamma}_1$ where δ is the power decay factor. Note that if $\delta = 0$, $\bar{\gamma}_k = \bar{\gamma}_1$ for $k \in \{1,\ldots,L\}$ and we obtain so-called uniform PDP (UPDP). Both EPDP and UPDP are commonly used in various studies. Semi-analytical simulation results are provided for the A-MRC performance as an independent check of our analytical results.

Figs. 3.1 and 3.2 plot the average and the variance of the number of the combined branches N_c versus the normalized threshold in independent Rayleigh fading channels with EPDPs. Both the average and the variance of N_c are highly dependent on the preset threshold $\hat{\gamma}_{\text{th}}$. As $\hat{\gamma}_{\text{th}}$ increases, $\bar{N}_c$ increases. When $\hat{\gamma}_{\text{th}}$ is chosen to be a medium value, $\bar{N}_c$ increases much faster and the variance of N_c becomes large. When $\hat{\gamma}_{\text{th}}$ is either very small or very large, $\bar{N}_c$ does not change much and the variance of N_c is small. As the channel power decay factor δ increases, the $\bar{N}_c$ increases and the variance of N_c changes more

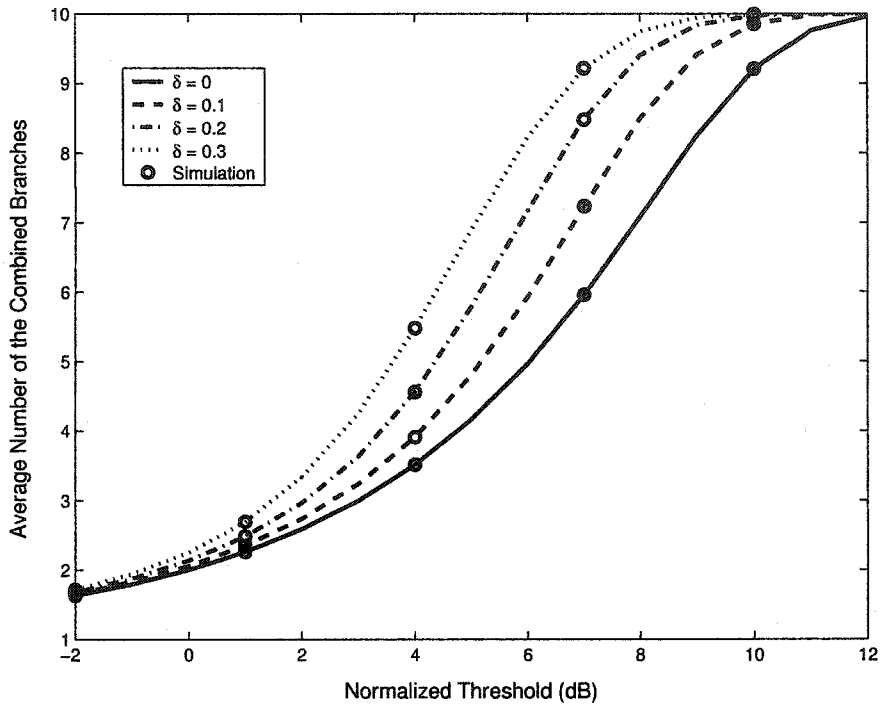

Figure 3.1: The average number of the combined branches.

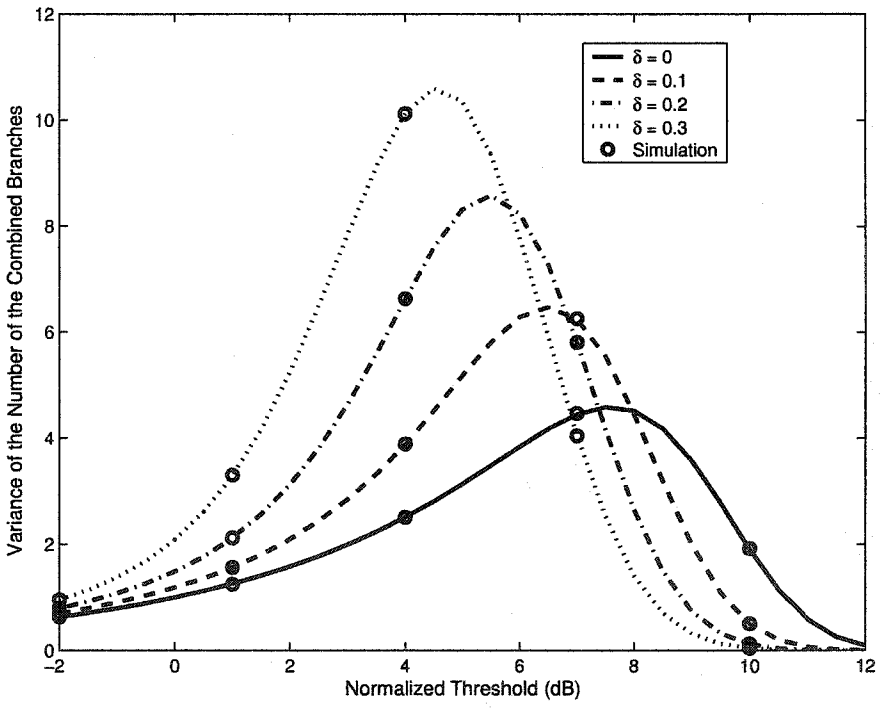

Figure 3.2: The variance of the number of the combined branches.

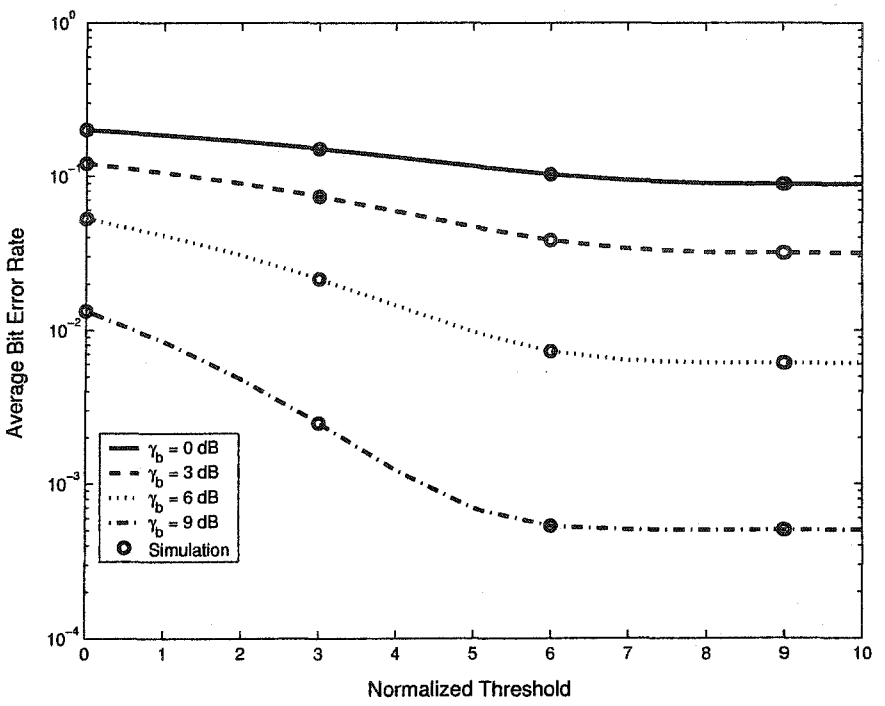

Figure 3.3: The average BER of BPSK with A-MRC as a function of the normalized threshold in independent Rayleigh fading channels with EPDP $\delta = 0.2$.

widely. This is much more pronounced in medium $\hat{\gamma}_{\text{th}}$ region.

Fig. 3.3 shows the average BER of BPSK with A-MRC as a function of the normalized threshold $\hat{\gamma}_{\text{th}}$. As expected, the average error rate performance depends on the preset threshold. As $\hat{\gamma}_{\text{th}}$ increases, the A-MRC performance improves because more branches are combined to form the output. However, due to the limit of the average received SNR γ_b, error floor occurs in high $\hat{\gamma}_{\text{th}}$ region. When $\hat{\gamma}_{\text{th}}$ approaches infinity, A-MRC is equivalent to MRC. As the average received SNR γ_b increases, the average BER decreases and the A-MRC performance becomes much more sensitive to the threshold $\hat{\gamma}_{\text{th}}$. From Figs. 3.1 and 3.3, increasing the threshold $\hat{\gamma}_{\text{th}}$ improves the A-MRC performance, but increases the average number of the combined branches $\bar{N}_c$, which results in higher computational complexity. Therefore, we should adjust $\hat{\gamma}_{\text{th}}$ to achieve a better tradeoff between performance and complexity.

Fig. 3.4 compares the performance of A-MRC with that of GSC(6, 10) in EPDP channels. The number of the combined branches is fixed in GSC(M, 10) while it is a random

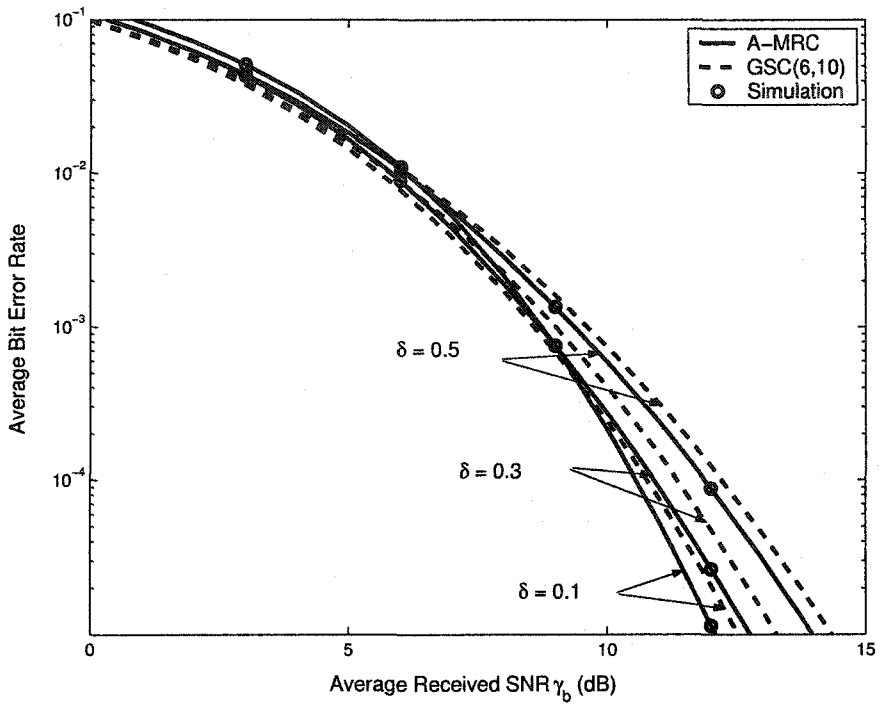

Figure 3.4: The average BER of BPSK with GSC(6, 10) and A-MRC in independent Rayleigh fading channels with different EPDPs $\delta = 0.1, 0.3, 0.5$.

Table 3.2: Choosing the normalized threshold $\hat{\gamma}_{\text{th}}$ (dB) in A-MRC with $L = 10$

	$\hat{\gamma}_{\text{th}}$	
	$\bar{N}_c = 5$	$\bar{N}_c = 6$
$\delta = 0.1$	5.197	6.058
$\delta = 0.2$	4.387	5.164
$\delta = 0.3$	3.635	4.379

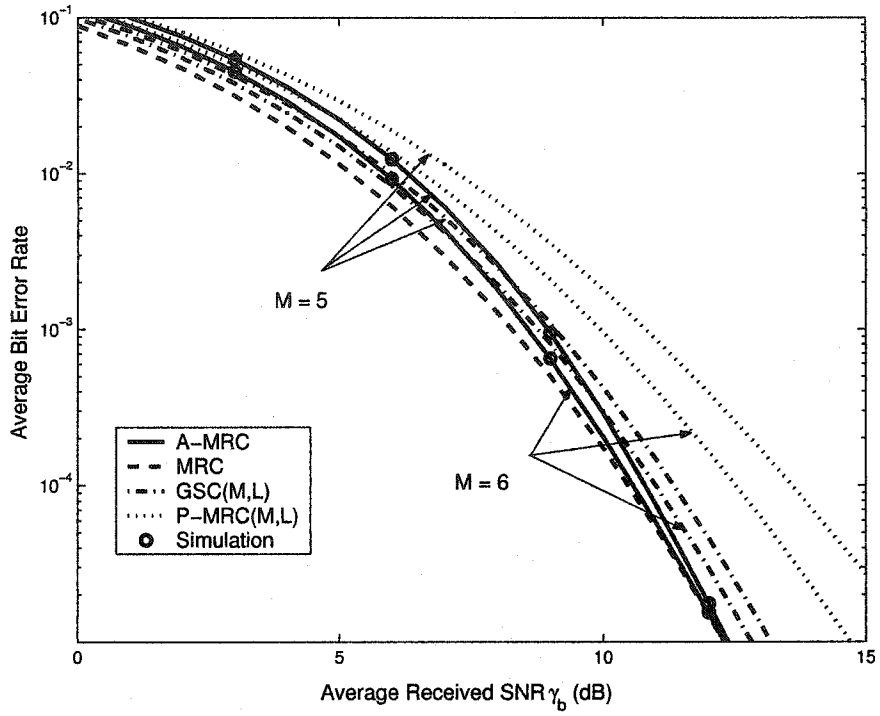

Figure 3.5: The average BER of BPSK with different diversity combining schemes in independent Rayleigh fading channels with EPDP $\delta = 0.2$.

variable in our A-MRC. To compare the performance on a fair basis, we choose the A-MRC threshold γ_{th}, such that the average numbers of the combined branches $\bar{N}_c$ is equal to M (see Table 3.2). Hence, the processing complexities of two combining schemes are almost the same on average. In fact, A-MRC is still simpler than GSC(M, L). Because less branches have to be measured and no sorting operation is required in our approach. Interestingly, as the power decay factor δ increases, the A-MRC performance degrades in higher SNRs but improves in lower SNRs, while the GSC(6, 10) performance becomes worse in all the SNRs. Hence, our approach can perform better than GSC(M, L) even in lower SNRs when the channel power decays fast, i.e. δ is large.

Figs. 3.5 and 3.6 compare the average BER performance of A-MRC with that of GSC(M, 10) and P-MRC(M, 10) in i.n.d. and i.i.d. Rayleigh fading channels, respectively. The A-MRC threshold γ_{th} is carefully chosen such that the average number of the combined branches is $\bar{N}_c = M$. The MRC performance is also plotted for comparison. Clearly, the P-MRC(M, L) performs the worst and MRC performs the best. When the channel has

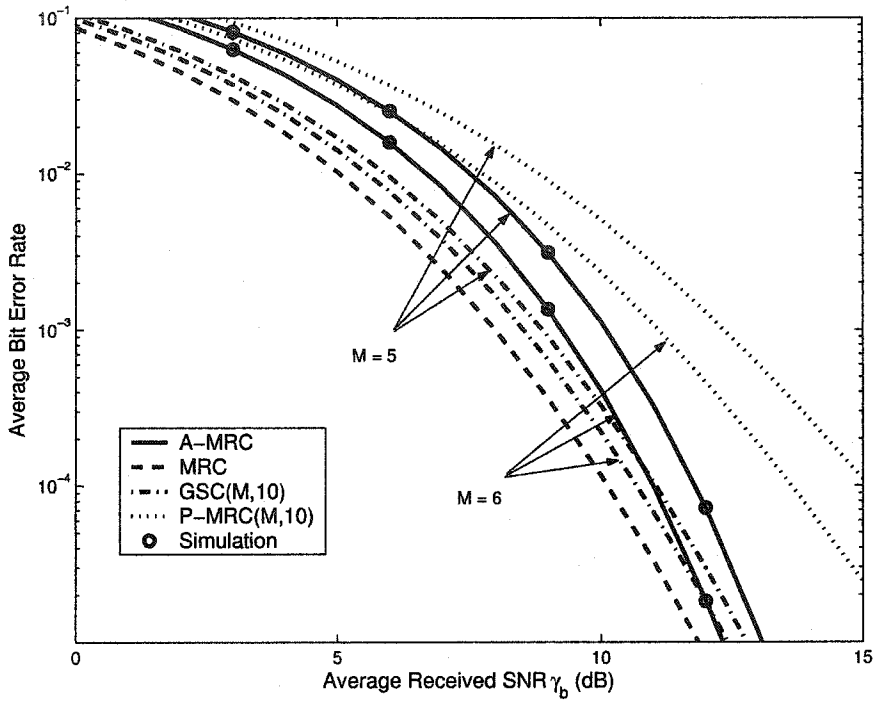

Figure 3.6: The average BER of BPSK with different diversity combining schemes in i.i.d. Rayleigh fading channels.

an EPDP, our A-MRC outperforms GSC(M, L) and approaches MRC in high SNRs (see Fig. 3.5). However, when the channel has a UPDP, our A-MRC does not perform well (see Fig. 3.6). As the average number of the combined branches M decreases, our A-MRC performs much worse than GSC(M, L). Therefore, our A-MRC is more suitable in non-identically distributed fading channels. In fact, UPDP rarely occurs in practical multi-path fading channels and is widely used as a worse-case benchmark.

Using (3.30) with (3.35), we plot the BER of binary DPSK with A-MRC in independent Nakagami-m fading channels when m is an integer in Fig. 3.7. We assume that the fading severity parameters on different branches are the same, i.e., $m_k = m$ for $k \in \{1, \ldots, L\}$. The BER of binary DPSK with MRC is plotted for comparison. As m increases (the fading condition improves), the performance of both MRC and A-MRC improves. However, the A-MRC performance does not improve as much as that of MRC. As the threshold $\hat{\gamma}_{\text{th}}$ increases, A-MRC behaves more like MRC.

Fig. 3.8 shows the impact of Gaussian estimation errors on the BER performance of

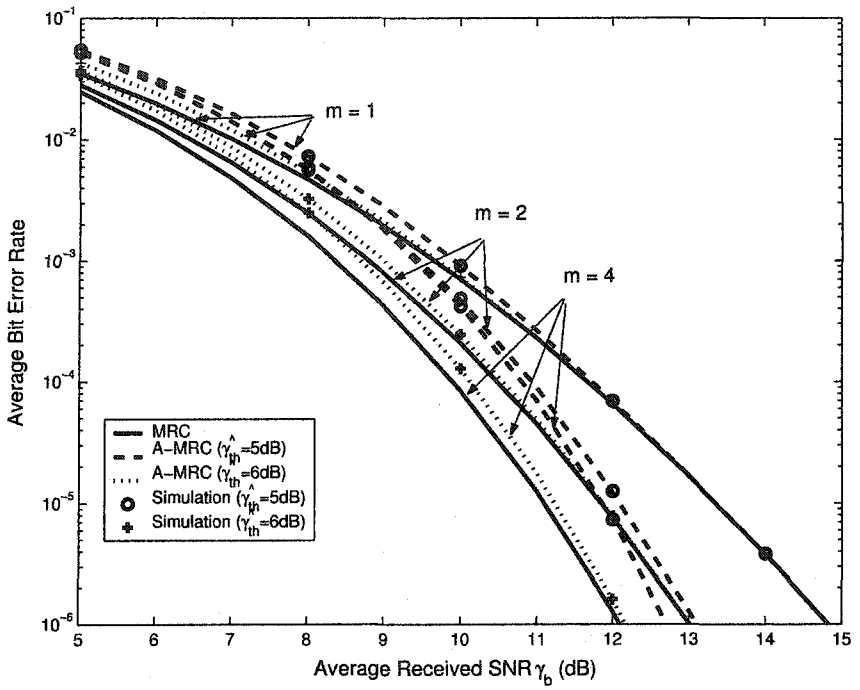

Figure 3.7: The average BER of binary DPSK with A-MRC in independent Nakagami-m fading channels with different fading severity parameters $m = 1, 2, 4$ and EPDP $\delta = 0.2$.

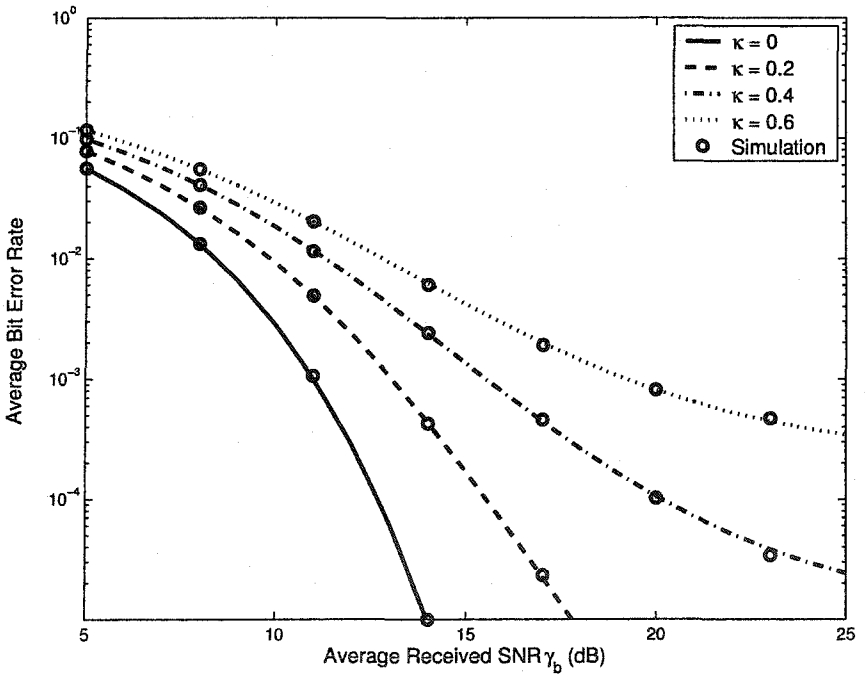

Figure 3.8: The average BER of BPSK with A-MRC with imperfect CSI in i.i.d. Rayleigh fading channels. The normalized threshold $\hat{\gamma}_{\text{th}} = \gamma_{\text{th}}/\bar{\gamma}_1 = 5\text{dB}$.

A-MRC with BPSK in i.i.d. Rayleigh fading channels. As expected, error floor is more obvious with the increasing κ which is defined as the ratio of the variance of the Gaussian estimation error to the variance of the actual channel gain. Simulation results prove the rightness of our analytical results.

3.5 Conclusion

In this chapter, we have developed a new diversity combining scheme, A-MRC, which adaptively combines the first N_c branches whose output SNR is above a preset threshold γ_{th}. This method measures the first N_c branches only. It avoids the sorting operation required in GSC(M, L) and allows the number of the combined branches N_c to vary according to the channel fading conditions. For performance analysis, we have derived the mgfs of the A-MRC output SNR in independent Rayleigh and Nakagami-m fading channels. Asymptotic analysis showed that the effective diversity order of A-MRC increases as the threshold increases. Using the output mgfs, we analyzed the performance of A-MRC with perfect CSI in independent Rayleigh fading channels and the performance of A-MRC with Gaussian channel estimation errors in i.i.d. Rayleigh fading channels. Numerical results showed that our proposed A-MRC outperforms GSC(M, L) when channel power decays rapidly. Our approach may achieve a better tradeoff between performance degradation and implementation complexity than GSC(M, L) in non-uniform dense multi-path fading channels.

Chapter 4

Performance Analysis of Diversity Combiners in Equally Correlated Fading Channels

In Chapters 2 and 3, we proposed two new diversity combiners and analyzed their performance in independent fading channels. However, the channel fading is usually correlated in practice. This chapter develops a novel approach for performance analysis of multi-branch diversity combiners in equally correlated fading channels. Section 4.1 reviews the analytical results for the performance of diversity combiners in the literature. Section 4.2 develops new representations for equally correlated Rayleigh, Ricean and Nakagami-m channel gains. Section 4.3 derives integral and infinite series expressions for the cdfs of the multi-branch SC output SNR in three types of equally correlated fading channels. These new results are then used to evaluate the average error rates, the outage probability and the output moments of multi-branch SC. Section 4.4 derives the cdfs and the moments of the multi-branch EGC output SNR and evaluates the average error rate performance of EGC in equally correlated fading channels. Numerical and semi-analytical simulation results that illustrate the effect of fading correlation on the performance of multi-branch SC and EGC are provided in Section 4.5. Section 4.6 concludes this chapter.

4.1 Introduction

Correlated fading among diversity branches can significantly degrade the performance of diversity systems. However, performance analysis of diversity combiners in correlated fad-

ing channels is inherently more difficult. The reason is that the joint distributions of the channel gains at different diversity branches are in general required. For arbitrary correlation patterns, such joint distributions are not available.

4.1.1 Equally Correlated Model

In this chapter, we study the performance of multi-branch diversity combiners in equally correlated Rayleigh, Ricean and Nakagami-m fading channels. The equally correlated model may be valid for a set of closely placed antennas [41]. It can also be used as a worst-case benchmark or as a rough approximation of arbitrary correlation pattern by replacing every element ρ_{jk} $(j \neq k)$ in the correlation matrix with the average value of ρ_{jk} $(j \neq k)$. However, experimental measurements have shown that for three equally placed antennas (a triangular antenna array), the fading correlation among them does not follow the equally correlated model [63].

4.1.2 Relation to the Previous Papers

While comprehensive theoretical results for the average error rate and the outage performance of multi-branch MRC systems in various correlated fading channels are available, by comparison, such performance analysis for multi-branch SC and EGC is not available. This is due to the lack of explicit expressions for the joint pdf of the branch SNRs for $L > 2$, when the channel gains are correlated.

The SC performance has therefore been comprehensively treated for various *independent* fading models and modulation methods [15, 19, 64–69]. For correlated fading, almost all results for SC deal with two branches ($L = 2$) or three branches ($L = 3$) (see [19, 70–77]). In the extensive list of papers dealing with SC, we know of only a few papers that address multi-branch ($L > 3$) SC in correlated fading channels. Exceptionally, Ugweje and Aalo [43] derive the pdf of the SC output SNR in correlated Nakagami-m fading channels as a multiple series of the generalized Laguerre polynomials. This work is based on the earlier work of Krishnamoorthy and Parthasarathy on the multi-variate gamma distribution [78]. They developed an orthogonal series expansion for the multivariate gamma chf in terms of the generalized Laguerre polynomials. However, the con-

vergence properties of this series appear to be poor and the complexity of this approach increases rapidly for $L > 3$. Zhang and Lu [44] have developed a general approach to analyze the multi-branch SC performance in correlated fading channels. The basic idea behind this approach is to express the joint pdf as an L-dimensional inverse integral of the joint chf and to manipulate a resulting kernel expression. However, their results require L-dimensional integration. For large L (> 3), this method is also fairly complicated. Mallik and Win [79] analyze the GSC(M, L) in equally correlated Nakagami-m fading channels using its output chf. All these methods utilize the joint chf of the branch SNRs and the complexity increases as L increases. Following Miller [80], Mallik [81] derives the joint pdf of the multi-variate Rayleigh distribution. However, the pdf expression again requires L-dimensional integration. Karagiannidis *et al.* derive the joint pdf of exponentially correlated Nakagami-m distribution [82] and apply this result with the Green's matrix to approximate the multi-variate Nakagami-m distribution [83]. Although such an approximation is accurate for the exponentially and linearly correlated models, it is not good for the equally correlated model.

Performance analysis of EGC is notoriously difficult. Even for independent fading, a closed-form solution to the pdf of the EGC output SNR is only known for dual-branch EGC in Rayleigh fading channels [65]. Different methods have therefore been developed to analyze the EGC performance. Brennan [18] numerically evaluates the distribution of the EGC output SNR in Rayleigh fading channels. Beaulieu and Abu-Dayya [65–67] apply an accurate approximation to the pdf of a sum of independent RVs. Annamalai *et al.* [1,2,84] use the Parseval theorem to transform the problem to the frequency domain. Zhang [68, 69] provides several closed-form solutions to the average BER using the chf of the decision variables. While much progress has been made regarding the EGC performance in independent fading channels, little is known about that in correlated fading channels. Only the dual-branch EGC in correlated fading channels has been completely solved. Mallik *et al.* [85] derive the average BER for coherent detected binary signals with dual-branch EGC in correlated Rayleigh fading channels. Tellambura and Annamalai [7] derive the chf of the EGC output SNR and utilize an infinite series representation for the complementary error function to obtain the average BER. In [86], an integral representation for the Gaussian

probability integral is used to derive the BER. As far as we know, theoretical performance results for multi-branch EGC in *correlated* fading channels do not exist for $L > 2$.

4.1.3 Our Contributions

We thus develop a new approach to analyze the performance of multi-branch SC and EGC in equally correlated Rayleigh, Ricean and Nakagami-*m* fading channels. The novel insight of our approach is that a set of independent Gaussian RVs can be linearly combined to form a set of equally correlated CGRVs. We extend the representations for the equally correlated Gaussian RVs [87, 88] to complex domain. Using this insight, we translate the problem of the SC and EGC performance in equally correlated fading to the problem of the SC and EGC performance in a *conditionally independent* fading environment. This reformulation allows us to extend known results for independent fading to analyze the multi-branch SC and EGC performance in correlated fading channels. We show that diversity benefits still exist in correlated fading channels. When the fading correlation is small, the diversity combiners perform as well as they do in independent fading channels. We also find that higher-order diversity systems are much more sensitive to the fading correlation. Correlated Ricean fading may cause larger performance loss than correlated Rayleigh fading. These observations may be useful in diversity system design.

It should be emphasized that our approach can be used to analyze not only SC and EGC, but also more general diversity combining schemes, such as GSC(M, L). For brevity, we do not give such results. Further, our new representations for equally correlated channel gains may also be useful in other applications such as co-channel interference modelling and multiple antenna systems.

4.2 Representations of the Channel Gains

Rayleigh, Ricean and Nakagami-*m* distributions are widely used to model the amplitude fluctuations of the received signals from different multi-path fading channels (Section 1.1.1). In this section, new representations for the equally correlated channel gains are developed for these fading models.

4.2.1 Correlated Rayleigh Envelopes

Since the envelope of a zero-mean CGRV is Rayleigh distributed (see the definition of the Rayleigh distribution in Section 1.1.1), Rayleigh envelopes can be associated with a set of CGRVs given by:

$$G_k = \left(\sqrt{1-\rho}\, X_k + \sqrt{\rho}\, X_0\right) + i\left(\sqrt{1-\rho}\, Y_k + \sqrt{\rho}\, Y_0\right) \tag{4.1}$$

where $k \in \{1, \ldots, L\}$, $0 \leq \rho \leq 1$, and $X_k, Y_k \sim N\left(0, \frac{1}{2}\right)$ are independent for any $k \in \{0, 1, \cdots, L\}$. That is, for any $j, k \in \{0, \ldots, L\}$,

$$E(X_k Y_j) = 0, \tag{4.2a}$$

$$E(X_k X_j) = E(Y_k Y_j) = \frac{1}{2}\delta_{kj}. \tag{4.2b}$$

The validity of (4.1) for non-negative ρ only may at first seem a significant limitation. However, the entire range for ρ is between $-\frac{1}{L-1}$ and 1 (the lower limit follows from the positive-definiteness constraint on the covariance matrix). For large L, we may therefore ignore the negative values $-\frac{1}{L-1} \leq \rho < 0$. However, a more complicated representation than (4.1) may be developed to handle negative ρ values.

Since $G_k \sim C\left(0, \frac{1}{2}\right)$, $|G_k|$ is Rayleigh distributed with the mean-square value

$$E(|G_k|^2) = 1. \tag{4.3}$$

The cross-correlation coefficient between any G_k and G_j $(k \neq j)$ equals to a constant,

$$\frac{E(G_k G_j^*)}{\sqrt{E(|G_k|^2)E(|G_j|^2)}} = \rho. \tag{4.4}$$

This specifies the correlation (fading correlation) between two complex Gaussian samples. However, it is required to relate this to the power correlation (i.e., the correlation between $|G_k|^2$ and $|G_j|^2$ where $k \neq j$) and the envelope correlation (i.e., the correlation between two Rayleigh samples $|G_k|$ and $|G_j|$ where $k \neq j$). It can be readily shown that the power correlation equals to the square of fading correlation [41], i.e.,

$$\rho_\eta = \rho^2, \tag{4.5}$$

and the envelope correlation can be expressed in terms of the fading correlation ρ as [13],

$$\rho_e = \frac{{}_2F_1\left(-\frac{1}{2}, -\frac{1}{2}; 1; \rho^2\right) - 1}{\frac{4}{\pi} - 1} \tag{4.6}$$

where ${}_2F_1(a, b; c; z)$ is the Gauss hypergeometric function defined as [3, Eq. (9.100)]

$${}_2F_1(a, b; c; z) = \sum_{n=0}^{\infty} \frac{(a)_n (b)_n}{(c)_n \, n!} z^n \tag{4.7}$$

where $(a)_n = \frac{\Gamma(a+n)}{\Gamma(a)} = a(a+1)\ldots(a+n-1)$ and $(a)_0 = 1$. For a given ρ_e, solving (4.6) yields ρ. Several solution methods are discussed in [89, 90] and we also provide a new, more general solution in (4.21). Thus, using (4.1) with (4.5) or (4.6), we can readily represent a set of equally correlated Rayleigh envelopes with a specified value of power correlation ρ_η or envelope correlation ρ_e.

Next, we introduce a 'trick' that enables performance analysis. We consider $X_0 = x_0$ and $Y_0 = y_0$ to be fixed. Then, $G_k \sim C\left(\sqrt{\rho}(x_0 + iy_0), \frac{1-\rho}{2}\right)$, are conditional independent for $k \in \{1, \ldots, L\}$. Performance analysis can now be carried out in two steps. First, conditional performance results, which are functions of $x_0^2 + y_0^2$, are obtained for the set of conditionally independent channel gains. The second step is to average the conditional results over the distribution of $X_0^2 + Y_0^2$.

4.2.2 Correlated Ricean Envelopes

The envelope of a non-zero mean CGRV is known to be Ricean distributed (see the definition of the Ricean distribution in Section 1.1.1). Assuming that the Rice factors at different diversity branches are identical, we represent the Ricean fading envelopes by using:

$$G_k = \left(\sqrt{1-\rho}\, X_k + \sqrt{\rho}\, X_0 + m_1\right) + i\left(\sqrt{1-\rho}\, Y_k + \sqrt{\rho}\, Y_0 + m_2\right) \tag{4.8}$$

where $k \in \{1, \ldots, L\}$ and $X_k, Y_k \sim N\left(0, \frac{1}{2}\right)$ are independent for any $k \in \{0, 1, \cdots, L\}$ and $m_1 + im_2$ is the non-zero LOS component.

Since $G_k \sim C\left(m_1 + im_2, \frac{1}{2}\right)$, $|G_k| \sim \mathcal{R}(m_1^2 + m_2^2, 1 + K)$, i.e., for any $k \in \{1, \ldots, L\}$, $|G_k|$ is a Ricean RV with the Rice factor

$$K = m_1^2 + m_2^2 \tag{4.9}$$

and the mean-square value

$$E(|G_k|^2) = 1 + K. \tag{4.10}$$

The fading correlation between any G_k and G_j ($k \neq j$) equals to a constant,

$$\frac{E\{[G_k - E(G_k)][G_j - E(G_j)]^*\}}{\sqrt{E[|G_k - E(G_k)|^2]E[|G_j - E(G_j)|^2]}} = \rho. \tag{4.11}$$

The power correlation between any $|G_k|^2$ and $|G_j|^2$ ($k \neq j$) can be obtained as [91, Eq. (2.4-9)]

$$\rho_\eta = \rho \frac{2K + \rho}{2K + 1}. \tag{4.12}$$

Thus, (4.12) and (4.8) can be used to represent the equally correlated Ricean fading envelopes with a specified value of power correlation.

4.2.3 Correlated Nakagami-m Envelopes

When the fading severity index (m) is an integer, a Nakagami-m envelope is the square root of the sum of squares of m independent Rayleigh RVs. Hence, we can associate the Nakagami-m fading envelopes with a set of Lm zero-mean CGRVs given by:

$$G_{kj} = \left(\sqrt{1-\rho}\, X_{kj} + \sqrt{\rho}\, X_{0j}\right) + i\left(\sqrt{1-\rho}\, Y_{kj} + \sqrt{\rho}\, Y_{0j}\right) \tag{4.13}$$

where $k \in \{1, \ldots, L\}$, $j \in \{1, \ldots, m\}$ and $X_{kj}, Y_{kj} \sim N\left(0, \frac{1}{2}\right)$ are independent for any $k \in \{0, 1, \ldots, L\}$ and $j \in \{1, \ldots, m\}$. That is, for any $k, l \in \{0, \ldots, L\}$ and $j, n \in \{1, \ldots, m\}$,

$$E(X_{kj} Y_{ln}) = 0, \tag{4.14}$$

$$E(X_{kj} X_{ln}) = E(Y_{kj} Y_{ln}) = \frac{1}{2}\delta_{kl}\delta_{jn}. \tag{4.15}$$

The fading correlation between any G_{kj} and G_{ln} is given by

$$\rho_g = \frac{E(G_{kj} G_{ln}^*)}{\sqrt{E(|G_{kj}|^2)E(|G_{ln}|^2)}} = \begin{cases} \rho, & k \neq l \text{ and } j = n, \\ 0, & j \neq n. \end{cases} \tag{4.16}$$

Let R_k^2 denote the summation of the absolute square of G_{kj}'s for $j = 1, \ldots, m$,

$$R_k^2 = \sum_{j=1}^{m} |G_{kj}|^2. \tag{4.17}$$

From (4.16), we find that for any fixed k, $G_{kj} \sim C\left(0, \frac{1}{2}\right)$ are independent for any $j \in \{1, \ldots, m\}$. Thus $R_k^2 \sim \chi_{2m}\left(0, \frac{1}{2}\right)$ is the sum of squares of m independent Rayleigh envelopes with constant cross-correlation coefficient (power correlation) given by [16]

$$\rho_\eta = \frac{E(R_k^2 R_l^2)}{\sqrt{E(R_k^4)E(R_l^4)}} = \rho^2, \quad k \neq l. \tag{4.18}$$

Therefore, $\{R_k\}$ is a set of equally correlated Nakagami-m fading envelopes with the mean-square value

$$E(R_k^2) = m. \tag{4.19}$$

The relationship between the power correlation ρ_η and the envelope correlation ρ_e is [16],

$$\rho_e = \frac{{}_2F_1(-\frac{1}{2}, -\frac{1}{2}; m; \rho_\eta) - 1}{\psi(m) - 1} \tag{4.20}$$

where $\psi(m) = \frac{\Gamma(m)\Gamma(m+1)}{\Gamma^2\left(m+\frac{1}{2}\right)}$. Note that for $m = 1$, (4.20) reduces to (4.6). Since there is no closed-form solution, for a given ρ_e, we may use a polynomial approximation for ρ_η. Expressing the hypergeometric function in the form of Gauss series [92, Eq. (15.1.1)] and using the reversion of power series [93, P. 138], we obtain the approximation for ρ_η as

$$\begin{aligned}\rho_\eta \approx 4xm - \frac{2m^2x^2}{m+1} - \frac{2(2m+1)m^3x^3}{(m+2)(m+1)^2} - \frac{5(5m+3)(2m+1)m^4x^4}{2(m+3)(m+2)(m+1)^3} \\ - \frac{(2m+1)(256m^3+843m^2+743m+198)m^5x^5}{2(m+4)(m+3)(m+2)^2(m+1)^4}\end{aligned} \tag{4.21}$$

where $x = \rho_e(\psi(m) - 1)$. Then using (4.18), we can immediately obtain the corresponding fading correlation ρ.

4.3 SC Performance in Equally Correlated Fading Channels

In this section, we derive the cdfs of the SC output SNR in equally correlated Rayleigh, Ricean and Nakagami-m fading channels. We show that the cdfs of the SC output SNR can be represented as a single-fold integral. Infinite series representations for the output cdfs are also derived. Using these new results, we evaluate the average error rates, the

outage probability and the output moments of multi-branch SC in equally correlated fading channels. Consequently, unlike the other existing methods [43, 44], any number of diversity branches can be handled as a single-fold integral (for the outage probability) or two-dimensional integral (for the error rate and the average output SNR). The complexity of our approach does not increase with the number of diversity branches.

4.3.1 Cdfs of the SC Output SNR

SC picks the best branch as the output. Its output SNR is given by (1.27). We can show that the output cdf of SC is given by

$$\begin{aligned} F_{\text{sc}}(y) &= \Pr(\gamma_1 \leq y, \ldots, \gamma_L \leq y) \\ &= \Pr\left(|G_1|^2 \leq E(|G_1|^2)\frac{y}{\bar{\gamma}_1}, \ldots, |G_L|^2 \leq E(|G_L|^2)\frac{y}{\bar{\gamma}_L}\right) \end{aligned} \tag{4.22}$$

where γ_k and $\bar{\gamma}_k$, $k \in \{1, \ldots, L\}$, are the instantaneous SNR and the average SNR associated with the k-th branch, which are given by (1.20) and (1.21), respectively. When the channel gains G_k's are independent, (4.22) can be evaluated using the cdfs of the branch powers $|G_k|^2$ as

$$F_{\text{sc}}(y) = \prod_{k=1}^{L} \Pr\left(|G_k|^2 \leq E(|G_k|^2)\frac{y}{\bar{\gamma}_k}\right) = \prod_{k=1}^{L} F_{|G_k|^2}\left(E(|G_k|^2)\frac{y}{\bar{\gamma}_k}\right). \tag{4.23}$$

However, if the channel gains are correlated, the joint cdf of $|G_k|^2$ is usually required to evaluate (4.22). In this section, we use the new representations for the channel gains to derive the cdfs of the SC output SNR in equally correlated fading channels. Our approach does not directly require the joint cdf of the correlated channel gain amplitudes.

Rayleigh Fading Channels

Careful inspection of (4.1) reveals that all G_k's contain two common RVs X_0 and Y_0. This is what ensures that the correlation between any two G_k and G_j is a *constant*. When X_0 and Y_0 are fixed ($X_0^2 + Y_0^2 = t$), the branch powers $|G_k|^2 \sim \chi_2\left(\sqrt{\rho t}, \frac{1-\rho}{2}\right)$ are independent, whose cdf is given by [6, Eq. (2-1-124)]

$$F_{|G_k|^2|T}(y\,|t) = \Pr\left(|G_k|^2 \leq y\,|t\right) = 1 - Q\left(\sqrt{\frac{2\rho t}{1-\rho}}, \sqrt{\frac{2y}{1-\rho}}\right). \tag{4.24}$$

Noting that the average power of G_k is given by (4.3) and using (4.23), we can readily obtain the conditional cdf of the SC output SNR as

$$F_{\mathrm{sc}|T}(y\,|t) = \left[1 - Q\left(\sqrt{\frac{2\rho t}{1-\rho}}, \sqrt{\frac{2y}{\bar{\gamma}(1-\rho)}}\right)\right]^L. \tag{4.25}$$

Notice that $T \sim \chi_2\left(0, \frac{1}{2}\right)$, where $T = X_0^2 + Y_0^2$, and its pdf is given by a special case of [6, Eq. (2-1-110)]

$$p_T(t) = e^{-t}, \quad t \geq 0. \tag{4.26}$$

Averaging the conditional cdf (4.25) over the distribution of T (4.26), we obtain the cdf of the multi-branch SC output SNR in equally correlated Rayleigh fading as a single-fold integral

$$\begin{aligned} F_{\mathrm{sc}}(y) &= \int_0^\infty F_{\mathrm{sc}|T}(y\,|t)\; p_T(t)\, dt \\ &= \int_0^\infty \left[1 - Q\left(\sqrt{\frac{2\rho t}{1-\rho}}, \sqrt{\frac{2y}{\bar{\gamma}(1-\rho)}}\right)\right]^L e^{-t}\, dt. \end{aligned} \tag{4.27}$$

Notice that Matlab provides the function NCX2CDF to compute the cdf of the non-central chi-square distribution, which is in the form of the Marcum Q-function. Therefore, we can readily evaluate (4.27) numerically using Matlab.

To the best of our knowledge, (4.27) is a novel result. It reduces the L-dimensional integration [44, Eq. (9)] necessary for the output cdf of SC in correlated fading channels to a single-fold integral, enabling the performance analysis of multi-branch SC in equally correlated Rayleigh fading. This new expression (4.27) for the SC output cdf reduces to the previous results for two special cases.

1. Independent Rayleigh fading ($\rho = 0$).

   Using the relation $I_0(0) = 1$ and $Q(0, x) = e^{-\frac{x^2}{2}}$, the cdf of the SC output SNR (4.27) simplifies to

   $$F_{\mathrm{sc}}(y) = \left[1 - e^{-\frac{y}{\bar{\gamma}}}\right]^L, \tag{4.28}$$

   which is equivalent to the well-known result [19, Eq. (10-4-12)].

2. Dual-branch SC ($L = 2$).

Integrating (4.27) by parts, we can show that the output cdf of dual-branch SC in correlated Rayleigh fading channels can be written as (see Appendix A)

$$F_{\text{sc}}(y) = 1 - 2e^{-\frac{y}{\bar{\gamma}}} Q\left(\sqrt{\frac{2y}{\bar{\gamma}(1-\rho^2)}}, \rho\sqrt{\frac{2y}{\bar{\gamma}(1-\rho^2)}}\right) + e^{-\frac{2y}{\bar{\gamma}(1-\rho^2)}} I_0\left[\frac{2\rho y}{\bar{\gamma}(1-\rho^2)}\right]. \tag{4.29}$$

This result is equivalent to the well-known expression [19, Eq. (10-10-8)].

Next, infinite series representation for computation of the SC output cdf in equally correlated Rayleigh fading channels is provided. Expressing the Marcum Q-function in an integral form [5], we rewire the output cdf (4.27) as

$$F_{\text{sc}}(y) = \int_0^{\infty} \left[\int_0^{\sqrt{\frac{2y}{\bar{\gamma}(1-\rho)}}} x e^{-\left(\frac{\rho t}{1-\rho}+\frac{x^2}{2}\right)} I_0\left(x\sqrt{\frac{2\rho t}{1-\rho}}\right) dx\right]^L e^{-t}\, dt. \tag{4.30}$$

Using an infinite series [92, Eq. (9.6.10)] for $I_0(x)$ and interchanging the order of integration and summation, we obtain an infinite series representation of the output cdf after some algebra as

$$F_{\text{sc}}(y) = (1-\rho) \sum_{k=0}^{\infty} \frac{k!\, a_k(y)}{(\rho L + 1 - \rho)^{k+1}} \tag{4.31}$$

where $a_k(y)$ can be computed recursively as

$$a_k(y) = \begin{cases} \left(1 - e^{-\eta}\right)^L, & k = 0, \\ \dfrac{\sum_{n=1}^{k} \dfrac{(nL - k + n)\rho^n}{n!} P(n+1, \eta)}{k\left(1 - e^{-\eta}\right)} a_{k-n}(y), & k \geq 1, \end{cases} \tag{4.32}$$

where $\eta = \frac{y}{\bar{\gamma}(1-\rho)}$ and $P(n, x)$ is the normalized incomplete gamma function, which can be evaluated using the finite series (3.22) when n is a positive integer:

$$P(n, x) = \frac{\gamma(n, x)}{\Gamma(n)} = 1 - e^{-x} \sum_{k=0}^{n-1} \frac{x^k}{k!}. \tag{4.33}$$

The number of the terms required in the infinite series (4.31) to achieve a target accuracy depends on several factors, including the fading correlation ρ, the normalized branch SNR $y/\bar{\gamma}$ and the diversity order L as well. Table 4.1 lists the results for a five significant figure accuracy over a range of values of ρ, y and L with the average branch SNR $\bar{\gamma} = 1$. As the fading correlation ρ or the branch SNR y or the diversity order L increases, more terms are required in (4.31) to achieve the target accuracy.

Table 4.1: The number of terms required in (4.31) to achieve five significant figure accuracy. ($\bar{\gamma} = 1$)

	$L = 3$			$L = 6$		
ρ	$y = -5$dB	$y = 0$dB	$y = 5$dB	$y = -5$dB	$y = 0$dB	$y = 5$dB
0.2	6	8	12	7	10	17
0.4	7	11	19	8	14	28
0.6	9	15	30	10	20	46
0.8	14	27	59	16	37	96

Differentiating (4.27) yields the pdf of the SC output SNR:

$$p_{\text{sc}}(y) = \frac{L}{\bar{\gamma}} e^{-\eta} \int_0^\infty e^{-t} \left[1 - Q\left(\sqrt{2\rho t}, \sqrt{2\eta}\right)\right]^{L-1} I_0\left(2\sqrt{\rho\eta t}\right) dt \tag{4.34}$$

where $\eta = \frac{y}{\bar{\gamma}(1-\rho)}$. There is no closed-form solution to this integral. However, in the case of $L = 2$, the output pdf can be written in terms of the Marcum Q-function:

$$p_{\text{sc}}(y) = \frac{2}{\bar{\gamma}} e^{-\frac{y}{\bar{\gamma}}} \left[1 - Q\left(\rho\sqrt{\frac{2y}{\bar{\gamma}(1-\rho^2)}}, \sqrt{\frac{2y}{\bar{\gamma}(1-\rho^2)}}\right)\right]. \tag{4.35}$$

This special case is already known [73, Eq. (11)].

Using the output pdf (4.34), we can also derive the corresponding output mgf as a two-dimensional integral

$$\begin{aligned} \phi_{\text{sc}}(s) = L(1-\rho) \int_0^\infty & e^{-[1+s\bar{\gamma}(1-\rho)]y} \\ & \times \int_0^\infty e^{-t} \left[1 - Q\left(\sqrt{2\rho t}, \sqrt{2y}\right)\right]^{L-1} I_0\left(2\sqrt{\rho y t}\right) dt\, dy. \end{aligned} \tag{4.36}$$

In the special case of dual-branch SC, the mgf can be expressed in closed-form [73],

$$\phi_{\text{sc}}(s) = \frac{2}{1+s\bar{\gamma}} - \frac{4(1-\rho^2)}{[s\bar{\gamma}(1-\rho^2)+2]^2 - 4\rho^2 - s\bar{\gamma}(1-\rho^2)\sqrt{[s\bar{\gamma}(1-\rho^2)+2]^2 - 4\rho^2}}. \tag{4.37}$$

Clearly, unlike previous results [44, 79], our new expressions (4.27), (4.34) and (4.36) are either single-fold or two-fold integrals and their computational complexity does not increase as the diversity order L increases.

Ricean Fading Channels

Using the representation for the equally correlated Ricean channel gains (4.8), we can also derive the output cdf of multi-branch SC in equally correlated Ricean channels. Fix $\left(X_0+\frac{m_1}{\sqrt{\rho}}\right)^2+\left(Y_0+\frac{m_2}{\sqrt{\rho}}\right)^2=t$, $|G_k|^2 \sim \chi_2\left(\sqrt{\rho t}, \frac{1-\rho}{2}\right)$ are independent, whose cdf is given by (4.24). Noting that the average power of Ricean channel gains is given by (4.10), we obtain the conditional output cdf as

$$F_{\mathrm{sc}|T}(y\,|t)=\left[1-Q\left(\sqrt{\frac{2\rho t}{1-\rho}}, \sqrt{\frac{2(1+K)y}{\bar{\gamma}(1-\rho)}}\right)\right]^L \tag{4.38}$$

where K is the Rice factor defined as (4.9). Also notice that $T \sim \chi_2\left(\sqrt{\frac{K}{\rho}}, \frac{1}{2}\right)$, where $T=\left(X_0+\frac{m_1}{\sqrt{\rho}}\right)^2+\left(Y_0+\frac{m_2}{\sqrt{\rho}}\right)^2$, and its pdf is given by [6, Eq.2-1-118]

$$p_T(t)=e^{-\left(\frac{K}{\rho}+t\right)} I_0\left(2\sqrt{\frac{Kt}{\rho}}\right). \tag{4.39}$$

Averaging the conditional output cdf (4.38) over the distribution of T (4.39), we obtain the output cdf of multi-branch SC in equally correlated Ricean fading channels as a single-fold integral

$$F_{\mathrm{sc}}(y)=e^{-\frac{K}{\rho}}\int_0^\infty\left[1-Q\left(\sqrt{\frac{2\rho t}{1-\rho}}, \sqrt{\frac{2(1+K)y}{\bar{\gamma}(1-\rho)}}\right)\right]^L e^{-t} I_0\left(2\sqrt{\frac{Kt}{\rho}}\right) dt \tag{4.40}$$

To the best of our knowledge, (4.40) is also a new result. Compared with the available result which requires L-dimensional integration [44], our result (4.40) is much easier to handle.

Similarly, we derive an infinite series representation for the output cdf of SC in equally correlated Ricean fading channels as

$$F_{\mathrm{sc}}(y)=(1-\rho)e^{-\frac{K}{\rho}}\sum_{k=0}^{\infty}\frac{k!}{(\rho L+1-\rho)^{k+1}}\sum_{j=0}^{k}\left[\frac{K(1-\rho)}{\rho}\right]^{k-j}\frac{a_j[(K+1)y]}{[(k-j)!]^2} \tag{4.41}$$

where $a_k(y)$ is given by (4.32).

Nakagami-m Fading Channels

When m is a positive integer, the channel gain representations (4.13) and (4.17) can be used to derive the output cdf of SC in equally correlated Nakagami-m fading channels. Fixing $\sum_{j=1}^{m}\left(X_{0j}^2+Y_{0j}^2\right)=t$, we obtain that the branch powers $R_k^2 \sim \chi_{2m}\left(\sqrt{\rho t}, \frac{1-\rho}{2}\right)$ are independent, whose cdf is given by [6, Eq. (2-1-124)],

$$F_{R_k^2|T}(y\,|t) = 1 - Q_m\left(\sqrt{\frac{2\rho t}{1-\rho}}, \sqrt{\frac{2y}{1-\rho}}\right). \tag{4.42}$$

Substituting the average power of Nakagami-m channel gains (4.19) and (4.42) into (4.23), we readily obtain the conditional output cdf of multi-branch SC as

$$F_{\mathrm{sc}|T}(y\,|t) = \left[1 - Q_m\left(\sqrt{\frac{2\rho t}{1-\rho}}, \sqrt{\frac{2my}{\bar{\gamma}(1-\rho)}}\right)\right]^L. \tag{4.43}$$

Also notice that $T \sim \chi_{2m}\left(0, \frac{1}{2}\right)$, where $T=\sum_{j=1}^{m}\left(X_{0j}^2+Y_{0j}^2\right)$, and its pdf may be found as [6, Eq. (2-1-110)]

$$p_T(t) = \frac{t^{m-1}e^{-t}}{(m-1)!}, \quad t \geq 0. \tag{4.44}$$

Averaging the conditional output cdf (4.43) over the distribution of T (4.44), we obtain the output cdf of multi-branch SC in equally correlated Nakagami-m fading channels as a single-fold integral

$$F_{\mathrm{sc}}(y) = \frac{1}{(m-1)!}\int_0^\infty \left[1 - Q_m\left(\sqrt{\frac{2\rho t}{1-\rho}}, \sqrt{\frac{2my}{\bar{\gamma}(1-\rho)}}\right)\right]^L t^{m-1}e^{-t}\,dt. \tag{4.45}$$

This novel result reduces to several well-known special cases. The output cdf of SC in independent Nakagami-m fading channels can be obtained by setting $\rho = 0$ in (4.45),

$$F_{\mathrm{sc}}(y) = \left[1 - Q_m\left(0, \sqrt{\frac{2my}{\bar{\gamma}}}\right)\right]^L = \left[1 - e^{-\frac{my}{\bar{\gamma}}}\sum_{k=0}^{M-1}\frac{1}{k!}\left(\frac{my}{\bar{\gamma}}\right)^k\right]^L, \tag{4.46}$$

which is equivalent to the result [52]. As expected, when $m = 1$, this new expression reduces to (4.27) for the equally correlated Rayleigh fading case. For dual-branch SC

($L = 2$), (4.45) is numerically checked against an infinite series for the output cdf derived from [94, Eq. (3)]. Both methods give exactly the same numerical values.

Infinite series representation for the SC output cdf in equally correlated Nakagami-m fading channels can also be obtained as:

$$F_{\text{sc}}(y) = \frac{(1-\rho)^m}{\Gamma(m)} \sum_{k=0}^{\infty} \frac{\Gamma(k+m)\, c_k(y)}{(\rho L + 1 - \rho)^{k+m}} \tag{4.47}$$

where

$$c_k(y) = \begin{cases} [P(m, \eta_m)]^L, & k = 0, \\ \displaystyle\sum_{n=1}^{k} \frac{(nL-k+n)\rho^n}{n!} P(m+n, \eta_m) \\ \qquad\qquad \Big/ \; kP(m, \eta_m) \; c_{k-n}(y), & k \geq 1, \end{cases} \tag{4.48}$$

where $\eta_m = \frac{my}{\bar{\gamma}(1-\rho)}$.

Differentiating (4.45) yields the output pdf of multi-branch SC in equally correlated Nakagami-m fading channels. For dual-branch ($L = 2$) SC, the output pdf reduces to

$$p_{\text{sc}}(y) = \frac{y^{m-1} m^m}{(m-1)!\bar{\gamma}^m} e^{-\frac{my}{\bar{\gamma}}} \left[1 - Q_m \left(\rho \sqrt{\frac{2my}{\bar{\gamma}(1-\rho^2)}}, \sqrt{\frac{2my}{\bar{\gamma}(1-\rho^2)}} \right) \right]. \tag{4.49}$$

This result is equivalent to that of [73]. These special cases reaffirm the rightness of (4.45).

4.3.2 Average Error Rate

In Chapters 2 and 3, we evaluated the average error rates of various digital modulations using the mgf of the diversity combiner output SNR. Here, since SC is being investigated, we show that the average error rates can be directly derived from the combiner output cdf. This can readily be done using integration by parts method:

$$\bar{P}_e = \int_0^{\infty} -P_e'(\gamma) F_{\text{out}}(\gamma)\, d\gamma \tag{4.50}$$

where $-P_e'(\gamma) = -\frac{d}{d\gamma} P_e(\gamma)$ denotes the negative derivative of the CEP $P_e(\gamma)$. According to the CEP forms of different digital modulations, we present the corresponding average error rates in terms of the SC output cdfs $F_{\text{sc}}(\gamma)$, which have already been derived for equally correlated Rayleigh, Ricean and Nakagami-m fading channels (4.27), (4.40), (4.45).

1. The CEP of BPSK, coherent BFSK and M-ary pulse amplitude modulation (PAM) is in the form of Q-function [6]

$$P_e(\gamma) = aQ\left(\sqrt{b\gamma}\right) \tag{4.51}$$

where $(a, b) = (1, 2)$ for BPSK, $(a, b) = (1, 1)$ for coherent BFSK, $(a, b) = \left(\frac{2(M-1)}{M}, \frac{6\log_2 M}{M^2-1}\right)$ for M-ary PAM. Substituting (4.51) into (4.50), we obtain the following expression for the average error rates

$$\bar{P}_e = \frac{a}{2}\sqrt{\frac{b}{2\pi}}\int_0^\infty \frac{e^{-\frac{b\gamma}{2}}}{\sqrt{\gamma}} F_{\text{sc}}(\gamma)\, d\gamma. \tag{4.52}$$

Notice that there is a removable singularity at $\gamma = 0$ in (4.52). That is, the integrand approaches 0 as $\gamma \to 0$, i.e.,

$$\lim_{\gamma\to 0} \frac{e^{-b\gamma/2}}{\sqrt{\gamma}} F_{\text{sc}}(\gamma) = 0. \tag{4.53}$$

When a numerical quadrature technique such as Gaussian quadrature is used, this singularity can be readily handled. Common mathematical software provides both Gaussian quadrature techniques and also the straightforward techniques such as Newton-Cotes formulas. All such techniques can readily be adapted to handle all the integral expressions derived in this section.

2. The CEP of non-coherent BFSK and binary DPSK can be expressed in an exponential form [6]

$$P_e(\gamma) = ae^{-b\gamma}. \tag{4.54}$$

where $(a, b) = (0.5, 1)$ for binary DPSK and $(a, b) = (0.5, 0.5)$ for non-coherent BFSK. Following the same procedure as the above, we obtain the average BER as

$$\bar{P}_e = ab\int_0^\infty e^{-b\gamma} F_{\text{sc}}(\gamma)\, d\gamma. \tag{4.55}$$

The CEP for non-coherent M-ary FSK can be expressed as a sum of exponential forms [6, Eq. (5-4-46)]. Thus, we can readily write down the average SER for M-ary FSK using (4.55)

$$\bar{P}_e = \sum_{n=1}^{M-1} \frac{(-1)^{n+1} nk}{(n+1)^2}\binom{M-1}{n}\int_0^\infty e^{-\frac{nk\gamma}{n+1}} F_{\text{sc}}(\gamma)\, d\gamma \tag{4.56}$$

where $k = \log_2 M$ is the number of bits per symbol.

3. The CEP of 4PSK, QAM, minimum-shift-keying (MSK) and coherent detected DPSK is in the following form [6]

$$P_e(\gamma) = aQ\left(\sqrt{b\gamma}\right) - cQ^2\left(\sqrt{b\gamma}\right) \tag{4.57}$$

where $(a, b, c) = (2, 2, 1)$ for 4PSK or MSK, $(a, b, c) = (2, 2, 2)$ for coherent detected DPSK and $(a, b, c) = \left(\frac{4(\sqrt{M}-1)}{\sqrt{M}}, \frac{3\log_2 M}{M-1}, \frac{4(\sqrt{M}-1)^2}{M}\right)$ for QAM. The corresponding average SER is obtained as

$$\bar{P}_e = \sqrt{\frac{b}{2\pi}} \int_0^\infty \frac{e^{-\frac{b\gamma}{2}}}{\sqrt{\gamma}} \left[\frac{a}{2} - cQ\left(\sqrt{b\gamma}\right)\right] F_{\text{sc}}(\gamma)\, d\gamma. \tag{4.58}$$

4. The CEP of $\pi/4$-QDPSK and non-coherent correlated BFSK can be written as [6,51]

$$P_e(\gamma) = Q\left(a\sqrt{\gamma}, b\sqrt{\gamma}\right) - \frac{1}{2} I_0(ab\gamma) e^{-\frac{a^2+b^2}{2}\gamma} \tag{4.59}$$

where $(a, b) = \left(\sqrt{2-\sqrt{2}}, \sqrt{2+\sqrt{2}}\right)$ and $(a, b) = \left(\sqrt{\frac{1-\sqrt{1-\lambda^2}}{2}}, \sqrt{\frac{1+\sqrt{1-\lambda^2}}{2}}\right)$ for $\pi/4$-QDPSK and correlated non-coherent BFSK, respectively, where λ is the correlation coefficient between the binary signals. Substituting (4.59) into (4.50), we obtain the average SER as

$$\bar{P}_e = \frac{a^2 - b^2}{4} \int_0^\infty e^{-\frac{(a^2+b^2)\gamma}{2}} I_0(ab\gamma) F_{\text{sc}}(\gamma)\, d\gamma. \tag{4.60}$$

4.3.3 Moments of the SC Output SNR

Using the output pdf (4.34) and the output mgf (4.36), the moments of the multi-branch SC output SNR in equally correlated Rayleigh fading channels can be readily determined. The average output SNR is obtained as a two-dimensional integral

$$\bar{\gamma}_{\text{sc}} = L\bar{\gamma}(1-\rho)^2 \int_0^\infty x e^{-x} \int_0^\infty e^{-t}[1 - Q(\sqrt{2\rho t}, \sqrt{2x})]^{L-1} I_0(2\sqrt{\rho x t})\, dt\, dx. \tag{4.61}$$

Similarly, we can readily derive higher-order moments of the SC output SNR and other useful measures, such as the central moments, the skewness, the kurtosis and the Karl Pearson's coefficient of variation [30] (see Section 1.2.3). Further simplification of these formulas seems to be impossible.

4.4 EGC Performance in Equally Correlated Fading Channels

The output cdfs and the average error rates of EGC in equally correlated Rayleigh and Ricean fading channels are next derived using our new representations for the equally correlated fading channel gains and the available results for the EGC performance in independent Ricean fading channels. We also derive the moments of the multi-branch EGC output SNR in three types of equally correlated fading channels.

4.4.1 Cdfs of the EGC Output SNR

Due to [67], the cdf of a sum of L i.i.d. Ricean RVs can be evaluated using an effective approximation:

$$F_V(K_f, \Omega_f, x) = \frac{1}{2} - \frac{2}{\pi} \sum_{\substack{n=1 \\ n \text{ is odd}}}^{\infty} \frac{(A_n)^L \sin(L\theta_n)}{n} \tag{4.62}$$

where $V = V_1 + \ldots + V_L$, $V_k \sim \mathcal{R}(K_f, \Omega_f)$ and

$$A_n = \sqrt{E^2[\cos(n\omega V_k)] + E^2[\sin(n\omega V_k)]}, \tag{4.63a}$$

$$\theta_n = \tan^{-1}\left(\frac{E[\sin(n\omega(V_k - \epsilon))]}{E[\cos(n\omega(V_k - \epsilon))]}\right) \tag{4.63b}$$

where $\epsilon = \frac{x}{L}$, $\omega = \frac{2\pi}{T}$ and T is the period of squarewave defined in [65]. Abu-Dayya and Beaulieu also provide solutions to $E[\cos(n\omega V_k)]$ and $E[\sin(n\omega V_k)]$ in [67]:

$$E[\cos(n\omega V_k)] = e^{-K_f} \sum_{j=0}^{\infty} \frac{K_f^j}{j!} {}_1F_1\left(j+1, \frac{1}{2}, -\frac{n^2\omega^2\Omega_f}{4(1+K_f)}\right), \tag{4.64a}$$

$$E[\sin(n\omega V_k)] = \frac{n\omega\sqrt{\Omega_f}e^{-K_f}}{\sqrt{1+K_f}} \sum_{j=0}^{\infty} \frac{\Gamma\left(j+\frac{3}{2}\right)}{(j!)^2} K_f^j \times {}_1F_1\left(j+\frac{3}{2}, \frac{3}{2}, -\frac{n^2\omega^2\Omega_f}{4(1+K_f)}\right) \tag{4.64b}$$

where ${}_1F_1(a, c; z)$ is the confluent hypergeometric function defined as [3, Eq. (9.210.1)]

$${}_1F_1(a, c; z) = \sum_{n=0}^{\infty} \frac{(a)_n}{(c)_n\, n!} z^n. \tag{4.65}$$

Hence, the cdf of a sum of Ricean RVs (4.62) can be computed using (4.63) and (4.64). The above results enable our derivation of the EGC output cdfs in equally correlated Rayleigh and Ricean fading channels.

Rayleigh Fading Channels

Using the new representation for equally correlated Rayleigh channel gains (4.1), we first calculate the cdf of the sum of equally correlated Rayleigh envelopes denoted by $R = |G_1| + \ldots + |G_L|$. Fix $X_0^2 + Y_0^2 = t$ in (4.1). Then $|G_k| \sim \mathcal{R}\left(\frac{\rho t}{1-\rho}, 1-\rho+\rho t\right)$ are independent and R is a sum of L i.i.d. Ricean RVs. Hence using (4.62), we obtain the conditional cdf of the sum of channel gain envelopes R as

$$F_{R|T}(y|t) = F_V\left(\frac{\rho t}{1-\rho}, 1-\rho+\rho t, y\right) \tag{4.66}$$

where $F_V(a, b, x)$ is given by (4.62). Averaging the conditional cdf (4.66) over the distribution of $T = X_0^2 + Y_0^2$ (4.26), we obtain the cdf of R as

$$F_R(y) = \int_0^\infty F_V\left(\frac{\rho t}{1-\rho}, 1-\rho+\rho t, y\right) e^{-t}\, dt. \tag{4.67}$$

Noticing the definition of the average branch SNR $\bar{\gamma}$ (1.21) and the average power of the Rayleigh channel gains $E(|G_k|^2)$ given by (4.3), we derive the cdf of the EGC output SNR (1.26) as

$$\begin{aligned} F_{\text{egc}}(y) &= \Pr(\gamma_{\text{egc}} \le y) = \Pr\left(\sum_{k=1}^{L} |G_k| \le \sqrt{\frac{Ly}{\bar{\gamma}}}\right) \\ &= \int_0^\infty F_V\left(\frac{\rho t}{1-\rho}, 1-\rho+\rho t, \sqrt{\frac{Ly}{\bar{\gamma}}}\right) e^{-t}\, dt. \end{aligned} \tag{4.68}$$

This novel result enables the evaluation of the outage probability of multi-branch EGC systems in equally correlated Rayleigh fading channels. We do not know any results on the multi-branch EGC performance in correlated fading channels. For the independent case, our new result (4.68) reduces to the well-known result [65, Eq. (5)]. Eq. (4.68) can be readily evaluated via numerical quadrature techniques with high accuracy (details omitted for brevity).

Ricean Fading Channels

When $\left(X_0+\frac{m_1}{\sqrt{\rho}}\right)^2+\left(Y_0+\frac{m_2}{\sqrt{\rho}}\right)^2=t$ in (4.8) is fixed, $|G_k|\sim\mathcal{R}\left(\frac{\rho t}{1-\rho},1-\rho+\rho t\right)$ are independent and $R=|G_1|+\ldots+|G_L|$ is a sum of L i.i.d. Ricean RVs whose conditional cdf is given by (4.66). Averaging the conditional cdf over the distribution of $T=\left(X_0+\frac{m_1}{\sqrt{\rho}}\right)^2+\left(Y_0+\frac{m_2}{\sqrt{\rho}}\right)^2$ (4.39), we obtain the cdf of the sum of equally correlated Ricean envelopes R as

$$F_R(y)=e^{-\frac{K}{\rho}}\int_0^\infty F_V\left(\frac{\rho t}{1-\rho},1-\rho+\rho t,y\right)e^{-t}I_0\left(2\sqrt{\frac{Kt}{\rho}}\right)dt. \tag{4.69}$$

Using the average power of the Ricean channel gains (4.10) with the average branch SNR (1.21), we can derive the cdf of the EGC output SNR as

$$F_{\text{egc}}(y)=e^{-\frac{K}{\rho}}\int_0^\infty F_V\left(\frac{\rho t}{1-\rho},1-\rho+\rho t,\sqrt{\frac{Ly(1+K)}{\bar{\gamma}}}\right)e^{-t}I_0\left(2\sqrt{\frac{Kt}{\rho}}\right)dt. \tag{4.70}$$

This is also a novel result. The outage probability of multi-branch EGC in equally correlated Ricean fading channels can be readily evaluated using (4.70).

4.4.2 Average Error Rate

Using the output cdfs (4.68) and (4.70) with (4.50), we may evaluate the average error rates of several digital modulations with multi-branch EGC in equally correlated Rayleigh and Ricean fading channels (see Section 4.3.2). Alternatively, we may use the chf-based approach to evaluate the average error rates [1].

With the aid of Parseval's theorem, the average error rates of different modulations with coherent EGC can be transformed to frequency domain as [1]

$$\begin{aligned}\bar{P}_e&=\int_0^\infty P_e(x)p_X(x)\,dx\\&=\frac{1}{2\pi}\int_{-\infty}^\infty G(\omega)\phi_X^*(\omega)\,d\omega\\&=\frac{2}{\pi}\int_0^{\frac{\pi}{2}}\frac{\psi(\tan\zeta)}{\sin(2\zeta)}\,d\zeta\end{aligned} \tag{4.71}$$

where $X = \sqrt{\gamma_{\text{out}}}$ is the amplitude of the combiner output SNR, $G(\omega)$ is the Fourier transform of the conditional error probability $P_e(x)$ with respect to x, $\phi_X(\omega)$ is the chf of X and $\psi(\omega) = \Re\left[\omega G(\omega)\phi_X^*(\omega)\right]$ where $\Re(z)$ is the real part of z.

Using Gauss-Chebyshev quadrature [92, Eq. (25.4.38)], we may obtain a rapidly converging series to approximate (4.71)

$$\bar{P}_e \approx \frac{1}{M}\sum_{n=1}^{M} \frac{\psi\left(\frac{1}{\sqrt{2}}\tan\theta_n\right)}{\sin 2\theta_n} \tag{4.72}$$

where $\theta = \frac{\pi(2n-1)}{2M}$. There is a tradeoff involved in the choice of M. A greater accuracy may be obtained using larger values, but at the expense of increasing computational complexity.

Note that $G(\omega)$ in (4.71) only depends on the modulation formats while $\phi_X(\omega)$ depends on the types of the fading channels and the diversity combiners. Since the expressions for $G(\omega)$ of a wide class of digital modulations can be readily found in [1, 2] (also see Table 4.2), we only need to derive the corresponding $\phi_X(\omega)$ to evaluate the average error rate performance of EGC $\bar{P}_e$ in equally correlated Rayleigh and Ricean fading channels.

Table 4.2: The Fourier Transform of the CEPs $G(\omega)$ [1,2].

Modulation Format $P_e(x)$	$G(\omega)$
$aQ\left(\sqrt{b}x\right)$	$\frac{a}{2\omega}\left[\frac{2}{\sqrt{\pi}}D\left(\frac{\omega}{\sqrt{2b}}\right)+i\left(1-e^{-\frac{\omega^2}{2b}}\right)\right]$ where $D(z)$ is the Dawson's integral [4].
ae^{-bx^2}	$\frac{a}{\sqrt{b}}\left[\frac{\sqrt{\pi}}{2}e^{-\frac{\omega^2}{4b}}+iD\left(\frac{\omega}{2\sqrt{b}}\right)\right]$
$aQ\left(\sqrt{b}x\right)-cQ^2\left(\sqrt{b}x\right)$	$\frac{a}{\omega\sqrt{\pi}}D\left(\frac{\omega}{\sqrt{2b}}\right)-\frac{1}{\omega\sqrt{\pi}}\left[D\left(\frac{\omega}{\sqrt{2b}}\right)-D\left(\frac{\omega}{2\sqrt{b}}\right)e^{-\frac{\omega^2}{4b}}\right]$ $+i\left\{\frac{a}{2\omega}\left(1-e^{-\frac{\omega^2}{2b}}\right)-\frac{c}{4\omega}\left[1-e^{-\frac{\omega^2}{2b}}-\frac{4}{\pi}D^2\left(\frac{\omega}{2\sqrt{b}}\right)\right]\right\}$

For subsequent use, we show the chf of X, the square root of the EGC output SNR, in i.i.d. Ricean fading channels here [1]

$$\tilde{\phi}_X(K_f,\xi,\omega) = \left[\frac{e^{-K_f}}{\pi}\int_0^{\pi} e^{\left(\frac{i\omega\xi+\sqrt{2K_f}\cos\theta}{2}\right)^2} D_{-2}\left(z(K_f,\xi,\theta)\right)\,d\theta\right]^L \tag{4.73}$$

where K_f is the Rice factor, $D_{-2}(z)$ is the parabolic cylinder function which is related to the confluent hypergeometric function as [3, Eq. (9.240)]

$$D_{-2}(z) = \exp\left(-\frac{z^2}{4}\right) {}_1F_1\left(1, \frac{1}{2}; \frac{z^2}{2}\right) - \sqrt{\frac{\pi}{2}} z \exp\left(\frac{z^2}{4}\right) \tag{4.74}$$

and

$$z(K_f, \xi, \theta) = -i\omega\xi - \sqrt{2K_f}\cos\theta, \tag{4.75a}$$

$$\xi = \sqrt{\frac{\bar{\gamma}\Omega_f}{2L(1+K_f)E(|G_k|^2)}} \tag{4.75b}$$

where Ω_f is the average power of the Ricean channel gain. Using (4.74), we may express (4.73) in terms of the confluent hypergeometric function as

$$\tilde{\phi}_X(K_f, \xi, \omega) = \left\{ \frac{e^{-K_f}}{\pi} \int_0^{\pi} \left[{}_1F_1\left(1, \frac{1}{2}, \frac{z^2(K_f, \xi, \theta)}{2}\right) - \sqrt{\frac{\pi}{2}} z(K_f, \xi, \theta) e^{\frac{z^2(K_f, \xi, \theta)}{2}} \right] d\theta \right\}^L \tag{4.76}$$

where $z(K_f, \xi, \theta)$ is defined as (4.75a).

Rayleigh Fading Channels

Recall that when $X_0^2 + Y_0^2 = t$ is fixed, $|G_k| \sim \mathcal{R}\left(\frac{\rho t}{1-\rho}, 1 - \rho + \rho t\right)$ are independent. The conditional chf of $X = \sqrt{\gamma_{\text{egc}}}$ can be obtained using (4.73) and (4.3) as

$$\phi_{X|T}(\omega|t) = \tilde{\phi}_X\left(\frac{\rho t}{1-\rho}, \sqrt{\frac{(1-\rho)\bar{\gamma}}{2L}}, \omega\right) \tag{4.77}$$

where $\tilde{\phi}_X(a, b, \omega)$ can be computed using (4.73) or (4.76). Averaging the conditional result over the distribution of T (4.26), we obtain the chf of X for equally correlated Rayleigh fading channels as

$$\phi_X(\omega) = \int_0^{\infty} \tilde{\phi}_X\left(\frac{\rho t}{1-\rho}, \sqrt{\frac{(1-\rho)\bar{\gamma}}{2L}}, \omega\right) e^{-t}\, dt. \tag{4.78}$$

Therefore, we may evaluate the average error rates of various digital modulations with multi-branch EGC in equally correlated Rayleigh fading channels using (4.78) and Table 4.2 with (4.71).

Ricean Fading Channels

Similarly, when $\left(X_0 + \frac{m_1}{\sqrt{\rho}}\right)^2 + \left(Y_0 + \frac{m_2}{\sqrt{\rho}}\right)^2 = t$ is fixed, $|G_k| \sim \mathcal{R}\left(\frac{\rho t}{1-\rho}, 1 - \rho + \rho t\right)$ are independent. Using $\tilde{\phi}_X(a, b, \omega)$ (4.73) or (4.76), we obtain the conditional chf of X as

$$\phi_{X|T}(\omega|t) = \tilde{\phi}_X\left(\frac{\rho t}{1-\rho}, \sqrt{\frac{(1-\rho)\bar{\gamma}}{2L(1+K)}}, \omega\right). \tag{4.79}$$

Averaging the conditional result over the distribution of T (4.39), we obtain the chf of X for equally correlated Ricean fading channels as

$$\phi_X(\omega) = e^{-\frac{K}{\rho}} \int_0^\infty \tilde{\phi}_X\left(\frac{\rho t}{1-\rho}, \sqrt{\frac{(1-\rho)\bar{\gamma}}{2L(1+K)}}, \omega\right) e^{-t} I_0\left(2\sqrt{\frac{Kt}{\rho}}\right) dt. \tag{4.80}$$

Substituting (4.80) with Table 4.2 to (4.71), we obtain the average error rates of different modulations with EGC in equally correlated Ricean fading channels.

4.4.3 Moments of the EGC Output SNR

Using the multinomial expansion, we obtain the moments of the EGC output SNR (1.26) as

$$\begin{aligned} m_n =& E(\gamma_{\text{egc}}^n) = \left(\frac{E_s}{LN_0}\right)^n E\left[(R_1 + \ldots + R_L)^{2n}\right] \\ =& (2n)! \left[\frac{\bar{\gamma}}{LE\left(R_k^2\right)}\right]^n \sum_{\substack{k_1,\cdots,k_L=0 \\ k_1+\cdots+k_L=2n}}^{2n} \frac{E\left(\prod_{j=1}^L R_j^{k_j}\right)}{\prod_{j=1}^L k_j!} \end{aligned} \tag{4.81}$$

where $R_k = |G_k|$, $k \in \{1, \ldots, L\}$, is the amplitude of the channel gain and $E(R_k^2) = E(|G_k|^2)$ are given by (4.3), (4.10) and (4.19) for equally correlated Rayleigh, Ricean and Nakagami-m fading channels, respectively. When R_k's are independent, (4.81) can be readily evaluated using the following property,

$$E\left(\prod_{j=1}^L R_j^{k_j}\right) = \prod_{j=1}^L \left[E\left(R_j^{k_j}\right)\right]. \tag{4.82}$$

However, it is an extremely complicated task to compute (4.81) when the joint pdf of correlated R_i's is unknown. Next, we use the new channel gain representations to derive the moments of the EGC output SNR in three types of equally correlated fading channels. Our approach does not directly require the joint pdf of the correlated channel gain amplitudes.

Rayleigh Fading Channels

We consider X_0 and Y_0 to be fixed ($X_0^2+Y_0^2 = t$) in (4.1). Then $R_k \sim \mathcal{R}\left(\frac{\rho t}{1-\rho}, 1-\rho+\rho t\right)$ are independent whose moments are given by [6, Eq. (2-1-146)]

$$\begin{aligned} E\left(R_j^{k_j}\right) =& (1-\rho)^{\frac{k_j}{2}} e^{-\frac{\rho t}{1-\rho}} \Gamma\left(1+\frac{k_j}{2}\right) {}_1F_1\left(1+\frac{k_j}{2}, 1; \frac{\rho t}{1-\rho}\right) \\ =& (1-\rho)^{\frac{k_j}{2}} \Gamma\left(1+\frac{k_j}{2}\right) {}_1F_1\left(-\frac{k_j}{2}, 1; -\frac{\rho t}{1-\rho}\right). \end{aligned} \tag{4.83}$$

Using the property (4.82) and substituting (4.83) into (4.81), we obtain the output moments of EGC conditioned on t as

$$m_n(t) = (2n)! \left[\frac{\bar{\gamma}(1-\rho)}{L}\right]^n \sum_{\substack{k_1,\cdots,k_L=0 \\ k_1+\cdots+k_L=2n}}^{2n} \left[\prod_{j=1}^{L} A(k_j) \, {}_1F_1\left(-\frac{k_j}{2}, 1; -\frac{\rho t}{1-\rho}\right)\right] \tag{4.84}$$

where

$$A(k_j) = \frac{\Gamma\left(1+\frac{k_j}{2}\right)}{k_j!}. \tag{4.85}$$

Averaging the conditional moments (4.84) over the distribution of T (4.26) and interchanging the order of integration and summation, we obtain the moments of the multi-branch EGC output SNR in equally correlated Rayleigh fading channels as

$$m_n = (2n)! \left[\frac{\bar{\gamma}(1-\rho)}{L}\right]^n \sum_{\substack{k_1,\cdots,k_L=0 \\ k_1+\cdots+k_L=2n}}^{2n} \left[I(k_1,\ldots,k_L) \prod_{j=1}^{L} A(k_j)\right] \tag{4.86}$$

where $I(k_1,\ldots,k_L)$ is a single-fold integral which can be expressed in terms of the L-th order Appell hypergeometric function [2, Eq. (C.1)] as

$$\begin{aligned} I(k_1,\ldots,k_L) &= \int_0^\infty e^{-t} \prod_{j=1}^{L} {}_1F_1\left(-\frac{k_j}{2}, 1; -\frac{\rho t}{1-\rho}\right) dt \\ &= F_A\left(1; -\frac{k_1}{2}, \cdots, -\frac{k_L}{2}; \underbrace{1, \cdots, 1}_{\text{L terms}}; x_1, \ldots, x_L\right) \end{aligned} \tag{4.87}$$

where $x_k = -\frac{\rho}{1-\rho}$ for $k \in \{1,\ldots,L\}$ and $F_A(\alpha; \beta_1,\ldots,\beta_n; \gamma_1,\ldots,\gamma_n; x_1,\ldots,x_n)$ is the n-th order Appell hypergeometric function defined as [3, (9.180.2)]

$$\begin{aligned} &F_A(\alpha; \beta_1,\ldots,\beta_n; \gamma_1,\ldots,\gamma_n; x_1,\ldots,x_n) = \\ &\sum_{p_1=0}^{\infty} \cdots \sum_{p_n=0}^{\infty} \frac{(\alpha)_{p_1+\cdots+p_n} (\beta_1)_{p_1} \cdots (\beta_n)_{p_n}}{(\gamma_1)_{p_1} \cdots (\gamma_n)_{p_n} \, p_1! \cdots p_n!} x_1^{p_1} \cdots x_n^{p_n} \end{aligned} \tag{4.88}$$

whose convergence region is defined by $|x_1| + \ldots + |x_L| < 1$ [95]. Obviously (4.87) only converges for $-\frac{1}{L-1} < \rho < \frac{1}{L+1}$. Applying a transformation formula for the higher transcendental function of F_A, we obtain a convergent expression for (4.87) as

$$I(k_1, \ldots, k_L) = \frac{1-\rho}{1+(L-1)\rho} F_A\left(1; \beta_1, \cdots, \beta_L; 1, \cdots, 1; z_1, \ldots, z_L\right) \tag{4.89}$$

where $\beta_j = 1 + \frac{k_j}{2}$ and $z_j = \frac{\rho}{1+(L-1)\rho}$ for $j \in \{1, \ldots, L\}$. Since $0 \leq \rho < 1$, $|z_1| + \ldots + |z_L| = \frac{L\rho}{L\rho+(1-\rho)} < 1$, i.e., the Appell hypergeometric function F_A in (4.89) converges. Therefore, the moments of the EGC output SNR in equally correlated Rayleigh fading channel can be calculated using (4.89) and (4.85) with (4.86).

As comparison, we present the moments of the MRC output SNR in equally correlated Rayleigh fading channels here. The pdf of the MRC output SNR in such channels is given by [41, Eq. (12)]. Hence, the output moments are obtained as

$$E(\gamma_{\text{mrc}}^n) = \bar{\gamma}^n \left[\frac{(1-\rho)^{1+n}(L+n-1)!}{(1-\rho+L\rho)(L-1)!} {}_2F_1\left(1, L+n; L; \frac{L\rho}{1-\rho+L\rho}\right)\right]. \tag{4.90}$$

Next we present some special cases of (4.86).

1. Average output SNR

   Using [2, Eq. (C.4)], we can simplify the average output SNR of EGC in equally correlated Rayleigh fading channel in terms of the Gaussian hypergeometric function [3, Eq. (9.100)] as

   $$\bar{\gamma}_{\text{egc}} = m_1 = \bar{\gamma}\left[1 + \frac{(L-1)\pi}{4} {}_2F_1\left(-\frac{1}{2}, -\frac{1}{2}; 1; \rho^2\right)\right]. \tag{4.91}$$

   When $\rho = 0$, (4.91) reduces to the well-known result [13, Eq. (5.2-20)],

   $$\bar{\gamma}_{\text{egc}} = \bar{\gamma}\left[1 + \frac{(L-1)\pi}{4}\right]. \tag{4.92}$$

2. I.i.d. Rayleigh fading

   In the independent case ($\rho = 0$), (4.86) reduces to a closed-form expression as

   $$m_n = (2n)!\left(\frac{\bar{\gamma}}{L}\right)^n \sum_{\substack{k_1, \cdots, k_L = 0 \\ k_1 + \cdots + k_L = 2n}}^{2n} \left[\prod_{j=1}^{L} A(k_j)\right]. \tag{4.93}$$

3. Dual-branch EGC

The moments of the dual-branch ($L = 2$) EGC output SNR can be written as

$$m_n = \frac{(2n)!\bar{\gamma}}{2} \sum_{k=0}^{2n} A(k)A(2n-k)\, {}_2F_1\left(-\frac{k}{2}, -\frac{2n-k}{2}; 1; \rho^2\right). \tag{4.94}$$

The second moments of the dual-branch EGC output SNR can also be simplified as

$$m_2 = \bar{\gamma}^2 \left[\frac{5}{2} + \frac{3}{2}\rho^2 + \frac{3\pi}{4}\, {}_2F_1\left(-\frac{3}{2}, -\frac{1}{2}; 1; \rho^2\right)\right]. \tag{4.95}$$

Ricean Fading Channels

Following the above procedure, we first fix $\left(X_0 + \frac{m_1}{\sqrt{\rho}}\right)^2 + \left(Y_0 + \frac{m_2}{\sqrt{\rho}}\right)^2 = t$ in (4.8) and obtain a set of conditional independent Ricean RVs, $|G_k| \sim \mathcal{R}\left(\frac{\rho t}{1-\rho}, 1-\rho+\rho t\right)$. Then (4.83) can be used with (4.81) to derive the output moments for a given t:

$$m_n(t) = (2n)!\left[\frac{\bar{\gamma}(1-\rho)}{L(1+K)}\right]^n \sum_{\substack{k_1,\cdots,k_L=0 \\ k_1+\cdots+k_L=2n}}^{2n} \left[\prod_{j=1}^{L} A(k_j)\, {}_1F_1\left(-\frac{k_j}{2}, 1; -\frac{\rho t}{1-\rho}\right)\right]. \tag{4.96}$$

Similarly, averaging the conditional output moments (4.96) over the distribution of T (4.39), we obtain the moments of the EGC output SNR in equally correlated Ricean fading channels as

$$m_n = (2n)!\left[\frac{\bar{\gamma}(1-\rho)}{(1+K)L}\right]^n \sum_{\substack{k_1,\cdots,k_L=0 \\ k_1+\cdots+k_L=2n}}^{2n} \left[J(k_1,\ldots,k_L)\prod_{j=1}^{L} A(k_j)\right] \tag{4.97}$$

where $A(k_j)$ is defined as (4.85) and

$$J(k_1,\ldots,k_L) = e^{-\frac{K}{\rho}} \int_0^\infty e^{-t} I_0\left(2\sqrt{\frac{Kt}{\rho}}\right) \prod_{j=1}^{L} {}_1F_1\left(-\frac{k_j}{2}, 1; -\frac{\rho t}{1-\rho}\right) dt. \tag{4.98}$$

Using an infinite series expression [92, Eq. (9.6.10)] for $I_0(x)$ and applying the integral identity [2, Eq. (C.1)] and the transformation formula of F_A [95], we may express (4.98) in terms of the L-th order Appell hypergeometric function

$$\begin{aligned} J(k_1,\ldots,k_L) = e^{-\frac{K}{\rho}} \sum_{l=0}^{\infty} \frac{1}{l!}\left(\frac{K}{\rho}\right)^l \left(\frac{1-\rho}{1+(L-1)\rho}\right)^{l+1} \\ \times F_A\left(l+1; \beta_1, \cdots, \beta_L; 1, \cdots, 1; z_1, \ldots, z_L\right) \end{aligned} \tag{4.99}$$

where $\beta_j = 1+\frac{k_j}{2}$ and $z_j = \frac{\rho}{1+(L-1)\rho}$ for $j \in \{1, \ldots, L\}$. The moments of the multi-branch EGC output SNR in equally correlated Ricean fading channels can thus be computed using (4.99) and (4.85) with (4.97).

The average output SNR of EGC in equally correlated Ricean fading channels can be simplified in terms of the hypergeometric function of two variables, i.e., the second order Appell hypergeometric function, as

$$\bar{\gamma}_{\text{egc}} = m_1 = \bar{\gamma}\left[1 + e^{-\frac{K}{\rho}}\frac{(1-\rho)^2(L-1)\pi}{4(1+\rho)(1+K)}\sum_{j=0}^{\infty}\frac{1}{j!}\left(\frac{K(1-\rho)}{\rho(1+\rho)}\right)^j \times F_A\left(j+1; \frac{3}{2}, \frac{3}{2}; 1, 1; \frac{\rho}{1+\rho}, \frac{\rho}{1+\rho}\right)\right]. \tag{4.100}$$

Notice that the second order Appell hypergeometric function is available in common mathematical software such as Maple and Mathematica.

Nakagami-m Fading Channels

When m is an integer, the equally correlated Nakagami-m channel gains can be represented by (4.13) and (4.17). Fixing $\sum_{j=1}^{m}\left(X_{0j}^2 + Y_{0j}^2\right) = t$, we obtain a set of i.i.d. channel gains, $R_j^2 \sim \chi_{2m}\left(\sqrt{\rho t}, \frac{1-\rho}{2}\right)$. The moments of R_j can be found [6, Eq. (2-1-146)]

$$E\left(R_j^{k_j}\right) = (1-\rho)^{\frac{k_j}{2}}\frac{\Gamma\left(m+\frac{k_j}{2}\right)}{(m-1)!}\,{}_1F_1\left(-\frac{k_j}{2}, m; -\frac{\rho t}{1-\rho}\right). \tag{4.101}$$

Applying (4.19) and (4.101) with the property (4.82), we obtain the output moments of EGC conditioned on t as

$$m_n(t) = (2n)!\left[\frac{\bar{\gamma}(1-\rho)}{mL}\right]^n \sum_{\substack{k_1,\cdots,k_L=0 \\ k_1+\cdots+k_L=2n}}^{2n}\left[\prod_{j=1}^{L} B(k_j)\,{}_1F_1\left(-\frac{k_j}{2}, m; -\frac{\rho t}{1-\rho}\right)\right] \tag{4.102}$$

where

$$B(k_j) = \frac{\Gamma\left(m+\frac{k_j}{2}\right)}{(m-1)!\,k_j!}. \tag{4.103}$$

Averaging the conditional output moments (4.102) over the distribution of T (4.44), we can obtain the moments of the EGC output SNR in equally correlated Nakagami-m fading

channels as

$$\mu_n = (2n)!\left[\frac{\bar{\gamma}(1-\rho)}{mL}\right]^n \sum_{\substack{k_1,\cdots,k_L=0 \\ k_1+\cdots+k_L=2n}}^{2n} \left[K(k_1,\ldots,k_L)\prod_{i=1}^{L} B(k_j)\right] \tag{4.104}$$

where $K(k_1,\ldots,k_L)$ can also be expressed in terms of the L-th order Appell hypergeometric function as

$$\begin{aligned} K(k_1,\ldots,k_L) &= \frac{1}{(m-1)!}\int_0^\infty t^{m-1}e^{-t}\prod_{j=1}^{L} {}_1F_1\left(-\frac{k_j}{2}, m; -\frac{\rho t}{1-\rho}\right) dt \\ &= \frac{1}{(m-1)!}\left(\frac{1-\rho}{1+(L-1)\rho}\right)^m \\ &\quad \times F_A\left(m; \beta_1, \cdots, \beta_L; m, \cdots, m; z_1, \ldots, z_L\right). \end{aligned} \tag{4.105}$$

where $\beta_j = m + \frac{k_j}{2}$ and $z_j = \frac{\rho}{1+(L-1)\rho}$ for $j \in \{1,\ldots,L\}$. Combining (4.105) with (4.103) and (4.104), we can readily compute the moments of the multi-branch EGC output SNR in equally correlated Nakagami-m fading channels.

The average output SNR of EGC can be simplified as

$$\bar{\gamma}_{\text{egc}} = m_1 = \bar{\gamma}\left[1 + \frac{(L-1)\Gamma^2(m+\frac{1}{2})}{m\left[(m-1)!\right]^2}\, {}_2F_1\left(-\frac{1}{2}, -\frac{1}{2}; m; \rho^2\right)\right]. \tag{4.106}$$

4.5 Numerical Results

Several numerical results are given to illustrate the effect of fading correlation on the performance of multi-branch SC and EGC in several equally correlated fading channels. In all the figures, ρ is the fading correlation, L is the diversity order and $\hat{\gamma} = \frac{\gamma}{\bar{\gamma}}$ is the normalized branch SNR. Note that semi-analytical simulation results (denoted by circles or plus signs) are provided as an independent check of our analytical results. We use the Cholesky decomposition approach [96] to generate the equally correlated complex Gaussian variables and transform them to the Rayleigh, Ricean and Nakagami-m envelopes.

Fig. 4.1 shows the effect of diversity order L on the output cdf $F_{\text{sc}}(\hat{\gamma})$ of SC in equally correlated Rayleigh. The case of $L = 1$ represents a situation with no diversity. As expected, diversity gain can still be achieved even with correlated fading. The maximum

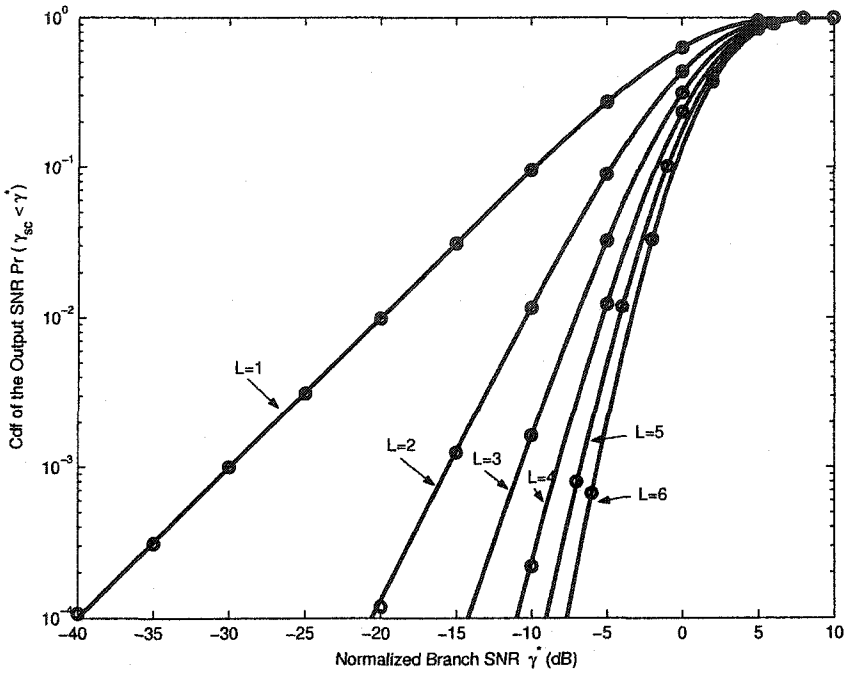

Figure 4.1: The cdf of the SC output SNR in equally correlated Rayleigh fading with different diversity orders. $\rho = 0.5$.

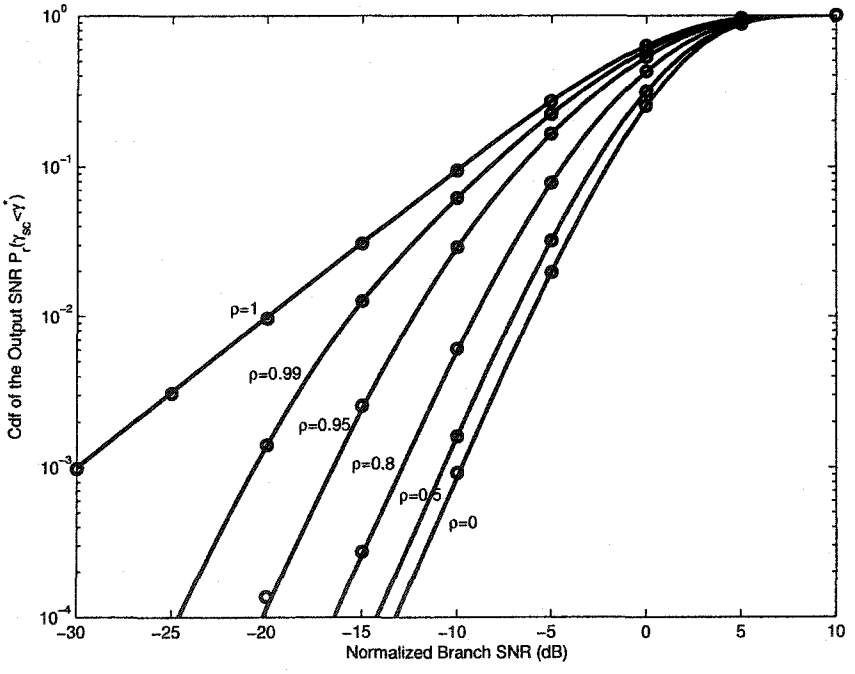

Figure 4.2: The cdf of the 4-branch SC output SNR in equally correlated Rayleigh fading with different fading correlations.

additional diversity gain is achieved with dual-branch diversity. With increasing L, the additional diversity gain diminishes, as is the case for independent fading.

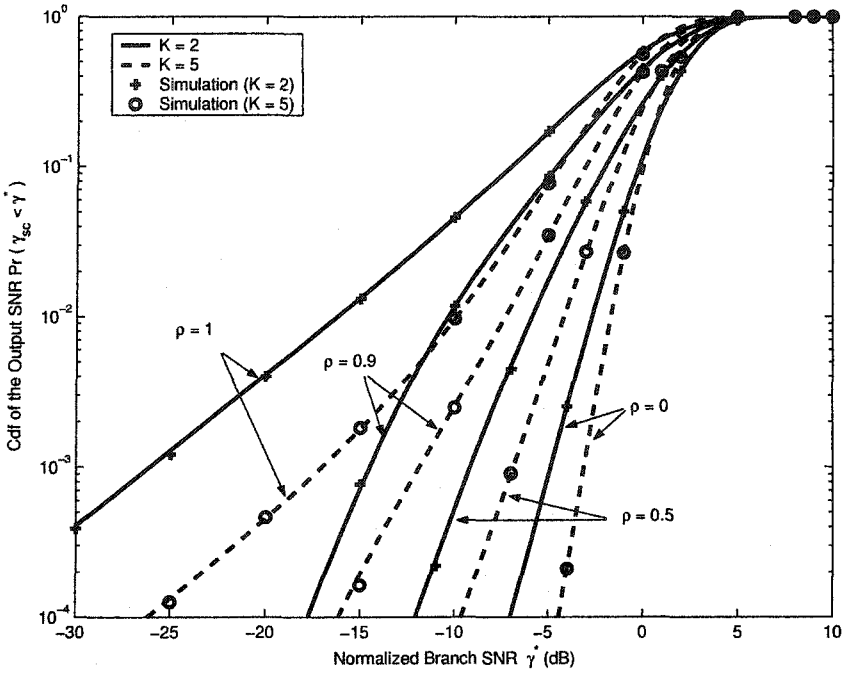

Figure 4.3: The cdf of the 4-branch SC output SNR in equally correlated Ricean fading with different fading correlations.

Figs. 4.2, 4.3 and 4.4 show the impact of fading correlation ρ on the output cdf of 4-branch SC in equally correlated Rayleigh, Ricean and Nakagami-m fading channels, respectively. The cases of $\rho = 0$ and $\rho = 1$ represent independent fading and the single branch case, respectively. Observe that the maximum diversity gain will not be achieved when correlated fading exists. The diversity gain decreases as ρ increases. However, the diversity gain is still available even with high correlation. We can also see that, in the low correlation case, where ρ is small, the performance of SC is comparable to that in the independent case. However, in heavily correlated fading channels, where ρ tends to 1, a minute increase of ρ will cause severe degradation of the SC performance.

Fig. 4.5 shows the impact of fading correlation ρ on the BER of BPSK with 4-branch SC in equally correlated Rayleigh fading channels. The correlation between the diversity branches results in significant loss in performance. As ρ increases, the performance of SC

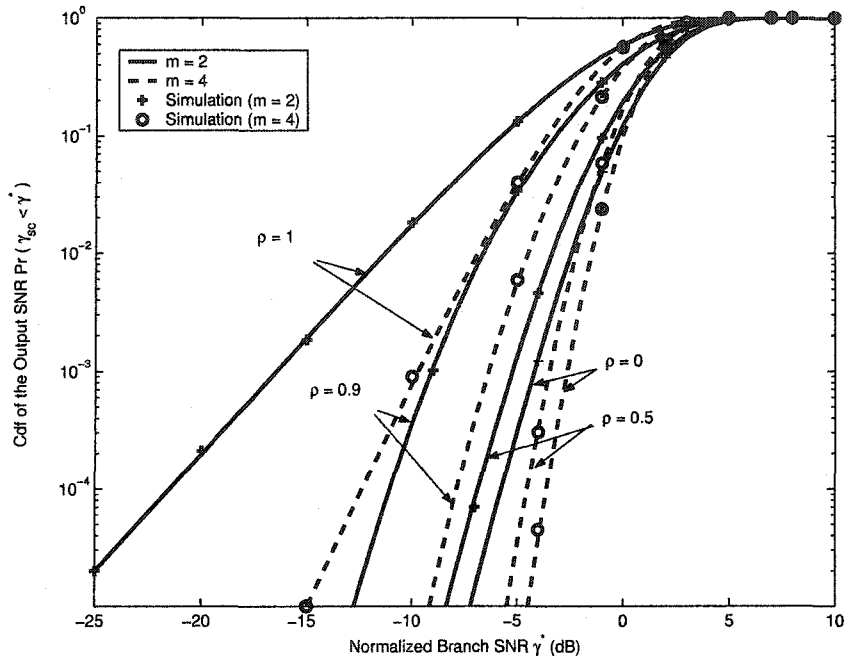

Figure 4.4: The cdf of the 4-branch SC output SNR in equally correlated Nakagami-*m* fading with different fading correlations.

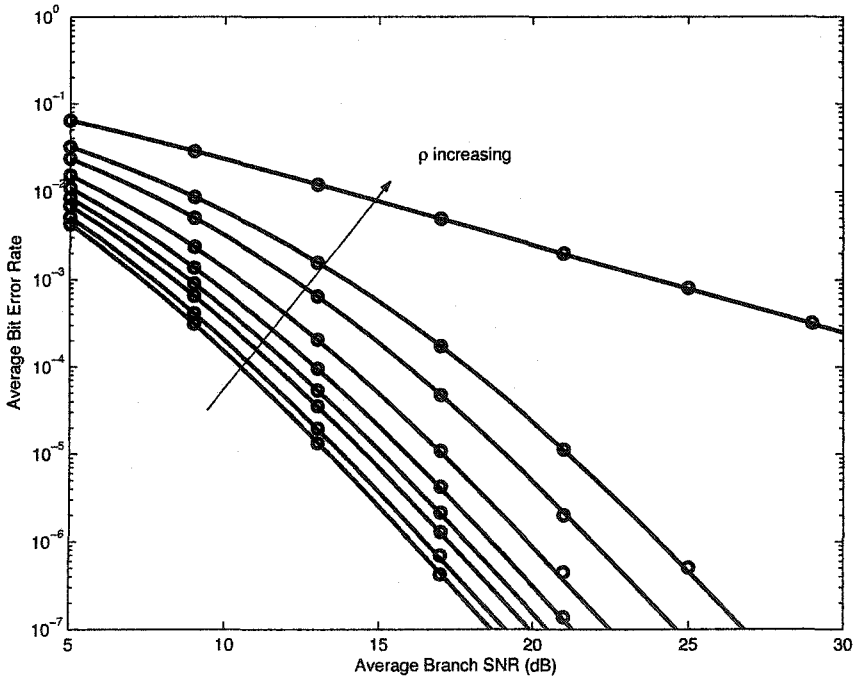

Figure 4.5: The average BER of BPSK with 4-branch SC in equally correlated Rayleigh fading channels. $\rho \in \{0, 0.3, 0.5, 0.6, 0.7, 0.8, 0.9, 0.95, 1\}$.

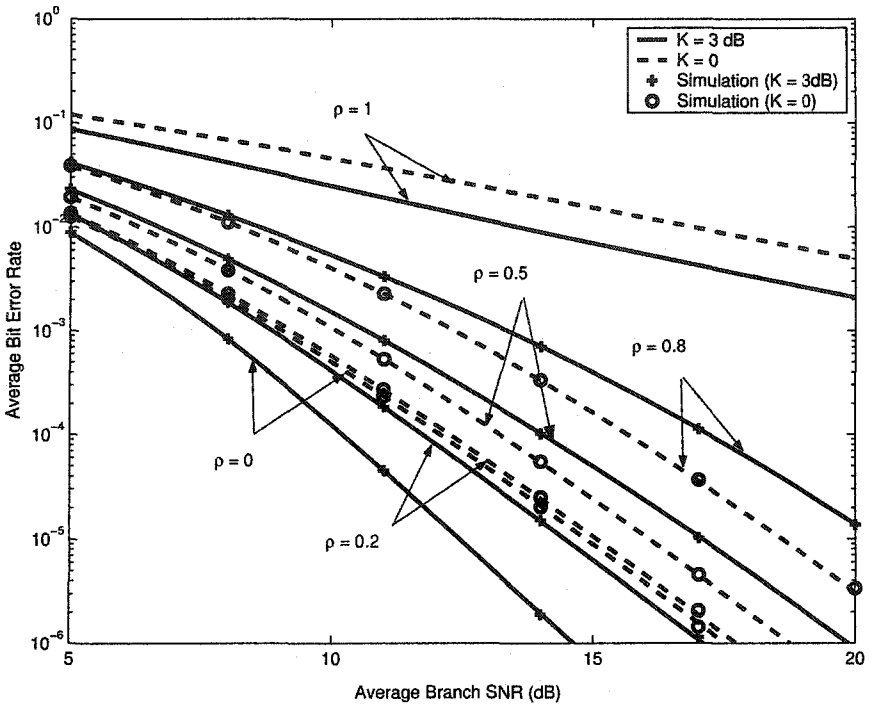

Figure 4.6: The average BER of binary DPSK with 4-branch SC in equally correlated Ricean fading channels with different fading correlations and Rice factors. $\rho \in \{0, 0.2, 0.5, 0.8, 1\}$, $K \in \{0, 3\text{dB}\}$.

degrades and the rate of degradation also increases.

Fig. 4.6 shows the impact of fading correlation ρ on the BER of binary DPSK with SC in equally correlated Rayleigh ($K = 0$) and Ricean fading channels. As ρ increases, the SC performance in both correlated Rayleigh and Ricean fading channels degrades. However, the SC performance in correlated Ricean fading degrades more rapidly in the low correlation case, but more slowly in the high correlation case than that in Rayleigh fading channels. This observation can be explained by the relationship between the fading correlation ρ and the power correlation ρ_η. As ρ increases, the ρ_η of Ricean fading (4.12) increases more rapidly when ρ is small but more slowly when ρ is large than that of Rayleigh fading (4.5). That is, Ricean fading is more sensitive than Rayleigh fading in the low correlation case, but less sensitive in the high correlation case. We also find that the impact of fading correlation in both Rayleigh and Ricean fading is more pronounced in the high SNR region.

Fig. 4.7 shows the impact of the fading correlation ρ on the performance of multi-

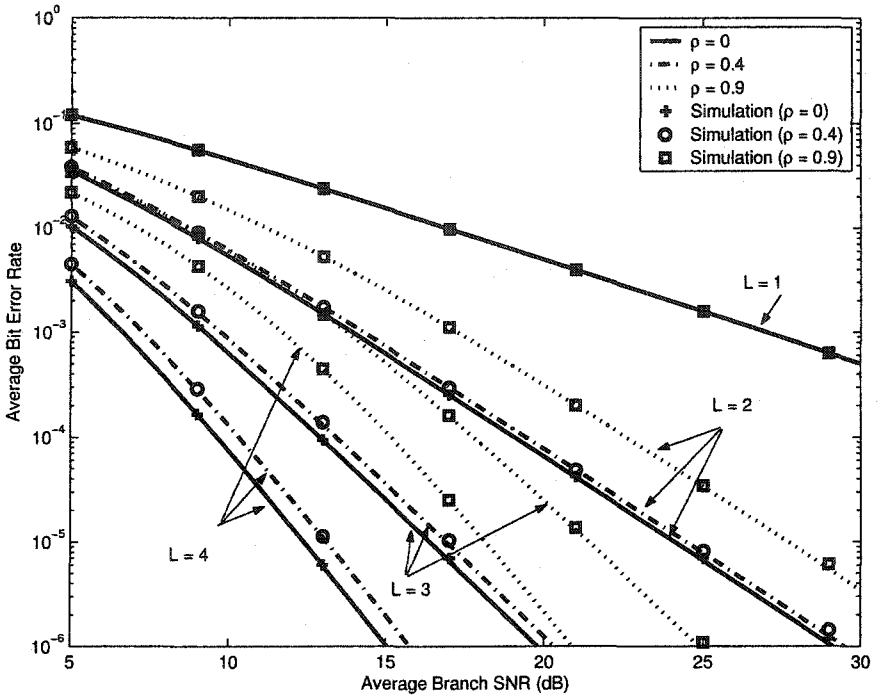

Figure 4.7: The average BER of binary DPSK with multi-branch EGC in equally correlated Rayleigh fading channels. $\rho \in \{0, 0.4, 0.9\}$.

branch EGC in equally correlated Rayleigh fading channels. As expected, the diversity gain can still be achieved even in highly correlated fading channels. Similar to the SC performance, the maximum diversity gain is achieved with dual-branch diversity. With increasing L, the additional diversity gain diminishes. This is more pronounced in higher SNRs. We also observe that, as ρ increases, the performance of binary DPSK degrades more rapidly when L is large. That is, higher-order diversity combiners are more sensitive to the fading correlation.

Fig. 4.8 shows the BER of binary DPSK with EGC in equally correlated Rayleigh ($K = 0$) and Ricean fading channels. For independent fading ($\rho = 0$), EGC always performs better in Ricean fading than Rayleigh fading. For correlated fading, the opposite occurs in the high SNRs. The same unexpected behavior has occurred for the SC performance (see Fig. 4.6). These surprising observations may also be explained by using the definition of fading correlation ρ (4.11). The fading correlation is defined as the correlation between two underlying CGRVs G_k and G_j ($k \neq j$). However, from (4.5) and (4.12), we

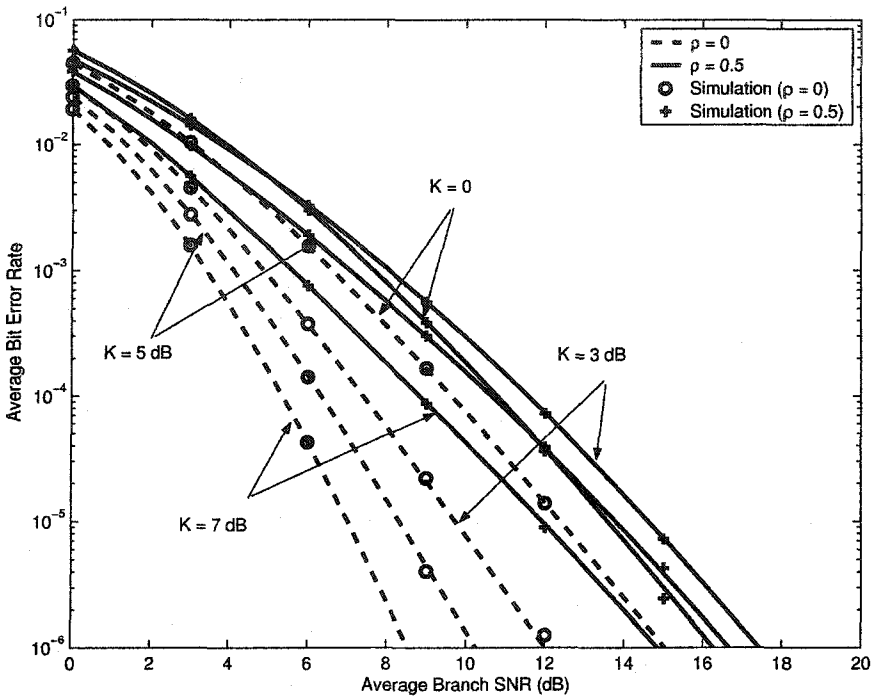

Figure 4.8: The average BER of binary DPSK with 4-branch EGC in equally correlated Ricean fading channels with different fading correlations and Rice factors. $\rho \in \{0, 0.5\}$, $K \in \{0, 3\text{dB}, 5\text{dB}, 7\text{dB}\}$.

find that for a certain value of ρ, the power correlation ρ_η of Ricean fading is larger than that of Rayleigh fading, that is the combined branches are more highly correlated in Ricean fading channels. Hence, two opposing mechanisms influence the diversity combiner performance in Ricean fading channels. First, the LOS component improves the performance. Second, the larger power correlation than that in Rayleigh fading channels degrades the performance. When the second mechanism dominates, the Ricean fading channel can be worse than the Rayleigh fading channel. Chang and McLane [97] have observed this situation for square-law combiners.

4.6 Conclusion

In this chapter, we have developed new representations for equally correlated Rayleigh, Ricean and Nakagami-*m* fading gains and these enable the performance analysis of multi-branch SC and EGC in correlated fading. We have derived analytical results for the average

error rates, the outage probability and the output moments of multi-branch SC and EGC in such channels. We have therefore solved the long-standing open problem of the multi-branch SC and EGC performance in equally correlated fading channels. Numerical results show that diversity benefits still exist in correlated fading channels, although the maximum diversity gain will not be achieved when fading is correlated. Higher-order diversity combiners are more sensitive to the fading correlation. We also observed and explained that the performance of diversity systems in correlated Ricean fading channels can be worse than that in correlated Rayleigh fading channels.

Chapter 5

Joint Distribution Functions of Three or Four Correlated Rayleigh RVs and Their Application in Diversity System Analysis

The channel gain representations developed in Chapter 4 only hold for equally correlated fading channels. For arbitrarily correlated fading channels, simple analytical results for the performance of multi-branch SC, EGC and GSC(M, L) are unknown. In this chapter, we derive new infinite series representations for the joint cdfs of the tri-variate and a certain class of quadri-variate Rayleigh distributions, which enable us to analyze the performance of 3-branch and 4-branch diversity combiners in arbitrarily correlated Rayleigh fading channels. Section 5.1 gives a short background introduction. Section 5.2 derives new infinite series representations for the joint pdfs and the joint cdfs of the tri-variate and a certain class of quadri-variate Rayleigh distributions. Bounds on the truncation errors of the infinite series, the joint moments and the joint chf of the tri-variate Rayleigh distribution are also derived. Section 5.3 presents some applications of the new results. Section 5.4 provides several numerical and simulation results. Section 5.5 concludes this chapter.

5.1 Introduction

The Rayleigh distribution is frequently used to model the received signal amplitudes in urban and suburban areas [10]. The joint pdf of a set of L correlated Rayleigh RVs is required for some performance analysis problems which include determining the impact of

fading correlation on diversity systems and modelling fading processes [13, 19, 98–100]. The pdf of **bivariate** correlated Rayleigh RVs has been derived by Rice [101]. Tan and Beaulieu [94] derived an infinite series representation for this **bivariate** joint cdf. It is exceedingly difficult to derive the joint pdf of the multi-variate correlated Rayleigh distribution and, indeed, Schwartz, Bennett and Stein claim that such joint pdf cannot be found [19]. Consequently, many published papers treating SC and EGC in correlated Rayleigh fading are limited to the dual-branch case [19, 73, 85, 86].

However, since the envelopes of multiple correlated CGRVs are Rayleigh distributed, the underlying complex Gaussian joint pdf can be converted to the polar form to give the joint pdf of amplitudes and phases and, in principle, the phase terms can be integrated out to give the joint amplitude pdf. Following this approach, Mallik [81] derives the joint pdf of the multi-variate Rayleigh distribution, which requires L-dimensional integration. Miller [102] derives an infinite series of products of the modified Bessel functions for the joint pdf of three correlated Rayleigh RVs. While this holds for arbitrary correlation models, it is intractable to derive the infinite series representation for the joint pdf when $L > 3$ using this approach. All the available results therefore treat restricted correlation models. For example, Blumenson and Miller [103] derive the joint pdf of L correlated Rayleigh RVs, providing the inverse covariance matrix $\mathbf{\Phi}$ of the underlying Gaussian RVs is tri-diagonal (i.e. $\phi_{ij} = 0$ if $|i-j| > 1$). The exponential correlation model generates this particular pattern. Using Blumenson and Miller's result [103], Karagiannidis *et al.* [77, 82] derive a joint distribution that holds only for **exponentially** correlated Nakagami fading channels.

In this chapter, we use Miller's result [102] to derive new infinite series representations for the joint pdf, cdf, moments and chf of three arbitrarily correlated Rayleigh RVs. For four correlated Rayleigh RVs, we generalize Blumenson and Miller's result [103] (which is limited to tri-diagonal inverse covariance matrices) to the case where the inverse covariance has five non-zero diagonals (i.e. only ϕ_{14} and ϕ_{41} need to be zero). Our tri-variate and quadri-variate cdf series generalize Tan and Beaulieu's series for the bivariate Rayleigh cdf [94]. Although there are many applications of the new pdf and cdf expressions, 3-branch and 4-branch diversity systems are particularly of interest. For diversity systems in

arbitrarily correlated Rayleigh channels, we evaluate the performance of 3-branch SC and derive the upper and lower bounds for the output ccdf of multi-branch ($L > 3$) SC. We further derive the moments of the 3-branch EGC output SNR and the output mgf of the GSC(2,3) receiver.

5.2 Tri-Variate and Quadri-Variate Distributions

This section derives infinite series representations for the joint pdf and the joint cdf of the tri-variate and a special class of quadri-variate Rayleigh distributions. The quadri-variate case considered in this section is more general than previous results [82]. New bounds for the truncation error of the infinite series are developed. The joint moments and the joint chf of the tri-variate Rayleigh distribution are also derived.

5.2.1 Joint Pdf and Cdf of Tri-Variate Rayleigh Distribution

Let $\boldsymbol{G} = \{G_1, G_2, G_3\}$ be joint CGRVs with zero means and positive definite covariance matrix $\boldsymbol{\Psi}$. We may write G_k in terms of polar coordinates as,

$$G_k = R_k \exp(i\Theta_k), \quad k \in \{1, 2, 3\}, \tag{5.1}$$

where $R_k = |G_k|$ is the envelope of G_k. Thus, $\boldsymbol{R} = \{R_1, R_2, R_3\}$ is a set of Rayleigh RVs and $\boldsymbol{\Theta} = \{\Theta_1, \Theta_2, \Theta_3\}$ is a set of jointly distributed phases. The joint pdf $p_{\boldsymbol{R},\boldsymbol{\Theta}}(\boldsymbol{r}, \boldsymbol{\theta})$ of $\boldsymbol{R}$ and $\boldsymbol{\Theta}$ can be related to the density $p_{\boldsymbol{G}}(\boldsymbol{g})$ of $\boldsymbol{G}$. Hence, the marginal density $p_{\boldsymbol{R}}(\boldsymbol{r})$ can be obtained by integrating out $p_{\boldsymbol{R},\boldsymbol{\Theta}}(\boldsymbol{r}, \boldsymbol{\theta})$ over $\boldsymbol{\theta}$ [80, 102]. This approach yields

$$\begin{aligned} p_{\boldsymbol{R}}(r_1, r_2, r_3) =& 8 \det(\boldsymbol{\Phi}) r_1 r_2 r_3 e^{-(r_1^2\phi_{11} + r_2^2\phi_{22} + r_3^2\phi_{33})} \sum_{k=0}^{\infty} \varepsilon_k (-1)^k \cos(k\chi) \\ & \times I_k(2r_1 r_2 |\phi_{12}|)\ I_k(2r_2 r_3 |\phi_{23}|)\ I_k(2r_3 r_1 |\phi_{31}|) \end{aligned} \tag{5.2}$$

where ε_k is the Neumann factor ($\varepsilon_0 = 1$, $\varepsilon_k = 2$ for $k = 1, 2, \cdots$) and

$$\chi = \chi_{12} + \chi_{23} + \chi_{31}, \tag{5.3}$$

and $\boldsymbol{\Phi}$ is the inverse covariance matrix

$$\boldsymbol{\Phi} = \boldsymbol{\Psi}^{-1} = \begin{bmatrix} \phi_{11} & \phi_{12} & \phi_{13} \\ \phi_{12}^* & \phi_{22} & \phi_{23} \\ \phi_{13}^* & \phi_{23}^* & \phi_{33} \end{bmatrix}, \quad \phi_{jk} = |\phi_{jk}| e^{i\chi_{jk}}. \tag{5.4}$$

The expression (5.2) is not much useful as it is not in a product form of the variables r_1, r_2 and r_3. Representing the modified Bessel function by an infinite series [92, Eq. (9.6.10)], we readily obtain an infinite series representation for the joint pdf as

$$p_{\boldsymbol{R}}(r_1, r_2, r_3) = 8 \det(\boldsymbol{\Phi}) e^{-(r_1^2\phi_{11}+r_2^2\phi_{22}+r_3^2\phi_{33})} \sum_{k=0}^{\infty} \varepsilon_k (-1)^k \cos(k\chi) \sum_{l,m,n=0}^{\infty} \frac{|\phi_{12}|^{2l+k}}{l!(l+k)!} \times \frac{|\phi_{23}|^{2m+k}|\phi_{31}|^{2n+k}}{m!(m+k)!n!(n+k)!} r_1^{2(l+n+k)+1} r_2^{2(l+m+k)+1} r_3^{2(m+n+k)+1}. \quad (5.5)$$

Note that (5.5) is in a product form of r_1, r_2, r_3 and is therefore suitable for our purposes. The joint tri-variate cdf is now given by

$$F_{\boldsymbol{R}}(\lambda_1, \lambda_2, \lambda_3) = 8(\det \boldsymbol{\Phi}) \sum_{k=0}^{\infty} \varepsilon_k (-1)^k \cos(k\chi) \sum_{i,j,k=0}^{\infty} \frac{|\phi_{12}|^{2l+k}|\phi_{23}|^{2m+k}|\phi_{31}|^{2n+k}}{l!(l+k)!m!(m+k)!n!(n+k)!} \times \int_0^{\lambda_1} r_1^{2(l+n+k)+1} e^{-r_1^2\phi_{11}} dr_1 \int_0^{\lambda_2} r_2^{2(l+m+k)+1} e^{-r_2^2\phi_{22}} dr_2 \times \int_0^{\lambda_3} r_3^{2(m+n+k)+1} e^{-r_3^2\phi_{33}} dr_3. \quad (5.6)$$

Making the transformation $x_1 = r_1^2\phi_{11}$, $x_2 = r_2^2\phi_{22}$ and $x_3 = r_3^2\phi_{33}$ and using the definition of the incomplete gamma function [92], we obtain the infinite series representation for the joint tri-variate cdf as

$$F_{\boldsymbol{R}}(\lambda_1, \lambda_2, \lambda_3) = \frac{\det(\boldsymbol{\Phi})}{\phi_{11}\phi_{22}\phi_{33}} \sum_{k=0}^{\infty} \varepsilon_k (-1)^k \cos(k\chi) \sum_{l,m,n=0}^{\infty} C\, \nu_{12}^{l+\frac{k}{2}} \nu_{23}^{m+\frac{k}{2}} \nu_{31}^{n+\frac{k}{2}} \times \gamma(\delta_1, \lambda_1^2\phi_{11})\, \gamma(\delta_2, \lambda_2^2\phi_{22})\, \gamma(\delta_3, \lambda_3^2\phi_{33}) \quad (5.7)$$

where χ is defined as (5.3) and

$$C = \frac{1}{l!\,(n+k)!\,m!\,(l+k)!\,n!\,(m+k)!}, \quad (5.8a)$$

$$\nu_{jk} = \frac{|\phi_{jk}|^2}{\phi_{jj}\phi_{kk}}, \quad (5.8b)$$

$$\delta_1 = l + n + k + 1, \quad (5.8c)$$

$$\delta_2 = m + l + k + 1, \quad (5.8d)$$

$$\delta_3 = n + m + k + 1, \quad (5.8e)$$

which will be used throughout this chapter for brevity. The cdf (5.7) holds for any arbitrary 3×3 correlation matrix. Let us consider two commonly used spatial correlation models.

1. Equally correlated model

   The equally correlated model is valid for a set of closely-placed antennas [41]. The normalized correlation matrix of this model is given by $\psi_{jk} = \rho$ $(j \neq k)$ and $\psi_{jj} = 1$, where $-\frac{1}{2} \leq \rho < 1$. It can be shown that $\chi = \chi_{12} + \chi_{23} + \chi_{31} = 3\pi$. Thus, the joint cdf (5.7) reduces to

$$F_{\boldsymbol{R}}(\lambda_1, \lambda_2, \lambda_3) = \frac{(1-\rho)(1+2\rho)^2}{(1+\rho)^3} \sum_{k=0}^{\infty} \varepsilon_k \sum_{l,m,n=0}^{\infty} C \left(\frac{\rho}{1+\rho}\right)^{\delta_1+\delta_2+\delta_3-3} \times \gamma\left(\delta_1, \frac{(1+\rho)\lambda_1^2}{1+\rho-2\rho^2}\right) \gamma\left(\delta_2, \frac{(1+\rho)\lambda_2^2}{1+\rho-2\rho^2}\right) \gamma\left(\delta_3, \frac{(1+\rho)\lambda_3^2}{1+\rho-2\rho^2}\right). \tag{5.9}$$

2. Exponentially correlated model

   The exponentially correlated model can be used to describe the correlation among equally-spaced linear antenna arrays [82]. The normalized correlation matrix of this model is described as $\psi_{jk} = E(G_j G_k^*) = \rho^{|j-k|}$, where $0 \leq \rho < 1$. It can then be shown that $\phi_{31} = \phi_{13} = 0$. Thus the joint cdf can be simplified considerably to

$$F_{\boldsymbol{R}}(\lambda_1, \lambda_2, \lambda_3) = \frac{1-\rho^2}{1+\rho^2} \sum_{l,m=0}^{\infty} \frac{1}{(l!)^2\,(m!)^2} \left(\frac{\rho^2}{1+\rho^2}\right)^{l+m} \gamma\left(l+1, \frac{\lambda_1^2}{1-\rho^2}\right) \times \gamma\left(l+m+1, \frac{(1+\rho^2)\lambda_2^2}{1-\rho^2}\right) \gamma\left(m+1, \frac{\lambda_3^2}{1-\rho^2}\right) \tag{5.10}$$

   which is equivalent to [82, Eq. (6)].

5.2.2 Joint Pdf and Cdf of Quadri-Variate Rayleigh Distribution

Blumenson and Miller [103] derive the joint pdf and the joint cdf of the multi-variate Rayleigh distribution. However, their expression is only valid when the inverse covariance matrix satisfies $\phi_{jk} = 0$ for $|j-k| > 1$ (i.e. for the matrix in (5.11), both ϕ_{13} and ϕ_{24} would be zero). However, we can derive more general results than [103], and we consider the inverse covariance matrix given by

$$\boldsymbol{\Phi} = \boldsymbol{\Psi}^{-1} = \begin{bmatrix} \phi_{11} & \phi_{12} & \phi_{13} & 0 \\ \phi_{12}^* & \phi_{22} & \phi_{23} & \phi_{24} \\ \phi_{13}^* & \phi_{23}^* & \phi_{33} & \phi_{34} \\ 0 & \phi_{24}^* & \phi_{34}^* & \phi_{44} \end{bmatrix}, \quad \phi_{jk} = |\phi_{jk}| e^{i\chi_{jk}}. \tag{5.11}$$

We show that the joint pdf of the quadri-variate Rayleigh distribution with positive definite Ψ and its Φ satisfying (5.11) can be obtained as a product of the modified Bessel functions of the first kind (see Appendix B)

$$p_R(r_1, r_2, r_3, r_4) = 16\det(\Phi) r_1 r_2 r_3 r_4 e^{-(r_1^2\phi_{11}+r_2^2\phi_{22}+r_3^2\phi_{33}+r_4^2\phi_{44})} \sum_{j=0}^{\infty}\sum_{k=-\infty}^{\infty} \varepsilon_j (-1)^{j+k}$$
$$\times \cos[i(\chi_{12}+\chi_{23}+\chi_{31}) + k(\chi_{23}+\chi_{34}+\chi_{42})]\, I_j(2r_1r_2|\phi_{12}|) \quad (5.12)$$
$$\times I_j(2r_1r_3|\phi_{13}|)\, I_k(2r_2r_4|\phi_{24}|)\, I_k(2r_3r_4|\phi_{34}|)\, I_{j+k}(2r_2r_3|\phi_{23}|).$$

To the best of our knowledge, (5.12) is a novel result which allows evaluation of 4-branch diversity combiners in several kinds of correlated fading channels. Eq. (5.12) reduces to previous results for two special cases. We believe that an expression akin to (5.12) *cannot* be derived unless $\phi_{14} = 0$. Thus, this appears to be the most general quadri-variate case that yields an infinite series solution. Moreover, if ϕ_{14} is not zero in a given application, we may choose a "best" approximation of Φ satisfying (5.11).

1. Independent Rayleigh envelopes

   Since the covariance matrix Ψ for independent Rayleigh RVs is diagonal, the inverse covariance matrix Φ is also diagonal, which is given by $\phi_{jk} = 0\,(j \neq k)$ and $\phi_{jj} = 1$ for $j, k \in \{1, \cdots, 4\}$. Therefore, our new expression (5.12) can be simplified to

   $$p_R(\lambda_1, \lambda_2, \lambda_3, \lambda_4) = \frac{16 r_1 r_2 r_3 r_4}{\psi_{11}\psi_{22}\psi_{33}\psi_{44}} e^{-\left(\frac{r_1^2}{\psi_{11}}+\frac{r_2^2}{\psi_{22}}+\frac{r_3^2}{\psi_{33}}+\frac{r_4^2}{\psi_{44}}\right)}, \quad (5.13)$$

   which is the product of four independent Rayleigh pdfs [6, Eq. (2-1-128)].

2. Exponentially correlated Rayleigh envelopes

   Substituting $\phi_{24} = \phi_{13} = 0$ into (5.12), we obtain the joint pdf of the exponentially correlated quadri-variate Rayleigh distribution

   $$p_R(r_1, r_2, r_3, r_4) = \frac{16 r_1 r_2 r_3 r_4}{(1-\rho^2)^3} e^{-\left(\frac{r_1^2+r_4^2}{1-\rho^2}+\frac{(1+\rho^2)(r_2^2+r_3^2)}{1-\rho^2}\right)} I_0\left(\frac{2r_1r_2\rho}{1-\rho^2}\right) \quad (5.14)$$
   $$\times I_0\left(\frac{2r_3r_4\rho}{1-\rho^2}\right) I_0\left(\frac{2r_2r_3\rho}{1-\rho^2}\right)$$

   where $\rho = \psi_{12} = E(G_1 G_2^*)$. This expression is equivalent to the previous result [82, Eq. (3)].

Expanding $I_m(x)$ in infinite series and integrating (5.12) yield an infinite series representation for the corresponding joint cdf

$$F_R(\lambda_1,\lambda_2,\lambda_3,\lambda_4) = \frac{\det(\Phi)}{\phi_{11}\phi_{22}\phi_{33}\phi_{44}} \sum_{j=0}^{\infty}\sum_{k=-\infty}^{\infty} \varepsilon_j (-1)^{j+k} \cos\omega \sum_{l,m,n,u=0}^{\infty} \nu_{12}^{l+\frac{j}{2}} \nu_{13}^{m+\frac{j}{2}} \nu_{24}^{n+\frac{|k|}{2}}$$
$$\times \nu_{34}^{u+\frac{|k|}{2}} \frac{\gamma(u+|k|+n+1, \lambda_4^2\phi_{44})\, \gamma(l+j+m+1, \lambda_1^2\phi_{11})}{l!\,m!\,n!\,u!\,(l+j)!\,(m+j)!\,(u+|k|)!\,(n+|k|)!} \sum_{v=0}^{\infty} \nu_{23}^{v+\frac{|j+k|}{2}}$$
$$\times \frac{\gamma\left(m+n+v+\tau+1, \lambda_2^2\phi_{22}\right)\gamma\left(m+u+v+\tau+1, \lambda_3^2\phi_{33}\right)}{v!\,(v+\frac{|j+k|}{2})!} \tag{5.15}$$

where $\omega = j(\chi_{12}+\chi_{23}+\chi_{31}) + k(\chi_{23}+\chi_{34}+\chi_{42})$ and $\tau = (|j+k|+|k|+j)/2$. We observe that both (5.5) and (5.12) are series of the product of the modified Bessel functions. For brevity, we only discuss the tri-variate Rayleigh distribution and its applications in the rest of this chapter. Similar results can be obtained for the special class of quadri-variate Rayleigh distribution.

5.2.3 Truncation Error

Assume that the cdf series (5.7) is limited to K, L, M and N terms in the variables k, l, m and n, respectively. The remaining terms constitute the truncation error. It is desirable to obtain a simple bound for the truncation error because such a bound is useful for studying the impact of correlation Ψ on the truncation error. Unfortunately, this is not always possible. For example, Tan and Beaulieu [94] derive a truncation error bound in terms of the confluent hypergeometric functions, where the relationship between the correlation ρ and the truncation error is not immediately evident. Here we provide an alternative method to bound the truncation error.

We notice that the incomplete gamma function $\gamma(a,x) \le \Gamma(a)$ and $|\cos(\chi)| \le 1$. The truncation error of (5.7) can therefore be upper bounded by

$$|E_T| \le \sum_{k=K}^{\infty}\sum_{l=0}^{\infty}\sum_{m=0}^{\infty}\sum_{n=0}^{\infty} G(k,l,m,n) + \sum_{k=0}^{K-1}\sum_{l=L}^{\infty}\sum_{m=0}^{\infty}\sum_{n=0}^{\infty} G(k,l,m,n)$$
$$+ \sum_{k=0}^{K-1}\sum_{l=0}^{L-1}\sum_{m=M}^{\infty}\sum_{n=0}^{\infty} G(k,l,m,n) + \sum_{k=0}^{K-1}\sum_{l=0}^{L-1}\sum_{m=0}^{M-1}\sum_{n=N}^{\infty} G(k,l,m,n) \tag{5.16}$$

where

$$G(k,l,m,n) = \frac{\det(\Phi)}{\phi_{11}\phi_{22}\phi_{33}}\varepsilon_k \binom{l+n+k}{l}\binom{l+m+k}{m} \times \binom{m+n+k}{n} \nu_{12}^{l+\frac{k}{2}} \nu_{23}^{m+\frac{k}{2}} \nu_{31}^{n+\frac{k}{2}}. \tag{5.17}$$

Further simplification of (5.16) is complicated. Due to the space limitation, we only provide an upper bound for the truncation error in the special case of exponentially correlated models where $\phi_{13} = 0$. This leads to

$$\begin{aligned} |E_T| \leq & \frac{1-\rho^2}{1+\rho^2}\left[\sum_{l=L}^{\infty}\sum_{m=0}^{\infty}\binom{l+m}{m}\left(\frac{\rho^2}{1+\rho^2}\right)^{l+m} + \sum_{l=0}^{L-1}\sum_{m=M}^{\infty}\binom{l+m}{m}\left(\frac{\rho^2}{1+\rho^2}\right)^{l+m}\right] \\ = & 1 - \frac{1-\rho^2}{1+\rho^2}\sum_{l=0}^{L-1}\sum_{m=0}^{M-1}\binom{l+m}{M}\left(\frac{\rho^2}{1+\rho^2}\right)^{l+m} \\ \leq & 1-(1-\rho^4)\left[1-\left(\frac{\rho^2}{1+\rho^2}\right)^{L}\right]\left[1-\left(\frac{\rho^2}{1+\rho^2}\right)^{M}\right]. \end{aligned} \tag{5.18}$$

As expected, the upper bound for the truncation error increases as ρ increases and decreases as the number of terms increases.

5.2.4 Joint Moments and Chf of Tri-Variate Rayleigh Distribution

Moments and chf are often used to characterize the RVs. Using the infinite series representation for the joint tri-variate pdf (5.5), we derive the corresponding joint moments and joint chf.

If $\alpha, \beta, \theta > -2$, the joint moments are given by

$$\begin{aligned} E(r_1^{\alpha} r_2^{\beta} r_3^{\theta}) = & \int_0^{\infty}\int_0^{\infty}\int_0^{\infty} r_1^{\alpha} r_2^{\beta} r_3^{\theta} p_R(r_1, r_2, r_3)\, dr_3 dr_2 dr_1 \\ = & \frac{\det(\Phi)}{\phi_{11}^{1+\frac{\alpha}{2}}\phi_{22}^{1+\frac{\beta}{2}}\phi_{33}^{1+\frac{\theta}{2}}} \sum_{k=0}^{\infty}\varepsilon_k(-1)^k\cos(k\chi) \sum_{l,m,n=0}^{\infty} C\, \nu_{12}^{l+\frac{k}{2}} \nu_{23}^{m+\frac{k}{2}} \nu_{31}^{n+\frac{k}{2}} \\ & \times \Gamma\left(\delta_1 + \frac{\alpha}{2}\right)\Gamma\left(\delta_2 + \frac{\beta}{2}\right)\Gamma\left(\delta_3 + \frac{\theta}{2}\right). \end{aligned} \tag{5.19}$$

The joint moments have many applications. We will show that statistical moments of the output SNR of certain diversity systems can be evaluated using (5.19).

The joint chf of the tri-variate Rayleigh distribution is defined as the statistical average

$$\begin{aligned}\phi(v_1, v_2, v_3) =& E[e^{i(v_1 r_1 + v_2 r_2 + v_3 r_3)}] \\ =& \left(\frac{\det \Phi}{\phi_{11}\phi_{22}\phi_{33}}\right) \sum_{k=0}^{\infty} \varepsilon_k (-1)^k \cos(k\chi) \sum_{l,m,n=0}^{\infty} C\, v_{12}^{l+\frac{k}{2}} v_{23}^{m+\frac{k}{2}} v_{31}^{n+\frac{k}{2}} \\ & \times e^{-\left(\frac{v_1^2}{8\phi_{11}} + \frac{v_2^2}{8\phi_{22}} + \frac{v_3^2}{8\phi_{33}}\right)} \frac{(2\delta_1 - 1)!(2\delta_2 - 1)!(2\delta_3 - 1)!}{2^{\delta_1+\delta_2+\delta_3-3}} \\ & \times D_{-2\delta_1}\left(\frac{-iv_1}{\sqrt{2\phi_{11}}}\right) D_{-2\delta_2}\left(\frac{-iv_2}{\sqrt{2\phi_{22}}}\right) D_{-2\delta_3}\left(\frac{-iv_3}{\sqrt{2\phi_{33}}}\right). \end{aligned} \tag{5.20}$$

5.3 Applications

The new results developed in the last section enable the performance analysis of several 3-branch and 4-branch diversity systems in arbitrarily correlated Rayleigh fading channels. This section presents four possible applications.

5.3.1 Performance Analysis of 3-Branch SC

The cdf of the 3-branch SC output SNR can be readily derived using (5.7) and (1.27) as

$$F_{\text{SC}}(x) = F_{\boldsymbol{R}}\left(\sqrt{\frac{x\psi_{11}}{\bar{\gamma}_1}}, \sqrt{\frac{x\psi_{22}}{\bar{\gamma}_2}}, \sqrt{\frac{x\psi_{33}}{\bar{\gamma}_3}}\right). \tag{5.21}$$

Eq. (5.21) holds for any arbitrary 3×3 correlation matrix. For independent fading channels, the cdf of the 3-branch SC output SNR (5.21) reduces to

$$F_{\text{SC}}(x) = (1 - e^{-\frac{x}{\bar{\gamma}_1}})(1 - e^{-\frac{x}{\bar{\gamma}_2}})(1 - e^{-\frac{x}{\bar{\gamma}_3}}), \tag{5.22}$$

which is equivalent to the well-known result [19, 10-4-9]. Replacing λ_k with $\sqrt{\frac{x\psi_{kk}}{\bar{\gamma}_k}}$ in (5.9) and (5.10), we obtain simplified expressions for the output cdf of 3-branch SC in equally and exponentially correlated fading channels. For example, the cdf of 3-branch SC in equally correlated fading channel is given by

$$\begin{aligned} F_{\text{SC}}(x) =& \frac{(1-\rho)(1+2\rho)^2}{(1+\rho)^3} \sum_{k=0}^{\infty} \varepsilon_k \sum_{l,m,n=0}^{\infty} C \left(\frac{\rho}{1+\rho}\right)^{\delta_1+\delta_2+\delta_3-3} \gamma\left(\delta_1, \frac{(1+\rho)x}{(1+\rho-2\rho^2)\bar{\gamma}}\right) \\ & \times \gamma\left(\delta_2, \frac{(1+\rho)x}{(1+\rho-2\rho^2)\bar{\gamma}}\right) \gamma\left(\delta_3, \frac{(1+\rho)x}{(1+\rho-2\rho^2)\bar{\gamma}}\right). \end{aligned} \tag{5.23}$$

We have checked (5.23) numerically against an alternative cdf expression (4.40). Both the methods give exactly the same numerical values.

The convergence rate of the cdf series (5.21) depends not only on the correlation among the branch signals Ψ but also on the normalized branch SNRs $x/\bar{\gamma}_k$. Without loss of generality, we investigate the convergence property of the cdf series for the equally correlated case. Table 5.1 lists the number of terms required in each sum of (5.23) to achieve five significant figure accuracy for different correlations ρ and the normalized branch SNRs $x/\bar{\gamma}$. The total number of terms required is equal to $K \times L \times M \times N$, where K, L, M, N denote the number of terms required in the variables k, l, m and n, respectively. We find that the cdf series (5.23) converges much faster as the correlation or the normalized branch SNR decreases.

Table 5.1: The number of terms needed in (5.23) to achieve five significant figure accuracy.

	$x/\bar{\gamma} = 0$dB	$x/\bar{\gamma} = 5$dB
$\rho = 0.2$	$K = 2, L = M = N = 3$	$K = 3, L = M = N = 4$
$\rho = 0.5$	$K = L = M = N = 4$	$K = L = M = N = 5$
$\rho = 0.8$	$K = 4, L = M = N = 6$	$K = 7, L = M = N = 10$

Average Error Rate

Eq. (5.21) can be readily used with (4.50) to derive single-integral expressions for the average error rates of various digital modulations with 3-branch SC in arbitrarily correlated Rayleigh fading channels (see 4.3.2 for details). In the following, we provide just two examples of such analysis for brevity.

1. BPSK and Coherent BFSK: Substituting the output cdf (5.21) into (4.52), we obtain the average BER of BPSK and coherent BFSK with 3-branch SC in arbitrarily correlated Rayleigh fading channels as

$$\bar{P}_e = \frac{\det(\Phi)}{\phi_{11}\phi_{22}\phi_{33}} \sum_{k=0}^{\infty} \varepsilon_k (-1)^k \cos(k\chi) \sum_{l,m,n=0}^{\infty} C\, \nu_{12}^{l+\frac{k}{2}} \nu_{23}^{m+\frac{k}{2}} \nu_{31}^{n+\frac{k}{2}} \times \frac{a}{2}\sqrt{\frac{b}{2\pi}} \int_0^{\infty} x^{-\frac{1}{2}} e^{-\frac{bx}{2}} \gamma(\delta_1, d_1 x)\, \gamma(\delta_2, d_2 x)\, \gamma(\delta_3, d_3 x)\, dx \tag{5.24}$$

where $(a, b) = (1, 2)$ for BPSK, $(a, b) = (1, 1)$ for coherent BFSK and

$$d_k = \psi_{kk}\phi_{kk}/\bar{\gamma}_k, \quad k \in \{1, 2, 3\}. \tag{5.25}$$

Noticing the relation between the incomplete gamma function and the confluent hypergeometric function [3, Eq. (9.236.4)] and applying the integral identity [2, Eq. (C.1)] and the transformation formula of the Appell hypergeometric function [95], we obtain the average BER as

$$\begin{aligned}\bar{P}_e = & \frac{a\det(\mathbf{\Phi})}{\phi_{11}\phi_{22}\phi_{33}} \sum_{k=0}^{\infty} \varepsilon_k (-1)^k \cos(k\chi) \\ & \times \sum_{l,m,n=0}^{\infty} C \nu_{12}^{l+\frac{k}{2}} \nu_{23}^{m+\frac{k}{2}} \nu_{31}^{n+\frac{k}{2}} d_1^{\delta_1} d_2^{\delta_2} d_3^{\delta_3} \frac{2^{\delta-1}\Gamma\left(\delta+\frac{1}{2}\right)}{\sqrt{\pi} b^{\delta} \delta_1 \delta_2 \delta_3} \left(\frac{b}{2d+b}\right)^{\delta+\frac{1}{2}} \\ & \times F_A\left(\delta+\frac{1}{2}; 1, 1, 1; \delta_1+1, \delta_2+1, \delta_3+1; \frac{2d_1}{2d+b}, \frac{2d_2}{2d+b}, \frac{2d_3}{2d+b}\right)\end{aligned} \tag{5.26}$$

where d_k's are defined as (5.25) and

$$\delta = \delta_1 + \delta_2 + \delta_3 = 2(l + m + n) + 3(k + 1), \tag{5.27a}$$

$$d = d_1 + d_2 + d_3 = \sum_{k=1}^{3} \psi_{kk}\phi_{kk}/\bar{\gamma}_k. \tag{5.27b}$$

These notations will be used in the subsequent results.

2. Binary DPSK and Non-Coherent BFSK: Similarly, substituting (5.21) into (4.55), we obtain the average BER of binary DPSK and non-coherent BFSK after some algebra,

$$\begin{aligned}\bar{P}_e = & \frac{ab\det(\mathbf{\Phi})}{\phi_{11}\phi_{22}\phi_{33}} \sum_{k=0}^{\infty} \varepsilon_k (-1)^k \cos(k\chi) \\ & \times \sum_{l,m,n=0}^{\infty} C\, \nu_{12}^{l+\frac{k}{2}} \nu_{23}^{m+\frac{k}{2}} \nu_{31}^{n+\frac{k}{2}} d_1^{\delta_1} d_2^{\delta_2} d_3^{\delta_3} \frac{(\delta+1)!}{b^{\delta+1}\delta_1\delta_2\delta_3} \left(\frac{b}{b+d}\right)^{\delta+1} \\ & \times F_A\left(\delta+1; 1, 1, 1; \delta_1+1, \delta_2+1, \delta_3+1; \frac{d_1}{d+b}, \frac{d_2}{d+b}, \frac{d_3}{d+b}\right).\end{aligned} \tag{5.28}$$

Moments of the 3-Branch SC Output SNR

We can also obtain the moments of the 3-branch SC output SNR in arbitrarily correlated Rayleigh fading. Differentiating the cdf of the SC output SNR (5.21) with respect to x

yields the corresponding output pdf:

$$p_{\mathrm{sc}}(x) = \frac{\det(\mathbf{\Phi})}{\phi_{11}\phi_{22}\phi_{33}} \sum_{k=0}^{\infty} \varepsilon_k (-1)^k \cos(k\chi) \sum_{l,m,n=0}^{\infty} C\, \nu_{12}^{l+\frac{k}{2}} \nu_{23}^{m+\frac{k}{2}} \nu_{31}^{n+\frac{k}{2}} \times \gamma(\delta_1, d_1 x)\, \gamma(\delta_2, d_2 x)\, \gamma(\delta_3, d_3 x) \sum_{j=1}^{3} \frac{d_j^{\delta_j} x^{\delta_j - 1} e^{-d_j x}}{\gamma(\delta_j, d_j x)}. \tag{5.29}$$

Using (5.29), we can obtained the output moments as

$$E(\gamma_{\mathrm{sc}}^{\beta}) = \frac{\det(\mathbf{\Phi})}{\phi_{11}\phi_{22}\phi_{33}} \sum_{k=0}^{\infty} \varepsilon_k (-1)^k \cos(k\chi) \sum_{l,m,n=0}^{\infty} \frac{C\, \nu_{12}^{l+\frac{k}{2}} \nu_{23}^{m+\frac{k}{2}} \nu_{31}^{n+\frac{k}{2}} d_1^{\delta_1} d_2^{\delta_2} d_3^{\delta_3}}{b^{\delta+\beta}} \times (\delta+\beta-1)! \sum_{(u,v,w)} \frac{F_A\left(\delta+\beta; 1, 1; \delta_v+1, \delta_w+1; \frac{d_v}{d}, \frac{d_w}{d}\right)}{\delta_v \delta_w} \tag{5.30}$$

where $(u, v, w) \in \{(1, 2, 3), (2, 3, 1), (3, 1, 2)\}$.

Using (5.30), we can obtain other useful performance measures, such as the central moments, the skewness, the Kurtosis and the amount of fading.

5.3.2 Bounds for the Output Ccdf of Multi-Branch SC

Performance of multi-branch SC ($L > 3$) is completely known for independent fading branches. If, however, branch signals are allowed to be correlated (which is a much realistic assumption), known theoretical results are few and far between. In [43] and [44], the performance of multi-branch SC in correlated Rayleigh fading channel is analyzed. However, their results are fairly complicated for large $L(> 3)$. From a both practical and theoretical standpoint, performance bounds for multi-branch SC are therefore desirable. For this problem in its most general setting, we need to know the L-th order joint distribution of the instantaneous branch SNRs for any correlation structure. As mentioned before, unfortunately, it is impossible or extremely difficult to derive this joint pdf for $L > 3$. Using (5.5) and (5.7), we can handle any arbitrary correlation pattern for $L = 3$. Can we use our new results to obtain the performance bounds of multi-branch SC for $L > 3$? Strangely enough, the answer is yes. For this purpose, we need to use the Boole formula which shows that the probability that at least one of the L events $\{A_1, A_2, \cdots, A_L\}$ occurs

is given by [104]

$$\Pr\left(\bigcup_{u=1}^{L} A_u\right) = \underbrace{\sum_{u}^{L} \Pr(A_u)}_{S_1} - \underbrace{\sum_{\substack{u,v=1 \\ u<v}}^{L} \Pr(A_u \cap A_v)}_{S_2} + \underbrace{\sum_{\substack{u,v,w=1 \\ u<v<w}}^{L} \Pr(A_u \cap A_v \cap A_w)}_{S_3} \tag{5.31}$$
$$+ \cdots (-1)^{L-1} \Pr(A_1 \cap A_2 \cap \cdots \cap A_L).$$

Note that S_1 is the sum of the first order event probabilities ignoring any dependency among the events. However, S_2 is the sum of the pairwise event probabilities, which takes into consideration pairwise dependencies among the events. Using the fact that the sum of an even (or odd) number of terms on the right hand equation (5.31) provides a lower (or upper) bound of $\Pr\left(\bigcup_{u=1}^{L} A_u\right)$, we obtain the Bonferroni inequalities, of which the second is

$$S_1 - S_2 \leq \Pr\left(\bigcup_{u=1}^{L} A_u\right) \leq S_1 - S_2 + S_3. \tag{5.32}$$

We are now in a position to apply this to evaluate the performance of multi-branch SC in correlated Rayleigh fading channels. Let A_u denote the event that the instantaneous SNR of the u-th branch γ_u exceeds x: $A_u = \{\gamma_u > x\}$. Since the SC output SNR is the maximum of all the branch SNRs, when at least one branch SNR exceeds x, so does the SC output. Therefore, we readily bound the ccdf of the multi-branch SC output SNR by

$$\sum_{u=1}^{L} \Pr(\gamma_u > x) - \sum_{\substack{u,v=1 \\ u<v}}^{L} \Pr(\gamma_u > x, \gamma_v > x) \leq \Pr(\gamma_{sc} > x) \leq \sum_{u=1}^{L} \Pr(\gamma_u > x)$$
$$- \sum_{\substack{u,v=1 \\ u<v}}^{L} \Pr(\gamma_u > x, \gamma_v > x) + \sum_{\substack{u,v,w=1 \\ u<v<w}}^{L} \Pr(\gamma_u > x, \gamma_v > x, \gamma_w > x) \tag{5.33}$$

where $\Pr(\gamma_u > x)$ is the probability that any single branch SNR exceeds x and $\Pr(\gamma_u > x, \gamma_v > x)$ is the probability that any two branch SNRs exceed x simultaneously, which are given respectively by [19, Eqs. (10-4-8, A-7-1)]

$$\Pr(\gamma_u > x) = e^{-\frac{x}{\bar{\gamma}_u}}, \tag{5.34a}$$

$$\Pr(\gamma_u > x, \gamma_v > x) = e^{-\frac{x}{\bar{\gamma}_u}} \left[1 - Q\left(\sqrt{\frac{2x}{(1-\rho_{uv}^2)\bar{\gamma}_v}}, \rho_{uv}\sqrt{\frac{2x}{(1-\rho_{uv}^2)\bar{\gamma}_u}}\right)\right]$$

$$+ e^{-\frac{x}{\bar{\gamma}_v}} Q\left(\rho_{uv}\sqrt{\frac{2x}{(1-\rho_{uv}^2)\bar{\gamma}_v}}, \sqrt{\frac{2x}{(1-\rho_{uv}^2)\bar{\gamma}_u}}\right) \tag{5.34b}$$

where $\rho_{uv} = \psi_{uv}/\sqrt{\psi_{uu}\psi_{vv}}$ is the fading correlation between the u-th and the v-th branches, and $\Pr(\gamma_u > x, \gamma_v > x, \gamma_w > x)$ is the probability that any three branch SNRs exceed x simultaneously, which can be derived using (5.5) as

$$\Pr(\gamma_u > x, \gamma_v > x, \gamma_w > x) = \left(\frac{\det \Phi}{\phi_{uu}\phi_{vv}\phi_{ww}}\right) \sum_{k=0}^{\infty} \varepsilon_k (-1)^k \cos k(\chi_{uv} + \chi_{vw} + \chi_{wu})$$
$$\times \sum_{l,m,n=0}^{\infty} C\, \nu_{uv}^{l+\frac{k}{2}} \nu_{vw}^{m+\frac{k}{2}} \nu_{wu}^{n+\frac{k}{2}} \Gamma(\delta_1, d_u x)\Gamma(\delta_2, d_v x)\Gamma(\delta_3, d_w x). \tag{5.35}$$

5.3.3 Moments of the 3-Branch EGC Output SNR

The moments of the combiner output SNR can be used as alternative performance measures to the conventional average error rate analysis. The new expression (5.19) enables us to evaluate the moments of the output SNR of a 3-branch EGC system whose output is given by (1.26)

$$\gamma_{\text{egc}} = \frac{(r_1 + r_2 + r_3)^2 E_s}{3N_0}. \tag{5.36}$$

The moments of the output SNR can be obtained as (4.81)

$$E(\gamma_{\text{egc}}^n) = \left(\frac{\bar{\gamma}_1}{3\psi_{11}}\right)^n \sum_{\substack{k_1,k_2,k_3=0 \\ k_1+k_2+k_3=2n}}^{2n} \frac{(2n)!}{k_1!\,k_2!\,k_3!} E(r_1^{k_1} r_2^{k_2} r_3^{k_3}) \tag{5.37}$$

where $E(r_1^{k_1} r_2^{k_2} r_3^{k_3})$ can be computed using (5.19). The average output SNR of 3-branch EGC can be simplified as

$$\bar{\gamma}_{\text{egc}} = \bar{\gamma}_1 \left\{ \frac{1}{3} + \frac{\psi_{22}}{3\psi_{11}} + \frac{\psi_{33}}{3\psi_{11}} + \frac{2\det\Phi}{3\psi_{11}\phi_{11}\phi_{22}\phi_{33}} \sum_{k=0}^{\infty} \varepsilon_k (-1)^k \cos(k\chi) \right.$$
$$\times \sum_{l,m,n=0}^{\infty} \nu_{12}^{l+\frac{k}{2}} \nu_{23}^{m+\frac{k}{2}} \nu_{31}^{n+\frac{k}{2}} \left[\frac{\binom{\delta_3-1}{k}\Gamma\left(\delta_1+\frac{1}{2}\right)\Gamma\left(\delta_2+\frac{1}{2}\right)}{l!\,m!\,(l+k)!\,(n+k)!\sqrt{\phi_{11}\phi_{22}}} \right. \tag{5.38}$$
$$\left. \left. + \frac{\binom{\delta_2-1}{m}\Gamma\left(\delta_1+\frac{1}{2}\right)\Gamma\left(\delta_3+\frac{1}{2}\right)}{l!\,n!\,(m+k)!\,(n+k)!\sqrt{\phi_{11}\phi_{33}}} + \frac{\binom{\delta_1-1}{l}\Gamma\left(\delta_2+\frac{1}{2}\right)\Gamma\left(\delta_3+\frac{1}{2}\right)}{m!\,n!\,(l+k)!\,(m+k)!\sqrt{\phi_{22}\phi_{33}}} \right] \right\}.$$

To the best of our knowledge, (5.38) is a new result and provides the average SNR for the most general 3-branch EGC case. Similar results can be derived for higher-order moments and for 4-branch EGC. These are omitted for brevity.

5.3.4 Performance Analysis of 3-Branch GSC

GSC(M, L) achieves a good tradeoff between performance and implementation complexity [22, 105]. However, very few theoretical results are known for the GSC performance in correlated fading channels. The only published paper dealing with this topic is Mallik and Win [79], who analyze the performance of GSC(M, L) in **equally** correlated Nakagami fading. The distribution theory for order statistics of arbitrarily correlated RVs is not fully developed [104]. Our new result (5.7) enables the performance analysis of 3-branch GSC in arbitrarily correlated Rayleigh fading channels.

Since GSC(1,3) and GSC(3,3) are simply SC and MRC, these cases are not treated here. Instead, we consider the GSC(2,3) system, which combines the largest two branch SNRs to form the output:

$$\gamma_{\text{gsc}} = \gamma_{(1)} + \gamma_{(2)}. \tag{5.39}$$

We derive the joint cdf of $\gamma_{(1)}$ and $\gamma_{(2)}$ via the first principles as

$$\begin{aligned} F_{\gamma_{(1)},\gamma_{(2)}}(\beta,\alpha) &= \Pr(\gamma_1 \le \beta, \gamma_2 \le \alpha, \gamma_3 \le \alpha) + \Pr(\gamma_1 \le \alpha, \gamma_2 \le \beta, \gamma_3 \le \alpha) \\ &\quad + \Pr(\gamma_1 \le \alpha, \gamma_2 \le \alpha, \gamma_3 \le \beta) - 2\Pr(\gamma_1 \le \alpha, \gamma_2 \le \alpha, \gamma_3 \le \alpha) \end{aligned} \tag{5.40}$$

where $\beta \ge \alpha > 0$.

Applying (5.7) and differentiating (5.40) with respect to β and α yield the joint pdf of $\gamma_{(1)}$ and $\gamma_{(2)}$ as

$$\begin{aligned} p_{\gamma_{(1)},\gamma_{(2)}}(y,x) &= \frac{\det \boldsymbol{\Phi}}{\phi_{11}\phi_{22}\phi_{33}} \sum_{k=0}^{\infty} \varepsilon_k (-1)^k \cos(k\chi) \sum_{l,m,n=0}^{\infty} C\, \nu_{12}^{l+\frac{k}{2}} \nu_{23}^{m+\frac{k}{2}} \nu_{31}^{n+\frac{k}{2}} \\ &\quad \times \sum_{\substack{u,v,w=1 \\ u\neq v\neq w}} \gamma(\delta_w, d_w x) d_u^{\delta_u} d_v^{\delta_v} [x^{\delta_u - 1} y^{\delta_v - 1} e^{-(x d_u + y d_v)}] \end{aligned} \tag{5.41}$$

where $y \ge x > 0$.

The mgf of the GSC(2,3) output SNR is the defined as (1.3), i.e.,

$$M_{\text{gsc}}(s) = E(e^{-s\gamma_{\text{gsc}}}). \tag{5.42}$$

Thus, using (5.41), we can obtained the output mgf as

$$\begin{aligned} M_{\mathrm{gsc}}(s) &= \int_0^\infty \int_x^\infty p_{\gamma_{(1)},\gamma_{(2)}}(y,x) e^{-(x+y)s}\, dy\, dx \\ &= \frac{\det \mathbf{\Phi}}{\phi_{11}\phi_{22}\phi_{33}} \sum_{k=0}^{\infty} \varepsilon_k (-1)^k \cos(k\chi) \sum_{l,m,n=0}^{\infty} C\, \nu_{12}^{l+\frac{k}{2}} \nu_{23}^{m+\frac{k}{2}} \nu_{31}^{n+\frac{k}{2}} \\ &\quad \times \sum_{\substack{u,v,w=1 \\ u\neq v\neq w}} \left(\frac{d_v}{d_v+s}\right)^{\delta_v} d_u^{\delta_u} g(u,v,w) \end{aligned} \tag{5.43}$$

where

$$\begin{aligned} g(u,v,w) &= \int_0^\infty x^{\delta_u - 1} e^{-x(d_u+s)} \gamma(\delta_w, x d_w) \Gamma[\delta_v, (d_v+s)x]\, dx \\ &= \frac{d_w^{\delta_w}}{\delta_w} \left[\frac{(\delta_u+\delta_w-1)!(\delta_v-1)!}{(d_u+d_w+s)^{\delta_u+\delta_w}} {}_2F_1\left(\delta_u+\delta_w, 1; \delta_w; \frac{d_w}{d_w+d_u+s}\right) \right. \\ &\quad \left. + \frac{(\delta-1)!(d_v+s)^{\delta_v}}{\delta_v (d+2s)^{\delta}} F_A\left(\delta; 1, 1; \delta_w+1, \delta_v+1; \frac{d_w}{d+2s}, \frac{d_v+s}{d+2s}\right) \right]. \end{aligned} \tag{5.44}$$

Eq. (5.44) follows from [3, Eq. (9.236.4)] and [2, Eq. (C.1)]. Using the output mgf (5.43), the performance of various digital modulations with GSC(2,3) can be readily evaluated (see Section 2.4.1 for details).

5.4 Numerical Results

Numerical results are here provided to show the performance of 3-branch SC and EGC in arbitrarily correlated Rayleigh fading channels. Note that semi-analytical simulation results are provided for the 3-branch SC and EGC performance as an independent check of our analytical results. We use the Cholesky decomposition approach [96] to generate correlated complex Gaussian variables and their amplitudes give the required correlated Rayleigh envelopes.

Let us first consider an antenna array with normalized covariance matrix

$$\mathbf{\Psi} = \begin{pmatrix} 1.0000 & 0.2920 & 0.2998 & 0.1121 \\ 0.2920 & 0.6602 & 0.2031 & 0.1585 \\ 0.2998 & 0.2031 & 0.7625 & 0.1888 \\ 0.1121 & 0.1585 & 0.1888 & 0.6431 \end{pmatrix}. \tag{5.45}$$

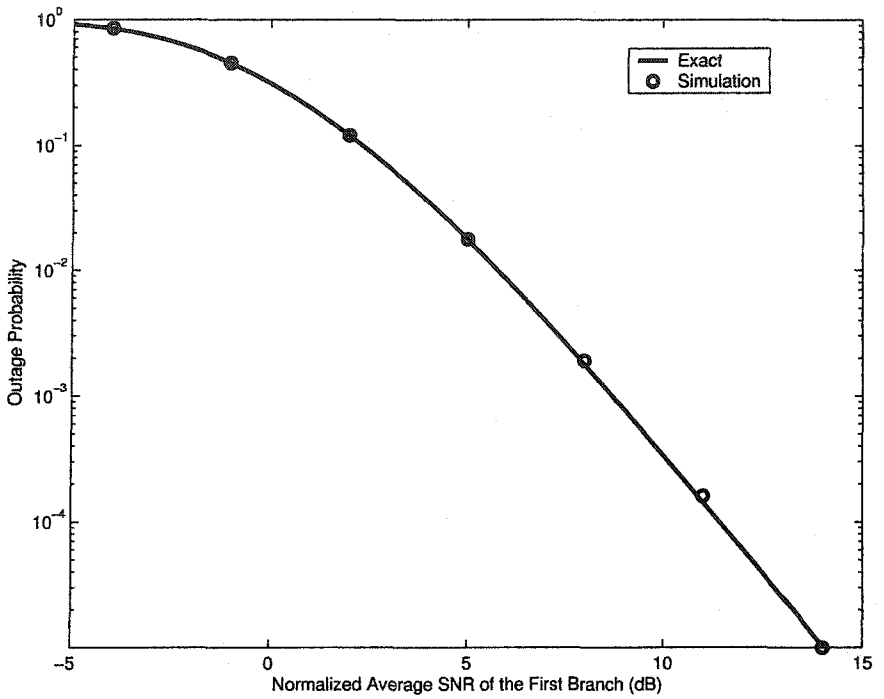

Figure 5.1: The outage probability of 4-branch SC versus the normalized average SNR of the first branch $\hat{\gamma}_T = \bar{\gamma}_1/\gamma_T$ in correlated Rayleigh fading channel.

The corresponding inverse covariance matrix now satisfies (5.11). Thus, using (5.15), we may evaluate the outage probability of 4-branch SC, as is shown in Fig. 5.1. Our numerical results agree with the simulation results.

Next, we consider only the performance of the 3-branch balanced SC and EGC (the average SNRs at all the branches are identical, i.e., $\bar{\gamma}_1 = \bar{\gamma}_2 = \bar{\gamma}_3 = \bar{\gamma}$) for brevity. A linear antenna array of three antennas, with equal antenna spacing d, is considered so that the distance between the j-th and the k-th antenna can be obtained as $|j-k|d$. Several statistical models have been proposed to describe the correlation between antennas. Clarke's two-dimensional isotropic scattering model assumes a uniform angle of arrival (AOA) distribution. The covariance between two antennas follows the zero-th order Bessel function $J_0(x)$ [15]:

$$\psi_{jk} = \bar{\gamma} J_0\left(2\pi \frac{|j-k|d}{\lambda}\right) \tag{5.46}$$

where λ is the carrier wavelength.

However, measurement data [106] suggests that a Gaussian AOA distribution is more

realistic than the uniform AOA distribution for GSM systems in rural and suburban areas. The AOA is assumed to be Gaussian distributed [107] with mean ϕ_0 and variance (angular spread) σ_ϕ. Hence, the covariance matrix of the underlying complex Gaussian components can be computed using [34, Eq. (33,34)] for different antenna spacing d. For example, when $\phi_0 = 30°$ and $\sigma_\phi = 10°$, the covariance matrix is given by

$$\Psi = \bar{\gamma} \begin{pmatrix} 1 & -0.60 + 0.45i & 0.13 - 0.30i \\ -0.60 - 0.45i & 1 & -0.60 + 0.45i \\ 0.13 + 0.30i & -0.60 - 0.45i & 1 \end{pmatrix} \tag{5.47}$$

for antenna spacing $d = 0.8\lambda$.

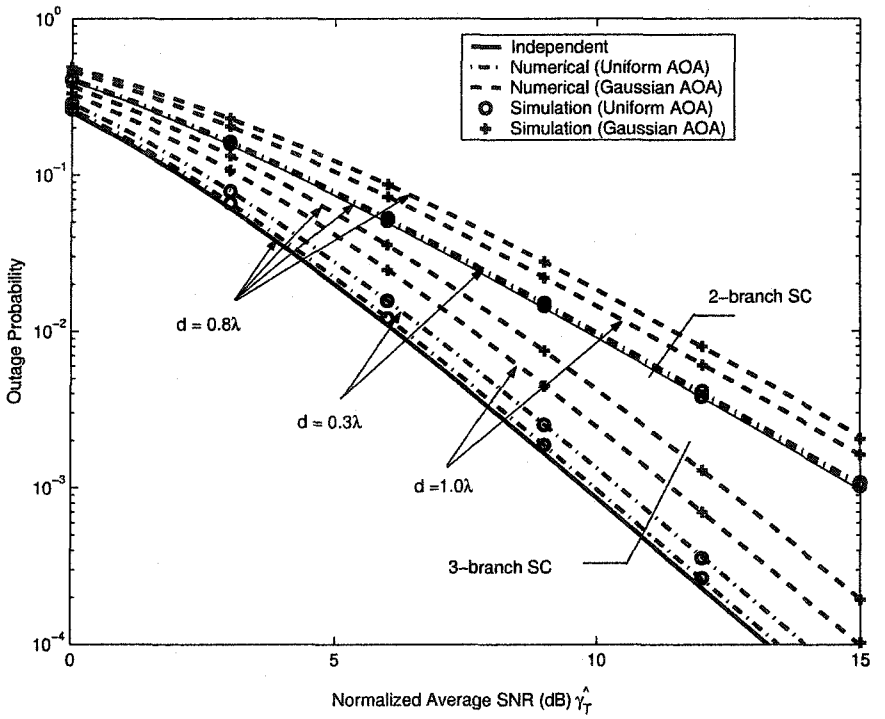

Figure 5.2: The outage probability of the balanced SC with two spacial correlation models (the uniform AOA model and the Gaussian AOA model with $\phi_0 = 30°$ $\sigma_\phi = 10°$).

Using our new results, we can evaluate the 3-branch SC and EGC performance with the above linear antenna arrays. The performance of 2-branch SC, which combines the first two antennas, is plotted for comparison.

Fig. 5.2 compares the outage probability of 3-branch SC with that of 2-branch SC for both the uniform AOA model and the Gaussian AOA model with $\phi_0 = 30°$ and $\sigma_\phi = 10°$.

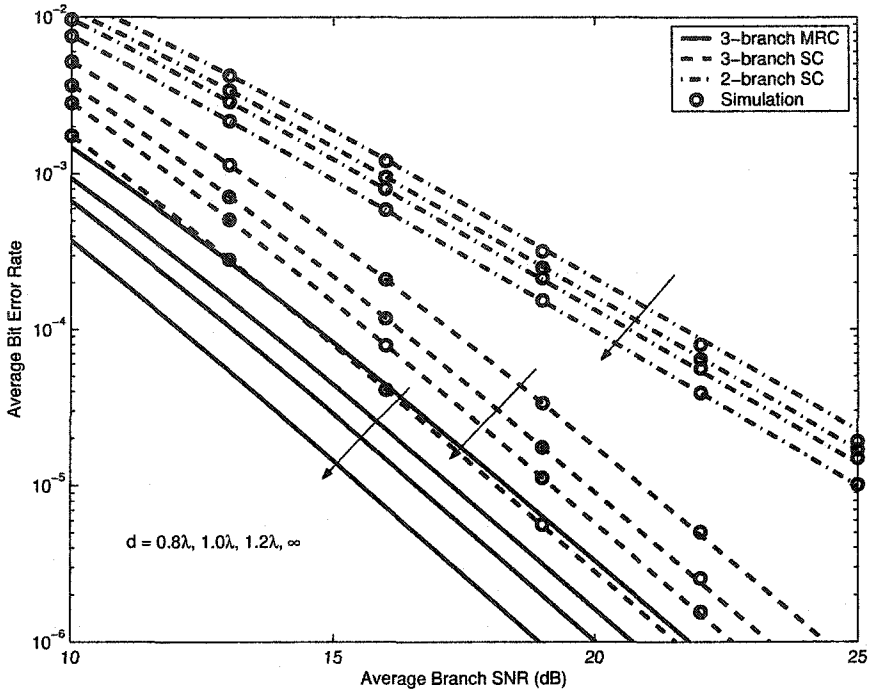

Figure 5.3: The average BER of binary DPSK with SC and MRC using the Gaussian AOA model with $\phi_0 = 30°$ $\sigma_\phi = 10°$. The antenna spacing $d \in \{0.8\lambda, 1.0\lambda, 1.2\lambda, \infty\}$.

The normalized average SNR is given by $\hat{\gamma}_T = \bar{\gamma}/\gamma_T$. The covariance matrices for the above two AOA models are determined using (5.46) and [34, Eq. (33,34)], respectively. A significant performance loss is caused by the insufficient antenna spacing. As antenna spacing d increases, the performance of 3-branch SC improves more rapidly than that of 2-branch SC. This effect is more pronounced in high SNRs. That is, 3-branch SC is more sensitive to the fading correlation than 2-branch SC. Compared with the uniform AOA distribution model, the Gaussian AOA model describes a worse case of spacial correlation.

Fig. 5.3 plots the average BER performance of SC. The Gaussian AOA correlation model with $\phi_0 = 30°$ and $\sigma_\phi = 10°$ is used. The MRC performance [108] is plotted for comparison. The performance gain of 3-branch MRC with respect to 3-branch SC is about 2.5dB, regardless of the antenna spacing. As the antenna spacing decreases, the correlation between branch signals increases and the diversity gain of 3-branch SC with respect to 2-branch SC diminishes.

Figs. 5.4 and 5.5 show the effect of the fading correlation ρ on the normalized average

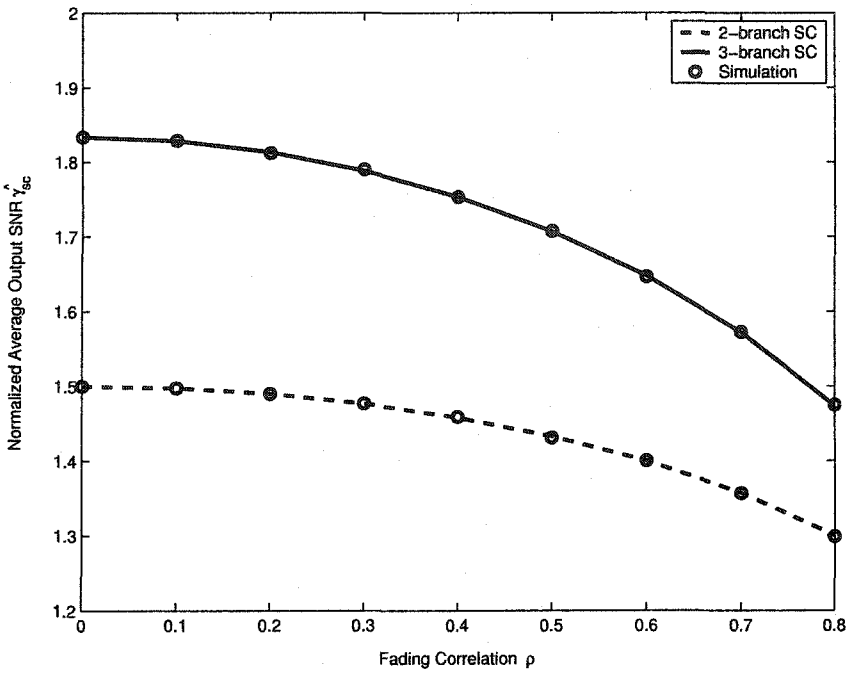

Figure 5.4: The normalized average output SNR of 3-branch SC in equally correlated Rayleigh fading. $\hat{\gamma}_{\rm sc} = \gamma_{\rm sc}/\bar{\gamma}$.

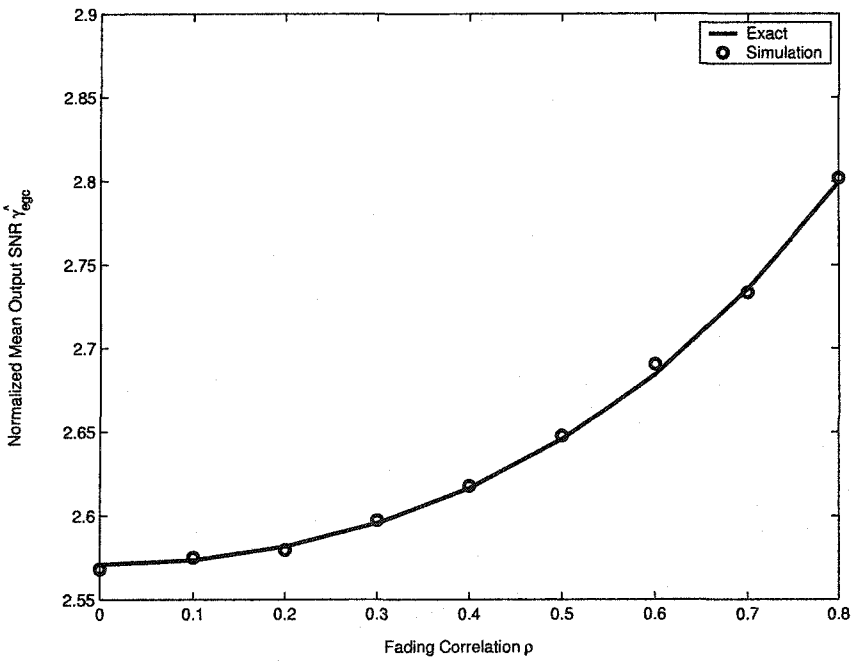

Figure 5.5: The normalized average output SNR of 3-branch EGC in equally correlated Rayleigh fading. $\hat{\gamma}_{\rm egc} = \gamma_{\rm egc}/\bar{\gamma}$.

output SNRs of SC and EGC, respectively. For simplicity, we consider equally correlated Rayleigh fading. As the fading correlation ρ increases, the average output SNR of 3-branch SC decreases more rapidly than that of 2-branch SC. This observation agrees with our expectation that 3-branch SC is more sensitive to the fading correlation. But, as fading correlation increases, the average output SNR of 3-branch EGC also increases. This contradicts the conventional wisdom that diversity combiner performance degrades with increasing correlation. However, it can be explained by (5.37). Since $E(R_j R_k) > E(R_j)E(R_k)$, $(j \neq k)$, for $\rho > 0$, the average output SNR of EGC in correlated fading channels is higher than that in independent fading channels [18]. As ρ approaches 1, the average output SNR of EGC approaches that of MRC. It should be noted that common EGC performance measures, such as BER, cannot be solely characterized by the average output SNR; they also depend on the higher moments. The average output SNR by itself is not a comprehensive metric for the EGC performance in correlated fading channels. Caution must be exercised when using the average output SNR as a performance measure. Performance measures that consider the higher-order moments of the combiner output SNR are required.

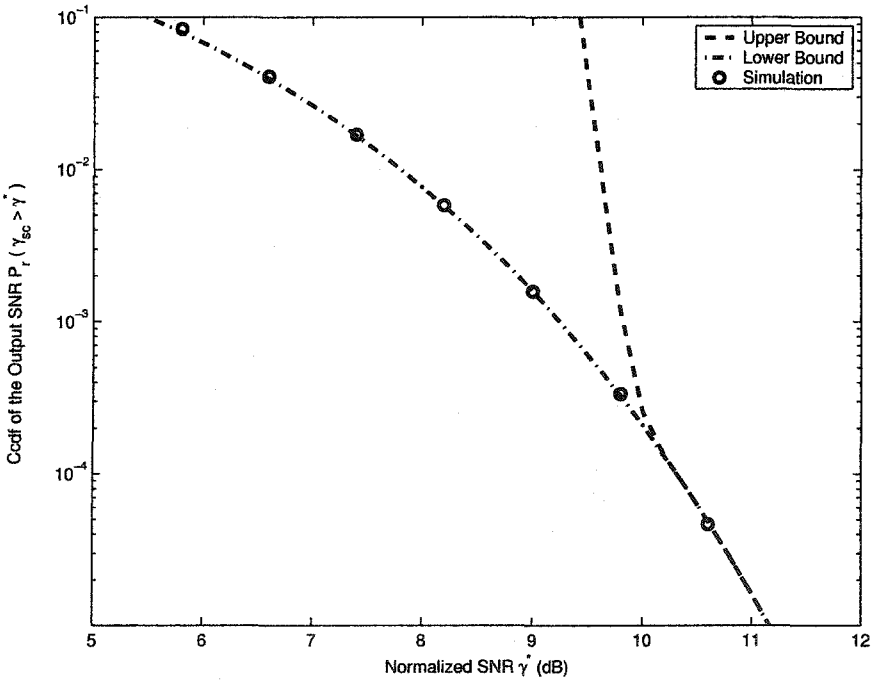

Figure 5.6: Bounds of the output ccdf of 5-branch SC.

Finally, let us consider a linear antenna array of five vertical omnidirectional antennas, with antenna spacing $d = 0.8\lambda$. The AOA is assumed to be Gaussian distributed [107] with mean $\phi_0 = 30°$ and variance (angular spread) $\sigma_\phi = 10°$. The covariance matrix of the underlying complex Gaussian components can be computed using [34, Eq. (33,34)]. Fig. 5.6 shows that our bounds fit the simulation results well in high SNRs. The lower bound is more accurate than the upper bound to predict the ccdf.

5.5 Conclusion

In this chapter, using Miller's classical approach, we have derived new infinite series representations for the joint pdf and the joint cdf of three and four correlated Rayleigh RVs. Several previous results have turned out to be special cases of our new results. Our results are canonical, in that they can accommodate any arbitrary 3×3 correlation matrix as well as a fairly general class of 4×4 correlation matrices. These representations pave the way for solving certain long-standing diversity problems. For example, the performance of 3-branch SC, EGC and GSC in arbitrarily correlated Rayleigh fading can now be evaluated analytically. To the best of our knowledge, these have never been developed up to now. Similarly, the performance of 4-branch diversity combiners in a fairly general correlation setting can now be completely solved using our results. Our novel use of Bonferroni's inequality allows the bounding of the multi-branch SC performance for arbitrary correlation structures among the diversity branches. Other applications may include finding transition probabilities for Markov modelling of the Rayleigh fading channel [109]. Finally, theoretical performance results of diversity systems in correlated fading are much scarce compared to that of independent fading. The results derived in this chapter partly redress this issue, while much more work remains to be done.

Chapter 6

Conclusion

For emerging very high data-rate wireless communications, the complexity of traditional diversity algorithms, such as MRC, can be prohibitive. This has motivated the development of several suboptimal diversity combining schemes whose performance is sacrificed for complexity reduction. In Chapters 2 and 3, we proposed two such diversity combining schemes, S-GSC and A-MRC, which achieve a flexible tradeoff between performance and implementation complexity in dense multi-path fading channels.

In Chapter 2, we studied the effect of the threshold on the performance of the recently-developed AT-GSC and found that AT-GSC performs even worse than SC when the threshold is high. Hence, we proposed a new hybrid scheme, named S-GSC, which combines all the branches with SNRs above the threshold. If all the branch SNRs drop below the threshold, S-GSC outputs the best branch. We also derived closed-form expressions for the mgf of the S-GSC output SNR in independent Rayleigh fading channels and applied the output mgfs to evaluate the average error rates, the outage probability and the output moments of S-GSC. We observed that S-GSC outperforms both AT-GSC and SC, while S-GSC is only slightly complicated than AT-GSC in terms of the average number of the combined branches. We also showed that both the performance and the processing complexity of S-GSC lie between those of MRC and SC.

Comparing the processing complexity of several diversity combiners, we found that the suboptimal GSC derivatives, such as GSC(M, L), AT-GSC and S-GSC, require measuring all the L diversity branches. The output of a RAKE receiver employing GSC schemes can only be formed after all the resolvable multi-paths arrived. This is both time-consuming

and power-consuming. In Chapter 3, we thus proposed an adaptive combining scheme, A-MRC, which combines the first N_c out of the L branches whose cumulative branch SNR exceeds the threshold. A-MRC only needs to measure the first N_c branches where N_c is adaptive to the channel fading conditions. We also derived analytical results for the mgf of the A-MRC output SNR in various independent fading channels and evaluated its average error rates, outage probability and output moments. We observed that A-MRC outperforms GSC(M, L) when the channel power decays fast. A-MRC is more suitable for non-uniform dense multi-path fading channels.

Experimental studies have shown that independent fading can hardly be achieved in practice. It is important to evaluate the performance of diversity combiners in correlated fading channels. In Chapters 4 and 5, we derived theoretical results for the performance of multi-branch ($L > 2$) diversity combiners in various correlated fading channels.

In Chapter 4, we developed new channel gain representations for equally Rayleigh, Ricean and Nakagami-m fading channels, which enable the performance analysis of various diversity combiners in such channels. We derived single-fold integral expression for the cdf of the multi-branch SC output SNR, which is much simpler than the available L-dimensional integrals. We also evaluated the average error rates of a wide class of digital modulations with SC directly from the output cdfs. Unlike the available results, the complexity of our new results does not increase as the diversity order L increases. Not aware of any results on the multi-branch EGC performance in correlated fading channels, we first derived analytical results for the average error rates and the output moments of multi-branch EGC in various equally correlated fading channels. We observed that diversity gain exists despite fading correlation and higher-order diversity combiners are more sensitive to the fading correlation. The performance of diversity combiners in correlated Ricean fading channels can be worse than that in correlated Rayleigh fading channels.

While Chapter 4 dealt with the equally correlated channel models, Chapter 5 investigated the performance of diversity combiners in arbitrarily correlated channels. We derived new infinite series representations for the joint distribution functions of the tri-variate and a certain class of quadri-variate Rayleigh distributions. Bounds for the truncation errors of the infinite series were also provided. Using these new representations, we derived new

theoretical results for the average error rates and the output moments of 3-branch SC, the output moments of 3-branch EGC and the mgf of the GSC(2,3) output SNR in arbitrarily correlated Rayleigh fading channels. We also provided bounds for the ccdf of the multi-branch SC output SNR.

We have thus partially solved some long-standing diversity problems.

6.1 Future Work

Future work in this area may include:

1. Analyze the performance of multi-branch EGC and GSC in arbitrarily correlated fading channels,
2. Analyze the performance of S-GSC and A-MRC in arbitrarily correlated fading channels,
3. Investigate the effect of channel PDPs on the performance of diversity combiners,
4. Investigate the effect of both Gaussian estimation errors and the fading correlation on the performance of diversity combiners,
5. Apply our new proposed S-GSC and A-MRC schemes to multiple input and multiple output (MIMO) systems.

Appendix A

Dual-Branch SC in Correlated Rayleigh Fading Channels

Here, we prove that our general cdf expression reduces to (4.29) in the case of dual-branch SC in correlated Rayleigh fading.

The output cdf of dual-branch SC can be written as

$$F_{\mathrm{sc}}(y) = \int_0^{\infty} \left[1 - Q\left(a\sqrt{2t}, b\right)\right]^2 e^{-t}\, dt \tag{A.1}$$

where

$$a = \sqrt{\frac{\rho}{1-\rho}}, \qquad b = \sqrt{\frac{2y}{\bar{\gamma}(1-\rho)}}. \tag{A.2}$$

Integrating (A.1) by parts using

$$u = \left[1 - Q\left(a\sqrt{2t}, b\right)\right]^2, \qquad dv = e^{-t}\, dt, \tag{A.3}$$

and using the results in [5], we obtain the output cdf as

$$F_{\mathrm{sc}}(y) = 1 + e^{-b^2} - 2e^{-\frac{b^2}{2(1+a^2)}} + 2e^{-\frac{b^2}{2}} A \tag{A.4}$$

where

$$A = ab \int_0^{\infty} e^{-\frac{(1+a^2)u^2}{2}} Q(au, b) I_1(abu)\, du. \tag{A.5}$$

Again, integrating (A.5) by parts using

$$u = e^{-\frac{(1+a^2)u^2}{2}} Q(au, b), \qquad dv = I_1(abu)\, du, \tag{A.6}$$

we obtain

$$A = -\frac{1}{2} e^{-\frac{b^2}{2}} + e^{\frac{a^2 b^2}{2(1+a^2)}} Q(\beta, \alpha) - \frac{1}{2} e^{-\frac{b^2}{2(1+2a^2)}} I_0(\alpha\beta) \tag{A.7}$$

where

$$\alpha = b\sqrt{\frac{1+a^2}{1+2a^2}} = \sqrt{\frac{2y}{\bar{\gamma}_c(1-\rho^2)}}, \tag{A.8}$$

$$\beta = \frac{a^2 b}{\sqrt{(1+a^2)(1+2a^2)}} = \rho\sqrt{\frac{2y}{\bar{\gamma}_c(1-\rho^2)}}. \tag{A.9}$$

Substituting (A.7) to (A.4), we finally obtain

$$\begin{aligned} F_{\mathrm{sc}}(y) &= 1 - 2e^{-\frac{b^2}{2(1+a^2)}} Q(\alpha,\beta) + e^{-\frac{(1+a^2)b^2}{1+2a^2}} I_0(\alpha\beta) \\ &= 1 - 2e^{-\frac{y}{\bar{\gamma}_c}} Q\left(\sqrt{\frac{2y}{\bar{\gamma}_c(1-\rho^2)}}, \rho\sqrt{\frac{2y}{\bar{\gamma}_c(1-\rho^2)}}\right) \\ &\quad + e^{-\frac{2y}{\bar{\gamma}_c(1-\rho^2)}} I_0\left[\frac{2\rho y}{\bar{\gamma}_c(1-\rho^2)}\right], \end{aligned} \tag{A.10}$$

which is exactly the expression in [19, Eq. (10-10-8)].

Appendix B

Derivation of (5.12)

Let $\boldsymbol{G} = \{G_1, G_2, G_3, G_4\}$ be jointly CGRVs with zero means and the inverse covariance matrix $\boldsymbol{\Phi}$ given by (5.11). The joint pdf $p_{\boldsymbol{R},\boldsymbol{\Theta}}(\boldsymbol{r}, \boldsymbol{\theta})$ of the corresponding amplitudes $\boldsymbol{R}$ and phases $\boldsymbol{\Theta}$ of $\boldsymbol{G}$ is given by [102]

$$p_{\boldsymbol{R},\boldsymbol{\Theta}}(\boldsymbol{r}, \boldsymbol{\theta}) = \frac{1}{\pi^4} |\det(\boldsymbol{\Phi})| r_1 r_2 r_3 r_4 e^{-\boldsymbol{g}^* \boldsymbol{\Phi} \boldsymbol{g}}. \tag{B.1}$$

The marginal density $p_{\boldsymbol{R}}(\boldsymbol{r})$ can therefore be obtained

$$p_{\boldsymbol{R}}(r_1, r_2, r_3, r_4) = \frac{1}{\pi^4} |\det \boldsymbol{\Phi}| r_1 r_2 r_3 r_4 \int_0^{2\pi} \int_0^{2\pi} \int_0^{2\pi} \int_0^{2\pi} e^{-\boldsymbol{g}^* \boldsymbol{\Phi} \boldsymbol{g}} \, d\theta_1 \, d\theta_2 \, d\theta_3 \, d\theta_4. \tag{B.2}$$

Writing G_k in terms of polar coordinates, we obtain

$$\begin{aligned} \boldsymbol{g}^* \boldsymbol{\Phi} \boldsymbol{g} =& r_1^2 \phi_{11} + r_2^2 \phi_{22} + r_3^2 \phi_{33} + r_4^2 \phi_{44} + 2 r_1 r_2 |\phi_{12}| \cos(\theta_1 - \theta_2 - \chi_{12}) \\ &+ 2 r_1 r_3 |\phi_{13}| \cos(\theta_1 - \theta_3 - \chi_{13}) + 2 r_2 r_3 |\phi_{23}| \cos(\theta_2 - \theta_3 - \chi_{23}) \\ &+ 2 r_2 r_4 |\phi_{24}| \cos(\theta_2 - \theta_4 - \chi_{24}) + 2 r_3 r_4 |\phi_{34}| \cos(\theta_3 - \theta_4 - \chi_{34}). \end{aligned} \tag{B.3}$$

Making variable transforms $\theta_1 - \theta_2 = u$, $\theta_2 - \theta_3 = v$ and $\theta_3 - \theta_4 = w$ and substituting (B.3) into (B.2), we obtain the pdf of $\boldsymbol{R}$ as

$$\begin{aligned} p_{\boldsymbol{R}}(r_1, r_2, r_3, r_4) =& \frac{2}{\pi^3} |\det \Phi| r_1 r_2 r_3 r_4 \exp[-(r_1^2 \phi_{11} + r_2^2 \phi_{22} + r_3^2 \phi_{33} + r_4^2 \phi_{44})] \\ & \int_0^{2\pi} \int_0^{2\pi} \int_0^{2\pi} \exp[-(a_1 \cos u + a_2 \sin u) - (a_3 \cos w + a_4 \sin w) \\ & - 2 r_2 r_3 |\phi_{23}| \cos(v - \chi_{23})] \, du \, dv \, dw \end{aligned} \tag{B.4}$$

where a_1, a_2, a_3 and a_4 depend on v, but not on u and w

$$a_1 = 2r_1r_2|\phi_{12}|\cos\chi_{12} + 2r_1r_3|\phi_{13}|\cos(v-\chi_{13}), \tag{B.5a}$$

$$a_2 = 2r_1r_2|\phi_{12}|\sin\chi_{12} - 2r_1r_3|\phi_{13}|\sin(v-\chi_{13}), \tag{B.5b}$$

$$a_3 = 2r_3r_4|\phi_{34}|\cos\chi_{34} + 2r_2r_4|\phi_{24}|\cos(v-\chi_{24}), \tag{B.5c}$$

$$a_4 = 2r_3r_4|\phi_{34}|\sin\chi_{34} - 2r_2r_4|\phi_{24}|\cos(v-\chi_{24}). \tag{B.5d}$$

Using the relationship [102]

$$\int_0^{2\pi} \exp[-(a\cos\theta + b\sin\theta)]\,d\theta = 2\pi I_0\left(\sqrt{a^2+b^2}\right), \tag{B.6}$$

and Neumann's addition theorem [110, P. 365], we obtain

$$\begin{aligned} p_{\boldsymbol{R}}(r_1,r_2,r_3,r_4) = {} & \frac{4}{\pi}(\det\boldsymbol{\Phi})r_1r_2r_3r_4\exp[-(r_1^2\phi_{11}+r_2^2\phi_{22}+r_3^2\phi_{33}+r_4^2\phi_{44})] \\ & \times\sum_{m=0}^{\infty}\sum_{n=0}^{\infty}\varepsilon_m\varepsilon_n I_m(2r_1r_2|\phi_{12}|)I_m(2r_1r_3|\phi_{13}|)I_n(2r_2r_4|\phi_{24}|)I_n(2r_3r_4|\phi_{34}|) \\ & \times\int_0^{2\pi} e^{-2r_2r_3|\phi_{23}|\cos(v-\chi_{23})}\{\cos[m(v+\chi_{12}-\chi_{13})+n(v+\chi_{34}-\chi_{24})] \\ & +\cos[m(v+\chi_{12}-\chi_{13})-n(v+\chi_{34}-\chi_{24})]\}\,dv. \end{aligned} \tag{B.7}$$

Using the relation [80, Eq. (3-3.14)], we obtain (5.12) after algebraic manipulation.

Bibliography

[1] A. Annamalai, C. Tellambura, and V. Bhargava, "Unified analysis of equal-gain diversity on Rician and Nakagami fading channels," in *Proc. IEEE WCNC 1999*, New Orleans, USA, Sept. 1999, vol. 1, pp. 10–14.

[2] A. Annamalai, C. Tellambura and V.K. Bhargava, "Equal-gain diversity receiver performance in wireless channels," *IEEE Trans. Commun.*, vol. 48, pp. 1732–1745, Oct. 2000.

[3] I. S. Gradshteyn and I. M. Ryzhik, *Table of Integrals, Series, and Products*, 5th ed. Academic Press, Inc., 1994.

[4] G. B. Rybicki, "Dawson's integral and the sampling theorem," *Computers in Physics*, vol. 3, no. 2, pp. 85–87, Mar. 1989.

[5] A. H. Nuttall, "Some integrals involving the Q_M function," *IEEE Trans. Inform. Theory.*, vol. 21, pp. 95–96, Jan. 1975.

[6] J. G. Proakis, *Digital Communications*, 3rd ed. New York: McGraw-Hill, 1995.

[7] C. Tellambura and A. Annamalai, *Wiley Encyclopedia of Telecommunications*, chapter Wireless Communications Systems Design, Wiley, Jan 2003.

[8] M. Patzold, *Mobile fading channels*. England: John Wiley, 2002.

[9] A. Papoulis, *Probability, Random Variables and Stochastic Process*, 3 rd ed. McGraw-Hill, Inc., 1991.

[10] W. R. Young, "Comparison of mobile radio transmission at 150, 450, 900, and 3700 MHz," *Bell Sys. Tech. J.*, vol. 31, pp. 1068–1085, 1952.

[11] H. W. Nylund, "Characteristics of small-area signal fading on mobile circuits in the 150 MHz band," *IEEE Trans. Veh. Technol.*, vol. 17, pp. 24–30, Oct. 1968.

[12] Y. Okumura, E. Ohmori, T. Kawano and K. Fukuda, "Field strength and its variability in VHF and UHF land mobile radio services," *Rev. Elec. Commun. Lab.*, vol. 16, pp. 825–873, Sept./Oct. 1968.

[13] W. C. Jakes, *Microwave Mobile Communications*. New York: IEEE Press, 1994.

[14] J. D. Parsons, *The mobile radio propagation channel*. London: Pentech Press, 1992.

[15] G. L. Stuber, *Principles of mobile communications*. Norwell, MA: Kluwer, 1996.

[16] M. Nakagami, "The m-distribution, a general formula of intensity distribution of rapid fading," in *Statistical Methods in Radio Wave Propagation*, W. G. Hoffman, Ed. Pergamon, Oxford, England, 1960.

[17] S. R. Saunders, *Antennas and propagation for wireless communication systems*. New York: John Wiley, 1999.

[18] D. G. Brennan, "Linear diversity combining techniques," *Proc. IRE*, vol. 47, pp. 1075–1102, June 1959.

[19] M. Schwartz, W. R. Bennett and S. Stein, *Communication Systems and Techniques*. New York: McGraw-Hill, 1966.

[20] G. Taricco, E. M. Biglieri and G. Caire, "Impact of channel-state information on coded transmission over fading channels with diversity reception," *IEEE Trans. Commun.*, vol. 47, pp. 1284–1287, Sept. 1999.

[21] A. I. Sulyman and M. Kousa, "Bit error rate performance of a generalized diversity selection combining scheme in Nakagami fading channels," in *Proc. IEEE WCNC 2000*, Chicago, IL, USA, September 2000, vol. 3, pp. 1080–1085.

[22] L. Yue, "Analysis of generalized selection combining techniques," in *Proc. IEEE VTC Spring 2000*, Tokyo, Japan, May 2000, vol. 2, pp. 1191–1195.

[23] M. K. Simon and M.-S. Alouini, "Performance analysis of generalized selection combining with threshold test per branch (T-GSC)," *IEEE Trans. Veh. Technol.*, vol. 51, no. 5, pp. 1018–1029, Sept. 2002.

[24] Y. Chen and C. Tellambura, "A new hybrid generalized selection combining scheme and its performance over fading channels," in *Proc. IEEE WCNC 2004*, Atlanta, USA, March 2004, vol. 2, pp. 926–931.

[25] A. Annamalai, G. Deora and C. Tellambura, "Unified analysis of generalized selection diversity with normalized threshold test per branch," in *Proc. IEEE WCNC 2003*, New Orleans, USA, Mar 2003, vol. 2, pp. 752–756.

[26] D. Cassioli, M. Z. Win, F. Vatalaro and A. F. Molisch, "Performance of low-complexity RAKE reception in a realistic UWB channel," in *Proc. IEEE ICC 2002*, New York, USA, May 2002, vol. 2, pp. 763–767.

[27] J. W. Craig, "A new, simple, and exact result for calculating the probability of error for two-dimension signal constellations,," in *IEEE MILCOM*. Oct. 1991, pp. 571–575, IEEE.

[28] A. Annamalai, C. Tellambura, and V. Bhargava, "A general method for calculating error probabilities over fading channels," in *Proc. IEEE ICC 2000*, New York, USA, May 2000, pp. 36–40.

[29] A. Annamalai, J. Su, and C. Tellambura, "Exact analysis of equal-gain diversity systems over fading channels," in *Proc. IEEE VTC Spring 2000*, Tokyo, Japan, May 2000, pp. 612–616.

[30] A. Stuart and K. Ord, *Kendall's Advanced Theory of Statistics*, 6th ed., vol. 1. New York: Oxford University Press, 1994.

[31] M. Win and J. Winters, "Analysis of hybrid selection/maximal-ratio combining in Rayleigh fading," *IEEE Trans. Commun.*, vol. 47, pp. 1773–1776, Dec. 1999.

[32] U. Charash, "Reception through Nakagami multipath channels with random delays," *IEEE Trans. Commun.*, vol. 27, no. 4, pp. 657–670, Apr. 1979.

[33] Mohamed-Slim Alouini, Marvin K. Simon, "Dual diversity over correlated log-normal fading channels," *IEEE Trans. Commun.*, vol. 50, no. 12, pp. 1946 –1959, Dec. 2002.

[34] J. Luo, J. R. Zeidler, and S. McLaughlin, "Performance analysis of compact antenna arrays with MRC in correlated Nakagami fading channels," *IEEE Trans. Veh. Technol.*, vol. 50, no. 1, pp. 267–277, Jan 2001.

[35] Samuel C. K. Ko and Ross D. Murch, "A diversity antenna for external mounting on wireless handsets," *IEEE Trans. Antennas Propagat.*, vol. 49, no. 5, pp. 840–842, May 2001.

[36] C. B. Dietrich, Jr., Kai Dietze, J. Randall Nealy and Warren L. Stutzman, "Spatial, polarization, and pattern diversity for wireless handheld terminals," *IEEE Trans. Antennas Propagat.*, vol. 49, no. 9, pp. 1271–1281, Sept. 2001.

[37] S.-S Jeng, G. T. Okamoto, G. Xu, H.-P. Lin and W. J. Vogel, "Experimental evaluation of smart antenna system performance for wireless communications," *IEEE Trans. Antennas Propagat.*, vol. 46, no. 6, pp. 749–757, June 1998.

[38] C. Braun, G. Engblom and C. Bechman, "Evaluation of antenna diversity performance for mobile handsets using 3-D," *IEEE Trans. Antennas Propagat.*, vol. 47, no. 11, pp. 1736–1738, Nov. 1999.

[39] J. N. Pierce and S. Stein, "Multiple diversity with nonindependent fading," *Proc. IRE*, vol. 48, pp. 196–211, Oct. 1960.

[40] C. Tellambura and V. K. Bhargava, "Error performance of MPSK trellis-coded modulation over nonindependent Rician fading channels," *IEEE Trans. Veh. Technol.*, vol. 47, pp. 152–162, Feb. 1998.

[41] V. A. Aalo, "Performance of maximal-ratio diversity systems in a correlated Nakagami-fading environment," *IEEE Trans. Commun.*, vol. 43, no. 8, pp. 2360–2369, Aug. 1995.

[42] P. Lombardo, G. Fedele and M. M. Rao, "MRC performance for binary signals in Nakagami fading with general branch correlation," *IEEE Trans. Commun.*, vol. 47, no. 1, pp. 44–52, Jan. 1999.

[43] O. C. Ugweje and V. A. Aalo, "Performance of selection diversity system in correlated Nakagami fading," in *Proc. IEEE VTC Spring 1997*, New York, NY, USA, May 1997, vol. 3, pp. 1488–1492.

[44] Q. T. Zhang and H. G. Lu, "A general analytical approach to multi-branch selection combining over various spatially correlated fading channels," *IEEE Trans. Commun.*, vol. 50, pp. 1066–1073, July 2002.

[45] C. Tellambura, A. J. Mueller and V. K. Bhargava, "Analysis of M-ary phase-shift keying with diversity reception for land-mobile satellite channels," *IEEE Trans. Veh. Technol.*, vol. 46, pp. 910–922, Nov. 1997.

[46] M. K. Simon and M.-S. Alouini, "A unified approach to the performance analysis of digital communication over generalized fading channels," *Proc. IEEE*, vol. 86, no. 9, pp. 1860–1877, Sept. 1998.

[47] M. S. Alouini and M. K. Simon, "An MGF-based performance analysis of generalized selection combining over Rayleigh fading channels," *IEEE Trans. Commun.*, vol. 48, pp. 401–415, Mar. 2000.

[48] R. F. Pawula, "A new formula for MDPSK symbol error probability," *IEEE Commun. Lett.*, vol. 2, no. 10, pp. 271–272, 1998.

[49] C. Tellambura and V. K. Bhargava, "Unified error analysis of DQPSK in fading channels," *IEE Elect. Lett.*, vol. 30, no. 25, pp. 2110–2111, Dec. 1994.

[50] M. K. Simon and M.-S. Alouini, "A unified approach to the probability of error for noncoherent and differentially coherent modulations over generalized fading channels," *IEEE Trans. Commun.*, vol. 46, no. 12, pp. 1625–1638, Dec. 1998.

[51] L. E. Miller and J. S. Lee, "BER expressions for differentially detected $\pi/4$ DQPSK modulation," *IEEE Trans. Commun.*, vol. 46, no. 1, pp. 71–81, Jan. 1998.

[52] A. Annamalai and C. Tellambura, "Error rates for Nakagami-m fading multichannel reception of binary and M-ary signals," *IEEE Trans. Commun.*, vol. 49, pp. 58–68, Jan. 2001.

[53] D. Cassioli, M. Z. Win and A. F. Molisch, "The ultra-wide bandwidth indoor channel: from statistical model to simulations," *IEEE J. Select. Areas. Commun.*, vol. 20, pp. 1247–1257, Aug 2002.

[54] A. Annanialai and C. Tellambura, "A new approach to performance evaluation of generalized selection diversity receivers in wireless channels," in *IEEE Vehicular Technology Conference*. 2001, pp. 2309–2313, IEEE.

[55] M. Z. Win and J. H. Winters, "Virtual branch analysis of symbol error probability for hybrid selection/maximal-ratio combining in Rayleigh fading," *IEEE Trans. Commun.*, vol. 49, pp. 1926–1934, Nov. 2001.

[56] Y. Ma and S. Pasupathy, "Performance of generalized selection combining on generalized fading," in *Proc. IEEE ICC 2003*, Anchorage, Alaska, USA, May 2003, vol. 5, pp. 3041–3045.

[57] Y. Chen, C. Tellambura, A. Annamalai, "Unified performance bounds for generalized selection diversity combining in independent generalized fading channels," *To appear in Canadian Journal of Electrical and Computer Engineering.*

[58] S. V. Amari and R. B. Misra, "Closed-form expressions for distribution of sum of exponential random variables," *IEEE Trans. Reliability*, vol. 46, no. 4, pp. 519, Dec 1997.

[59] Z. Wang and G. B. Giannakis, "A simple and general parameterization quantifying performance in fading channels," *IEEE Trans. Commun.*, vol. 51, pp. 1389–1398, 2003.

[60] P. G. Moschopoulos, "The distribution of the sum of independent gamma random variables," *Ann. Inst. Statist. Math.*, vol. 37, pp. 541–544, 1985.

[61] L. Hanzo, W. Webb and T. Keller, *Single- and Multi-carrier Quadrature Amplitude Modulation: Principles and Applications for Personal Communications, WLANs and Broadcasting*. New York: Wiley, 2002.

[62] M. J. Gans, "The effect of Gaussian error in maximal ratio combiners," *IEEE Trans. on Commun. Tech.*, vol. 19, pp. 492–500, Aug. 1971.

[63] Q. T. Zhang, "Maximal-ratio combining over Nakagami fading channels with an arbitrary branch covariance matrix," *IEEE Trans. Veh. Technol.*, vol. 48, no. 4, pp. 1141–1150, July 1999.

[64] F. J. Altman and W. Sichak, "A simplified diversity communication system for beyond the horizon links," *IRE Trans. Commun. Syst.*, vol. 4, pp. 50–55, Mar. 1956.

[65] N. C. Beaulieu, "An infinite series for the computation of the complementary probability distribution function of a sum of independent random variables and its application to the sum of Rayleigh random variables," *IEEE Trans. Commun.*, vol. 38, pp. 1463–1474, Sept. 1990.

[66] N. C. Beaulieu and A. A. Abu-Dayya, "Analysis of equal gain diversity on Nakagami fading channels," *IEEE Trans. Commun.*, vol. 39, no. 2, pp. 225–234, Feb. 1991.

[67] A. Abu-Dayya and N. C. Beaulieu, "Microdiversity on Ricean channels," *IEEE Trans. Commun.*, vol. 42, pp. 2258–2267, June 1994.

[68] Q. T. Zhang, "Probability of error for equal-gain combiners over Rayleigh channels: some closed-form solutions," *IEEE Trans. Commun.*, vol. 45, pp. 270–273, Mar. 1997.

[69] Q. T. Zhang, "A simple approach to probability of error for equal gain combiners over Rayleigh channels," *IEEE Trans. Veh. Technol.*, vol. 48, pp. 1151–1154, July 1999.

[70] Young-Chai Ko, M.-S. Alouini and M. K. Simon, "Average SNR of dual selection combining over correlated Nakagami-m fading channels," *IEEE Commun. Lett.*, vol. 4, pp. 12–14, Jan 2000.

[71] M. K. Simon and M.-S. Alouini, "A unified performance analysis of digital communication with dual selective combining diversity over correlated Rayleigh and Nakagami-m fading channels," *IEEE Trans. Commun.*, vol. 47, no. 1, pp. 33–44, Jan. 1999.

[72] C. Tellamura, A. Annamalai and V. K. Bhargava, "Contour integral representation for generalized Marcum-Q function and its application to unified analysis of dual-branch selection diversity over correlated Nakagami-m fading channels," in *Proc. IEEE VTC Spring 2000*, Tokyo, Japan, May 2000, vol. 2, pp. 1031–1034.

[73] C. Tellambura, A. Annamalai and V. K. Bhargava, "Closed-form and inifinite series solutions for the MGF of a dual-diversity selection combiner output in bivariate Nakagami fading," *IEEE Trans. Commun.*, vol. 51, pp. 539– 542, Apr. 2003.

[74] Liquan Fang, Guoan Bi and Alex C. Kot, "Performance of antenna diversity reception with correlated Rayleigh fading signals," *IEEE Trans. Commun.*, vol. 3, pp. 1593 –1597, 1999.

[75] Y. Wan and J. C. Chen, "Fading distribution of diversity techniques with correlated channels," *Proc. IEEE Int. Symp. Personal, Indoor, and Mobile Communications PIMRC'95*, vol. 3, pp. 1202–1206, Sept. 1995.

[76] G. K. Karagiannidis, "Performance analysis of SIR -based dual selection diversity over correlated Nakagami-m fading channels," *IEEE Trans. Veh. Technol.*, vol. 52, pp. 1207–1216, Sept. 2003.

[77] G. K. Karagiannidis, D. A. Zogas and S. A. Kotsopoulos, "Performance analysis of triple selection diversity over exponentially correlated Nakagami-*m* fading channels," *IEEE Trans. Commun.*, vol. 51, no. 8, pp. 1245–1248, Aug. 2003.

[78] A. S. Krishnamoorthy and M. Parthasarathy, "A multivariate gamma-type distribution," *Ann. Math. Statist.*, vol. 22, pp. 549–557, 1951.

[79] R. K. Mallik and M. Z. Win, "Analysis of hybrid selection/maximal-ratio combining in correlated Nakagami fading," *IEEE Trans. Commun.*, vol. 50, pp. 1372–1383, Aug. 2002.

[80] K. S. Miller, *Complex Scochastic Processes*. Addison-Wesley, 1974.

[81] R. K. Mallik, "On the multivariate Rayleigh and exponential distributions," *IEEE Trans. Inform. Theory*, vol. 49, pp. 1499–1515, June 2003.

[82] G. K. Karagiannidis, D. A. Zogas and S. A. Kotsopoulos, "On the multivariate Nakagami-*m* distribution with exponential correlation," *IEEE Trans. Commun.*, vol. 51, no. 8, pp. 1240– 1244, Aug. 2003.

[83] G. K. Karagiannidis, D. A. Zogas and S. A. Kotsopoulos, "An efficient approach to multivariate Nakagami-m distribution using Green's matrix approximation," *IEEE Trans. Wirel. Commun.*, vol. 2, pp. 883–889, Sept. 2003.

[84] A. Annamalai, C. Tellambura, and V. K. Bhargava, "Exact evaluation of maximal-ratio and equal-gain diversity receivers for M-ary QAM on Nakagami fading channels," *IEEE Trans. Commun.*, vol. 47, pp. 1335–1344, Sept. 1999.

[85] R. Mallik, M. Win, and J. Winters, "Performance of dual-diversity predetection EGC in correlated Rayleigh fading with unequal branch SNRs," *IEEE Trans. Commun.*, vol. 50, pp. 1041–1044, July 2002.

[86] A. Annamalai, V. Ramanathan and C. Tellambura, "Analysis of equal-gain diversity receiver in correlated fading channels," in *Proc. IEEE VTC Spring 2002*, Birmingham, Al, May 2002, vol. 4, pp. 2038 –2041.

[87] C. W. Dunnett and M. Sobel, "Approximations to the probability integral and certain percentage points of a multivariate analogue of student's t-distribution," *Biometrika*, vol. 42, no. 1/2, pp. 258–260, Jun 1955.

[88] S. S. Gupta, K. C. S. Pillai and G. P. Steck, "On the distribution of linear functions and ratios of linear functions of ordered correlated normal random variables with emphasis on range," *Biometrika*, vol. 51, pp. 143–151, 1964.

[89] R. B. Ertel and J. H. Reed, "Generation of two equal power correlated Rayleigh fading envelopes," *IEEE Commun. Lett.*, vol. 2, no. 10, pp. 276–278, 1998.

[90] N. C. Beaulieu, "Generation of correlated Rayliegh fading envelopes," *IEEE Commun. Lett.*, vol. 3, no. 6, pp. 172–174, June 1999.

[91] S. Chang, *Non-coherent orthogonal digital modulation in fading with correlated branch diversity*, Ph.D. thesis, Queen's Univ., Kingson, Ont., Canada, July 1994.

[92] M. Abramowitz and I. A. Stegun, *Handbook of Mathematical Functions with Formulas, Graphs, and Mathematical Tables*. New York: Dover, 1972.

[93] Murray R. Spiegel and John Liu, *Mathematical Handbook of Formulas and Tables*, 2nd ed. McGraw-Hill, 1999.

[94] C. C. Tan and N. C. Beaulieu, "Infinite series representations of the bivariate Rayleigh and Nakagami-m distributions," *IEEE Trans. Commun.*, vol. 45, no. 10, pp. 1159–1161, Oct. 1997.

[95] P. Appell and J. Kampé de Fériet, *Fonctions Hypergéométriques et Hypersphériques; Polynomes d'Hermite*. Paris: Gauthier-Villars, 1926.

[96] M. C. Jeruchim, P. Balaban and K. S. Shanmugan, *Simulation of communication systems: modeling, methodology and techniques*, 2 ed. New York: Kluwer academic/Plenum, 2000.

[97] S. Chang and P. J. McLane, "Bit-error-probability for noncoherent orthogonal singals in fading with optimum combining for correlated brach diversity," *IEEE Trans. Inform. Theory.*, vol. 43, Jan. 1997.

[98] A. A. Abu-Dayya and N. C. Beaulieu, "Analysis of switched diversity systems on generalised-fading channels," *IEEE Trans. Commun.*, vol. 42, no. 11, pp. 2959–2966, Nov. 1994.

[99] M. K. Simon and M.-S. Alouini, *Digital Communication over Fading Channels*, 1 ed. New York: Wiley, 2000.

[100] C. Tellambura and V. K. Bhargava, "A performance analysis of trellis coded modulation schemes in non-independent Rician fading channels," *Global Telecommunications Conference, 1993*, vol. 3, pp. 1424 –1428, 1993.

[101] S. O. Rice, "Mathematical analysis of random noise," *Bell Syst. Tech. J.*, vol. 23, pp. 282–332, 1944.

[102] K. S. Miller, "Complex Gaussian processes," *SIAM*, vol. 11, pp. 544–567, Oct. 1969.

[103] L. E. Blumenson and K. S. Miller, "Properties of generalized Rayleigh distributions," *Ann. Math. Statist.*, vol. 34, pp. 903–910, 1963.

[104] H. A. David, *Order statistics*, 2nd. ed. New York : Wiley, 1981.

[105] N. Kong, T. Eng, and L. B. Milstein, "A selection combining scheme for RAKE receivers," in *IEEE ICUPC*. 1995, pp. 426–430, IEEE.

[106] D. Aszetly, *On antenna arrays in mobile communication systems: fast fading and GSM base station receiver algorithm*, Ph.D. thesis, Royal Institute Technology, Stockholm, Sweden, Mar. 1996.

[107] J. Salz and J. H. Winters;, "Effect of fading correlation on adaptive arrays in digital mobile radio," *IEEE Trans. Veh. Technol.*, vol. 43, pp. 1049–1057, Nov. 1994.

[108] Y. Ma, C. C. Chai and T. J. Lim, "Unified analysis of error probability for MRC in correlated fading channels," *Electronics Letters*, vol. 35, no. 16, pp. 1314–1315, Aug. 1999.

[109] J. G. Kemeny and J. L. Snell, *Finite Markov Chains*. Princeton, NJ: Van Nostrand, 1960.

[110] G. N. Watson, *A Treatise on the theory of Bessel functions*. Univerisity Press, Cambridge, 1944.